Spring 1994

Analysis of Random Structure-Acoustic Interaction Problems Using Coupled Boundary Element and Finite Element Methods

Carl S. Pates III
Old Dominion University

ANALYSIS OF RANDOM STRUCTURE-ACOUSTIC INTERACTION PROBLEMS USING COUPLED BOUNDARY ELEMENT AND FINITE ELEMENT METHODS

by

Carl S. Pates, III
B.S., December 1989, Old Dominion University
M.S., December 1991, Old Dominion University

A Dissertation Submitted to the Faculty of
Old Dominion University in Partial Fulfillment of the
Requirement for the Degree of

DOCTOR OF PHILOSOPHY

in

ENGINEERING MECHANICS

OLD DOMINION UNIVERSITY
May, 1994

Approved by:

_____
Chuh Mei (Co-Director)

_____
Uday Shirahatti (Co-Director)

_____
Stephen Rizzi

_____
Gene Hou

_____
Glenn Lasseigne

ABSTRACT

ANALYSIS OF RANDOM STRUCTURE-ACOUSTIC INTERACTION PROBLEMS USING COUPLED BOUNDARY ELEMENT AND FINITE ELEMENT METHODS

Carl S. Pates III
Old Dominion University
Directors: Dr. Chuh Mei and Dr. Uday Shirahatti

A coupled boundary element(BEM)-finite element(FEM) approach is presented to accurately model structure-acoustic interaction systems. The boundary element method is first applied to interior, two and three-dimensional acoustic domains with complex geometry configurations. Boundary element results are very accurate when compared with limited exact solutions.

Structure-interaction problems are then analyzed with the coupled FEM-BEM method, where the finite element method models the structure and the boundary element method models the interior acoustic domain. The coupled analysis is compared with exact and experimental results for a simplistic model. Composite panels are analyzed and compared with isotropic results. The coupled method is then extended for random excitation. Random excitation results are compared with uncoupled results for isotropic and composite panels.

ACKNOWLEDGEMENTS

I would like to extend my thanks to Drs. Chuh Mei and Uday Shirahatti for their patience, guidance and knowledge. Not only did they teach me technical knowledge, and research skills, but they taught me ethical values and responsibilities. I would like to thank Drs. Stephen A. Rizzi, Gene Hou, and D.G. Lasseigne for their support and suggestions. I want to also extend my thanks to everyone at the Acoustics Division, at NASA Langley Research Center (NAG-1-1358), for their input and backing when I was there. To Dr. Robert Ash, thank you for opening my eyes and for helping me realize my graduate potential. Thank you for motivating me early in my career.

The ultimate credit for the perseverance and determination to complete this dissertation came from my loving parents. Throughout the years, they have always supported and contributed to my education. I also want to express my sincere gratification to my wife, Jo Ell. Without her total support and trust, none of this would have been possible.

TABLE OF CONTENTS

LIST OF TABLES

LIST OF FIGURES

LIST OF SYMBOLS

A,B,D	Laminate stiffness matrices
al,bl	Element length and width
AR	Singular element area
c	Medium sound speed
C	Modal damping matrix
C_c	Matrix simplification
c_m	Integration constant
C_b, C_m	Shape function derivative matrices
CPLG(ω)	Coupled system transfer matrix
d	Modal coordinates
E, E_{11}, E_{22}	Young's Modulus
$E[d^2]$	Mean square of modal displacement
$E[W^2]$	Mean square of displacement
f_{mod}	Modal force
F_e	External force
F_p	Acoustic force
F_T	Global force vector
G	Acoustic influence matrix
G_{12}	Shear modulus
h	Plate thickness
H	Acoustic influence matrix

$H_0^{(1)}$, $H_1^{(1)}$	Hankel function
$\hat{H}$	Influence matrix
H_{pact}	Acoustic pressure transfer function
H_s	Structural response function
H_u, H_v, H_w	Shape functions
i	$\sqrt{-1}$
I	Identity matrix
J_0, J_1	Bessel function of the 1st kind
k	Acoustic wavenumber
k_b	Element bending stiffness
k_m	Element membrane stiffness
k_{mb}, k_{bm}	Element coupling stiffness
k_{el}	Total Linear element stiffness
K	Global stiffness matrix
l	Element length (1-D element)
L	Acoustic duct length
L_2	Acoustic duct length of Middle Section
LOAD	Matrix simplification
LT	Load transformation matrix
m	Total element mass matrix
m_b	Element bending mass matrix
m_{um}, m_{vm}	Element inplane mass matrix
M_b	Bending moments
M	Global mass matrix
M_n	Modal mass

N	Inplane forces
p	Spatial part of acoustic pressure, P
p^*	Green's function for p
p_{act}	Coupled acoustic pressure
$p_b(t)$	Time dependent element pressure loading
p_{IN}	Input acoustic pressure
$P(x,y,z,t)$	Total acoustic pressure
$P_b(t)$	Global loading vector
$P_{bl}(t)$	Reduced Loading Vector
q	Normal derivative of p
q^*	Green's function of q
Q	Reduced stiffness matrix
$\overline{Q}$	Transformed reduced stiffness matrix
$\vec{r}$	Distance vector
R_o	Singular element radius
s	Condensation
S_{T0}, S_{T1}	Struve functions
S_2, S_1	Area of duct at location 2 and 1
S_A	Diagonal area matrix
$S_d(\omega)$	Spectral density of structure modal displacement
$SD(\omega)$	Matrix simplification
$SD_{IN}(\omega)$	Matrix simplification
$S_{IN}(\omega)$	Input spectral density
$S_p(f)$	Input spectral density (hertz)
$S_{pact}(\omega)$	Acoustic spectral density

S_{u_a}	Acoustic displacement spectral density
SSL	Sound source level (dB)
T	Transformation matrix
T_b, T_m	Element transformation matrices
u, v	Inplane displacement in x & y direction, respectively
u_a	Acoustic displacement
v_a	Acoustic velocity
w	Total element displacement
w_b	Element bending displacement
w_m	Element inplane displacement
W	Global degree of freedom vector
W_{ext}	External work
W_{int}	Internal work
Y_0, Y_1	Bessel function of the 2nd kind
z	Constant impedance boundary condition
z_o	Distance from mid-surface

Greek

α'	Angle between connecting elements
α, β	Generalized coordinates
α_t	Transmission loss coefficient
B	Adiabatic Bulk Modulus
β_o	Coordinate transformation
Δ	Dirac delta function
ζ	Damping ratio
ϵ	Total strain

ϵ_m	Membrane strain
ϵ_o	Coordinate transformation
γ	Shear strain
Γ	Acoustic boundary
Γ_f	Gamma function
κ	Plate curvature
ν_{12}, ν_{21}	Poisson's ratio
ω	Input frequency
ω_c	Cutoff frequency
ω_n	Structure natural frequency
Ω	Interior acoustic domain
Ω'	Exterior acoustic domain
ϕ	Composite lamination angle
ϕ_1	Middle duct section angle
Φ	Structure modal matrix
Φ_1, Φ_2	Interpolation function
Φ_b	Bending modal matrix
Φ_m	Membrane modal matrix
ρ_a	Acoustic medium density
ρ	Structure density
σ	Plate stress
θ	Angle between $\vec{r}$ and normal
ξ	Dimensionless parameter

Chapter 1

INTRODUCTION

1.1 Preliminary Remarks

Over the past few years, structural-acoustic interaction problems have shown enhanced interest in the aerospace and automotive industries. New supersonic aircraft designs such as the High-Speed Civil Transport (HSCT), the National Aero-Space Plane (NASP), and the Advanced Tactical Fighter (ATF) have lead to some very complicated engineering problems. Acoustic excitation of the fuselage has been one of the main concerns during certain flight operations. In Figure 1.1, the acoustic loads on a B-52 wing during take-off are shown. The acoustic sound pressure levels reach as high as 164 dB [1]. Systems on new supersonic aircraft will be highly random in nature with temperatures possibly reaching 2000°F and acoustic sound pressure levels of 190 dB, as shown in Figure 1.2 [2]. In such extreme environments, the structural-acoustic system can be driven into an extreme random regime from such things as turbulent boundary layers. Under such conditions, the coupling of the acoustic and the structure systems and determining their combined random responses become extremely important.

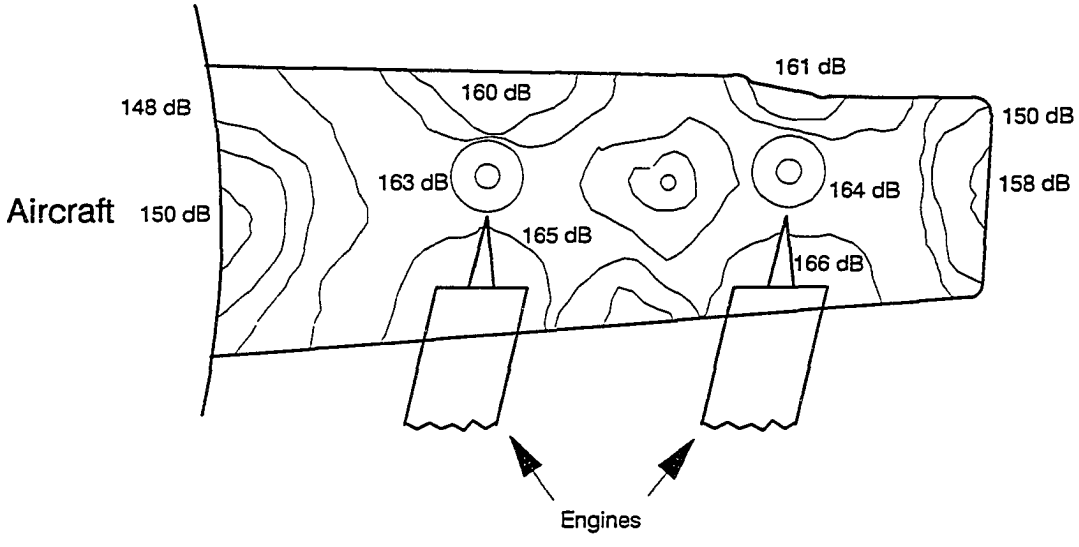

Figure 1.1 Acoustic Sound Pressure Levels on a B-52 Wing During Take-off.

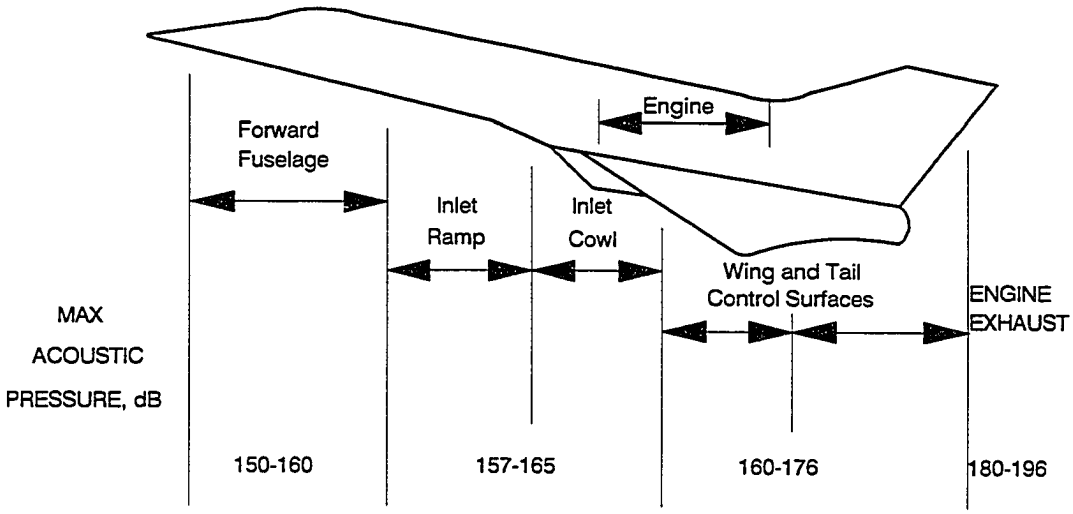

Figure 1.2 Expected Acoustic Sound Pressure Levels on NASP.

Due to the harsh environments generated during flight, structural design becomes critical and strength-to-weight ratios also become vitally important. In extreme environments, composite materials can have major advantages over isotropic materials in the random response of structural components. Composite materials offer adjustable design variables such as lamination angles, layer thicknesses and fiber/matrix composition ratios.

Due to the complex geometry of many structural problems, numerical methods have become the tool of choice. The finite element method (FEM) is a well established technique that offers many advantages when modelling the structure. The boundary element method (BEM) has become a popular technique when modelling acoustic domains. Recently, some attempts have been made to couple the boundary element method and the finite element method for solving structural-acoustic interaction problems. By coupling the two numerical techniques, the designer creates a very powerful tool for modelling real system behavior, including random response.

1.2 Review of Previous Work

Over the past 15 years, research on the indirect boundary element method (IBEM) and the direct boundary element method (DBEM) has increased. The DBEM solves directly for the acoustic pressures and velocities. The IBEM creates source potentials to model the boundary as acoustic sources and from

the potentials, acoustic pressures and velocities are obtained. The direct method is better suited to couple with the finite element method. The major differences between the IBEM and the DBEM have been documented [3-5].

Approximately, 80% of all boundary element papers dealing with acoustics are in the radiation and scattering area [6-14]. Acoustic radiation and scattering has also become an important research area for acoustic systems. The majority of research papers concerning internal domains have been in three-dimensional space. Two-dimensional problems present difficulties associated with the singularities of the Hankel function [15-19]. Research in three-dimensional duct systems has been conducted in three main areas. Room acoustics with acoustic sources started three-dimensional BEM research [20-22]. Another area of research has been in the design of mufflers. Here, the boundary element method has resulted in a very useful modelling tool for solving difficult geometry and boundary condition problems [23-26]. Research interest has also been directed towards the design of automobile cavities. The interior of automobiles can give rise to some very difficult geometry regions as well as reflecting and absorbing material boundary conditions [16,20,27,28].

Additional research in acoustics using the boundary element method includes element design and time domain solutions. Many types of boundary elements have been developed and used for acoustic domains. The first type of

elements used for acoustics were the constant, linear and quadratic elements [29]. Triangular and quadrilateral elements have become increasingly popular with boundary element users [5,10,30,31]. Limited research has been conducted on transient problems with time domain solutions [32,33]. Coupling the finite element and boundary element methods has been a main focus of the research community over the past ten years. The initial idea to couple the discretized equations of FEM and the boundary integral method was developed by Zienkiewicz, Kelly and Bettess in 1977 [34]. The boundary element and finite element methods have been coupled for many types of problems. Numerous publications have linked the two methods in structural dynamics. Crack propagation [35], soil-plate coupling [36], and beam and plate vibration systems are some typical examples. Specific beam and plate problems include studies on structures with cut-outs [37,38], varying BEM and FEM regions [39-42], and circular plates with slots [43]. The coupled BEM-FEM technique has been used to model fluid-filled tanks and spheres used in the Space Shuttle [44,45]. Coupling FEM and BEM for the Laplace equation has shown limited interest [34].

Modelling structure-acoustic interaction problems has also been at the forefront of current research over the past few years. Radiation and scattering problems have received much of the research attention, since the boundary element method handles infinite regions very well [46-51]. Yuying

studied acoustic radiation of floating plates with odd geometries [52]. Coupling of interior acoustic and structure problems has also been popular. In 1984, Suzuki, Imai and Ishiyama provided the initial formulation coupling the modal FEM and BEM [53]. Many articles use a well-known cavity-backed plate problem to compare results [53-56]. The cavity-backed plate problem was first analyzed by Guy and Bhattacharya in 1973 [57]. They provided valuable semi-analytical results using modal approximations and also experimental data. In 1992, Bokil derived an exact solution to the coupled cavity-backed plate problem using Laplace transforms [58]. After the coupling technique showed that it was accurate and versatile, many interesting real world problems have been modelled. Aircraft fuselage studies were conducted in 1991 by Fyfe, Coyette, and van Vooren [59]. Many authors have attempted to model complex geometries of automobile cavities [59-61]. Some automobile cavities have used complex boundary conditions including fiber and foam absorbing material [20,60]. Other interesting automotive problems have been studied such as engine block noise [59] and gearbox noise [62] reduction studies.

1.3 Objectives and Scope

The overall objective of the present study is to present a coupled boundary element and finite element technique to solve coupled structural-acoustic interaction problems for

harmonic and random response. To perform this task, four steps are required. The first objective is to develop and validate the boundary element method as an accurate numerical technique for acoustic domains. The second step is to acquire a finite element program to accurately model the structural system. The third objective involves coupling the boundary element method and the finite element method to model the total coupled system. Coupling the acoustic and plate displacements as well as the acoustic force becomes very important. The first three steps have been completed previously. The new contribution of this study includes the coupled BEM-FEM technique to model realistic problems, including composite materials and random responses of the acoustic and structural domains.

The boundary element method is well suited for interior and exterior acoustic problems. BEM reduces the dimensionality of the discretized domain by one dimension, thus making it very appealing for complex geometric domains. For instance, a three-dimensional domain is modelled by two-dimensional surface elements only. The two-dimensional acoustic problem is analyzed first. Two-dimensional domains are very difficult to model with BEM because of the singularities that occur in the assumed free-field pressure solution. Since the assumed pressure, or Green's function, contains the first and second order Bessel functions, the domain integral becomes singular at certain positions. This

study derives a new method of approximating these singular integrals. A few two-dimensional cases are modelled using linear and constant boundary elements including: mufflers, ducts with sudden area changes, and a three-section duct system. BEM results are compared with exact solutions for certain rectangular duct systems in Chapter 4.

Three-dimensional duct systems are also modelled in this study. Singular integrals are easily evaluated by a change of coordinate systems. BEM results are again compared versus exact solutions for rectangular duct domains in Chapter 4. Irregular-shaped ducts are also modelled to show the versatility of the boundary element method. Chapter 3 includes the coupled formulation for BEM and FEM. A brief introduction to the finite element formulation is given along with pertinent element-type information. Coupling techniques between BEM and FEM for random analysis is derived in Chapter 3. Chapter 4 includes the case results from each system listed above. Results include two and three-dimensional duct systems and coupled structural-acoustic interaction problems. Random effects are also shown for the coupled interaction problem. Concluding remarks and recommendations for future work are presented in Chapter 5.

Chapter 2

BOUNDARY ELEMENT FORMULATION

In this chapter, the governing equations are derived for two and three-dimensional acoustic domain problems. The system equations and solution procedures are also given.

The derivation begins with the wave equation and progresses with the derivation of the influence matrices, [H] and [G]. There is no stream flow considered and only the acoustic pressure is assumed present. Throughout this study, only linear acoustic and structure theory are used in the formulation.

2.1 Acoustic Wave Equation

The derivation of the linear wave equation is well defined and can be found in any acoustic text. The acoustic medium is assumed to be homogeneous, isotropic and perfectly elastic. The perfectly elastic assumption allows us to use the particle displacements and velocities of acoustic waves in the governing equations, similar to elastic waves in solids. No viscous or gravitational effects are considered in the

derivation. The equation of state of a perfect fluid medium is given as

$$P = Bs, \tag{2.1}$$

where B is the adiabatic bulk modulus and s is the condensation. Only small displacements are considered for the acoustic particle displacement and the acoustic pressure, P, is considered to be small compared with the equilibrium pressure. The equation of continuity can now be applied to a volume element. The linearized continuity equation is shown as

$$\frac{\partial s}{\partial t} + \nabla \cdot \vec{v}_a = 0, \tag{2.2}$$

where $\vec{v}_a$ is the particle velocity and ∇ is the divergence operator.

The next step is to apply Newton's second law to the equilibrium of forces on the acoustic particles, and thus the inviscid linearized Euler's equation is produced

$$\rho_a \frac{\partial \vec{v}_a}{\partial t} = -\nabla P, \tag{2.3}$$

where ρ_a is the density of the acoustic medium. Combining Equations (2.1), (2.2) and (2.3), and eliminating the condensation, s, yields the linearized wave equation

$$\nabla^2 P = \frac{1}{c^2}\frac{\partial^2 P}{\partial t^2}, \tag{2.4}$$

where c is defined as, $c=(B/\rho_s)^{1/2}$. A detailed derivation of the linear wave equation can be found in Kinsler and Frey [65]. The pressure in Equation (2.4) is represented as

$$P = P(x,y,t). \tag{2.5}$$

2.2 Two-Dimensional Formulation

Very little work has been done in the two-dimensional study of the boundary element method due to the difficulty in calculating the integrals of the fundamental solutions. ∇^2, from Equation (2.4), is the two-dimensional Laplacian operator given by

$$\nabla^2 = \frac{\partial^2}{\partial x^2} + \frac{\partial^2}{\partial y^2}.$$

The fundamental acoustic pressure response is given as

$$P = p(x,y)e^{i\omega t} \tag{2.6}$$

and thus the two-dimensional linear wave equation reduces to the Helmholtz equation,

$$\nabla^2 p + k^2 p = 0, \tag{2.7}$$

where k is the acoustic wavenumber and is represented as $k=\omega/c$. The value ω, is the acoustic input frequency. The variable p represents the pressure distribution and q is the

partial derivative of the pressure with respect to the normal or,

$$q=\frac{\partial p}{\partial n}=-i\rho_a\omega\overline{v}_a. \tag{2.8}$$

Equation (2.8) is a direct result from Euler's equation as seen in Equation (2.3). This condition will be utilized as the boundary condition of the sound pressure on the surface of the duct, where $\partial/\partial n$ is the outward normal derivative.

Noting that p is only a function of spatial coordinates, the method of weighted residuals statement of the Helmholtz equation is given by

$$\int_\Omega\left(\nabla^2 p+k^2 p\right)p^* d\Omega=0, \tag{2.9}$$

where the fundamental solution, p^*, is the free-field Green's function for the Helmholtz equation and satisfies

$$\nabla^2 p^*+k^2 p^*+\Delta=0, \tag{2.10}$$

in the domain Ω and Δ is the Dirac delta function. The fundamental solution for two-dimensional space and solution to Equation (2.10) is

$$p^*=\frac{i}{4}H_o^{(1)}(k\overline{r}), \tag{2.11}$$

and

$$q^* = \frac{-ik}{4} H_1^{(1)}(k\vec{r})\cos\theta, \qquad (2.12)$$

where $\vec{r}$ is the distance between the source point, S, and the observation point, B, as seen in Figure 2.1 and $H(k\vec{r})$ is the Hankel function [29]. The variable θ is the angle between the normal of the j^{th} element (observation point, B) and the distance vector, $\vec{r}$, which is between the source point, S, and the observation point as shown in Figure 2.1. Figure 2.1a is a model of a two-dimensional duct utilizing constant boundary elements. Figure 2.1b is a two-dimensional duct utilizing linear boundary elements. Note that both ducts have inlet and outlet boundaries as shown.

The Hankel function is defined as

$$H_o^{(1)}(k\vec{r}) = J_o(k\vec{r}) + iY_o(k\vec{r}),$$

and

$$H_1^{(1)}(k\vec{r}) = J_1(k\vec{r}) + iY_1(k\vec{r}), \qquad (2.13)$$

where J and Y are the Bessel functions of the first and second kind, respectively [66]. The subscripts on the Bessel functions can be identified as: 0 representing the zero order and 1 representing the first order. The definitions for the Bessel functions of the zero and first order are given as

$$\frac{d}{dx}Y_o(x) = -Y_1(x), \qquad \frac{d}{dx}J_o(x) = -J_1(x). \qquad (2.14)$$

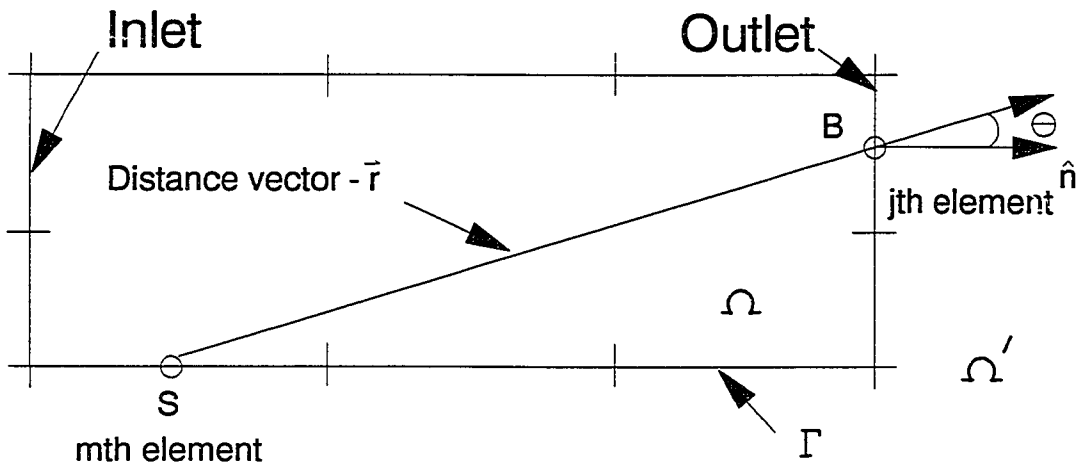

Figure 2.1a Duct Modelled with 2-D Constant Boundary Elements.

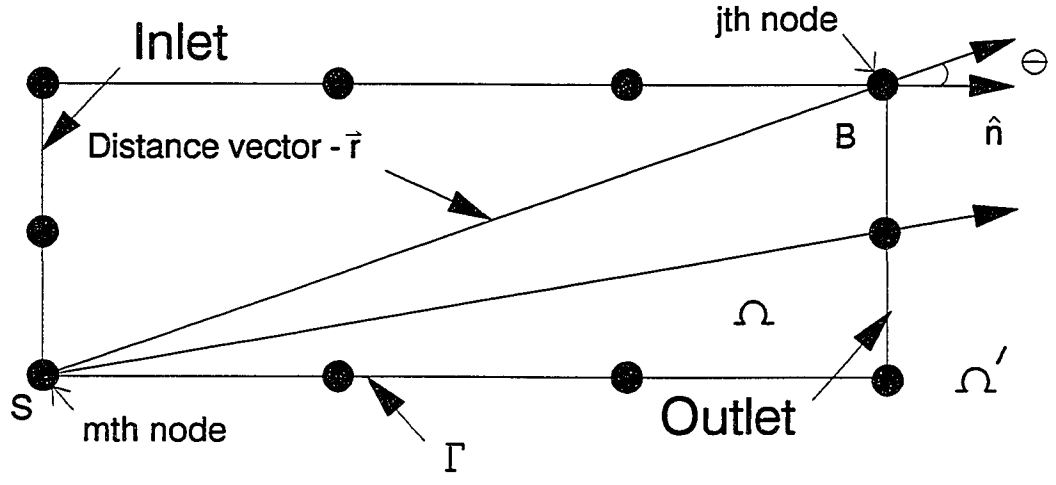

Figure 2.1b Duct Modelled with 2-D Linear Boundary Elements.

$H_o^{(1)}$ is the Hankel function of the first kind and zero order and $H_1^{(1)}$ is the Hankel function of the first kind and first order.

Integrating Equation (2.9) twice by parts and collecting terms, the governing equation becomes,

$$\int_\Omega (\nabla^2 p^* + k^2 p^*) p \, d\Omega = -\int_\Gamma q p^* d\Gamma + \int_\Gamma p q^* d\Gamma, \qquad (2.15)$$

where Γ represents the total boundary. The domain integral term in Equation (2.15) is evaluated by introducing the Dirac delta function from Equation (2.10), and thus reduces the integral to $-c_m p_m$. The c_m term is constant for each boundary element and is defined as,

$$\begin{aligned} c_m &= \frac{\alpha'}{2\pi} && \textit{on the boundary } (\Gamma) \\ c_m &= 0 && \textit{outside the boundary } (\Omega') \\ c_m &= \frac{1}{2} && \textit{on a smooth boundary } (\Gamma) \\ c_m &= 1 && \textit{inside the boundary } (\Omega) \end{aligned} \qquad (2.16)$$

where α' is the internal angle, in radians, between connecting elements and the subscript m represents the source element. For example, a smooth element has a c_m value of 1/2, since the angle at the representing node is π. For smooth constant elements, the angle is always π, since the representing node is at the center of the element. For linear elements, a corner element has a $\pi/2$ angle and a c_m value of 1/4. For linear elements, a c_m value is given for each node of the element. Figure 2.2 clearly shows the definition of the angle

α' for constant and linear elements. A complete derivation and description of the c_m value is given by Brebbia [29]. By introducing the Dirac delta function into the domain integral, the domain integral is reduced to a constant term and thus the governing equation reduces to only boundary expressions. This assumption of using the free-space Green's function is the backbone idea of the boundary element method.

Discretizing the boundary into elements, the governing equation can be written as,

$$c_m\, p_m + \sum_{j=1}^{N} \int_{\Gamma_j} q^* p \, d\Gamma = \sum_{j=1}^{N} \int_{\Gamma_j} p^* q \, d\Gamma, \qquad (2.17)$$

where N is the total number of elements and j represents the j^{th} element. The fundamental solutions from Equations (2.11) and (2.12) can now be substituted in Equation (2.17). At this point, one must decide which type of element to use. Extensive work has been completed using three types of elements: constant, linear, and quadratic elements. For the two-dimensional analysis, only constant and linear type elements are discussed. However, higher order elements can easily be derived and programmed. This study was not an attempt to employ higher order elements. Rather, the objective of this study is to understand and apply the governing equations of the boundary element method to model acoustic domains.

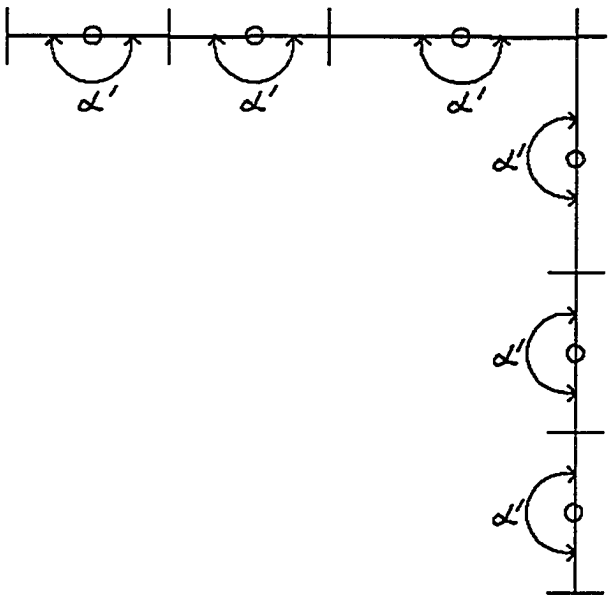

Figure 2.2a Definition of Angle α′ for 2-D Constant Boundary Elements.

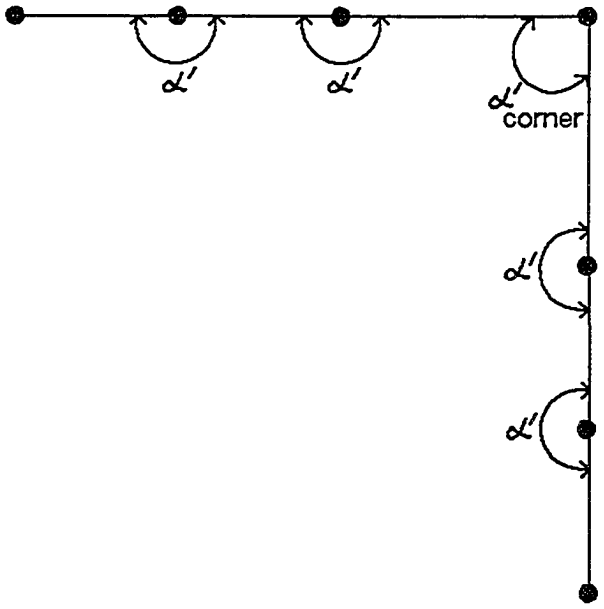

Figure 2.2b Definition of Angle α′ for 2-D Linear Boundary Elements.

2.2.1 Constant Elements

If constant elements are used, p and q are assumed constant over each element. The element is represented by a line and a node at the center of the element as seen in Figure 2.3 below.

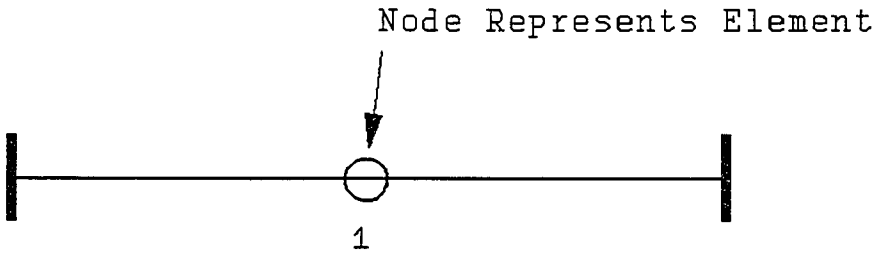

Figure 2.3 Two-Dimensional Constant Element.

Therefore, p and q can be extracted from the integral terms in Equation (2.17). Substituting p^* and q^*, from Equations (2.11) and (2.12), into Equation (2.17) and using constant elements,

$$c_m\, p_m + \sum_{j=1}^{N} \left(\int_{\Gamma_j} \left[-\frac{ik}{4} H_1^{(1)}(k\vec{r}) \right] \cos\theta \; d\Gamma \right) p_j = \sum_{j=1}^{N} \left(\int_{\Gamma_j} \left[\frac{i}{4} H_o^{(1)}(k\vec{r}) \right] d\Gamma \right) q_j . \qquad (2.18)$$

Note that p_j and q_j have been pulled outside of the boundary integrals. Also, note that the angle θ varies as the integral is enforced over the element. Equation (2.18) is the final form of the governing boundary element equation for constant elements.

2.2.2 Linear Elements

For linear boundary elements, p and q are defined in terms of their end nodal values and two interpolation functions Φ_1 and Φ_2. The linear element is represented by a line with nodes at each end of the element as shown in Figure 2.4.

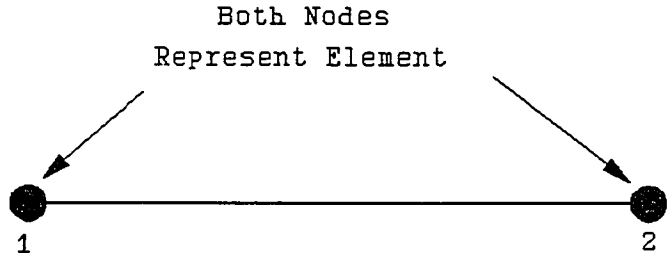

Figure 2.4 Two-Dimensional Linear Element.

The interpolation functions are

$$\Phi_1 = \frac{1}{2}(1-\xi),$$

and

$$\Phi_2 = \frac{1}{2}(1+\xi), \qquad (2.19)$$

where ξ is a dimensionless coordinate varying from -1 to +1. Now p and q can be expressed as

$$p(\xi) = \Phi_1 p^1 + \Phi_2 p^2 = \begin{bmatrix}\Phi_1 & \Phi_2\end{bmatrix} \begin{Bmatrix} p^1 \\ p^2 \end{Bmatrix} \qquad (2.20)$$

and

$$q(\xi) = \Phi_1 q^1 + \Phi_2 q^2 = \begin{bmatrix} \Phi_1 & \Phi_2 \end{bmatrix} \begin{Bmatrix} q^1 \\ q^2 \end{Bmatrix}. \qquad (2.21)$$

The values p^1, p^2, q^1, and q^2 in Equations (2.20) and (2.21) are the constant pressures and normal derivatives of pressure at nodes 1 and 2, as shown in Figure 2.4. Substituting the expressions for p and q from Equations (2.20) and (2.21) and the fundamental solutions for p^* and q^* from Equations (2.11) and (2.12) into the governing boundary element equation, the governing equation for linear boundary elements becomes

$$c_m p_m + \sum_{j=1}^{N} \left(\int_{\Gamma_j} \begin{bmatrix} \Phi_1 & \Phi_2 \end{bmatrix} \left[-\frac{ik}{4} H_1^{(1)}(k\vec{r}) \right] \cos\theta \, d\Gamma \right) \begin{Bmatrix} p_1 \\ p_2 \end{Bmatrix} = \sum_{j=1}^{2N} \left(\int_{\Gamma_j} \begin{bmatrix} \Phi_1 & \Phi_2 \end{bmatrix} \left[\frac{i}{4} H_o^{(1)}(k\vec{r}) \right] d\Gamma \right) \begin{Bmatrix} q_1^1 \\ q_1^2 \\ q_2^1 \\ q_2^2 \end{Bmatrix}. \qquad (2.22)$$

The right side of Equation (2.22) is summed from 1 to 2N because q is the variable of the integral. In other words, there is one q value coming into the node and one q value going out of the node. So one boundary node has two q values, one q in and one q out, as shown in Figure 2.5. The subscript on q represents the node number and the superscript represents incoming or outgoing, (1=out, 2=in). Accounting for the difference in q values, requires considerable more computational time and effort than constant elements. In Equation (2.22), note that only the Φ_1 and Φ_2 values vary with

coordinate location and the p's and q's are constant nodal values.

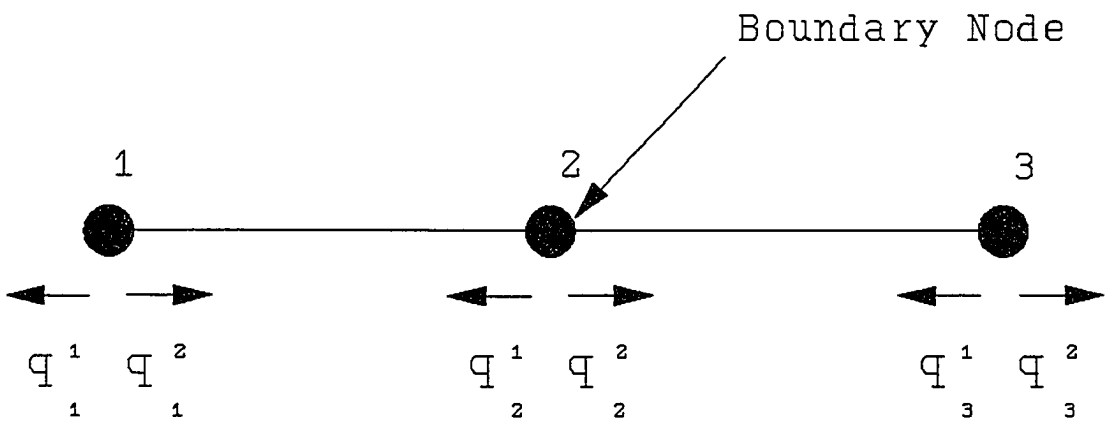

Figure 2.5 Definition of q Values for Linear Elements.

2.3 Three-Dimensional Formulation

Over the past few years, a vast amount of research has been performed on three-dimensional acoustic problems using the boundary element method. Most of the research has been in the acoustic scattering and radiation areas. More research has been done on three-dimensional domains than two-dimensional domains because two-dimensional problems involve Bessel functions and three-dimensional problems involve exponential functions. Thus integration solutions are much easier to work with in three-dimensions.

The three-dimensional formulation is very similar to the two-dimensional formulation. The same governing boundary element equation exists for three-dimensions,

$$c_m\, p_m + \sum_{j=1}^{N} \int_{\Gamma_j} q^* p \, d\Gamma = \sum_{j=1}^{N} \int_{\Gamma_j} p^* q \, d\Gamma, \qquad (2.23)$$

where the c_m value is evaluated from Equation (2.16) in the same manner as the two-dimensional analysis. Since constant elements were found to give very accurate solutions compared with linear elements, only constant elements are used in the three-dimensional analysis. Therefore, p and q can be extracted from the integrals in Equation (2.23). A three-dimensional constant element is defined by four boundary nodes and represented by a node at the center of the element as seen in Figure 2.6.

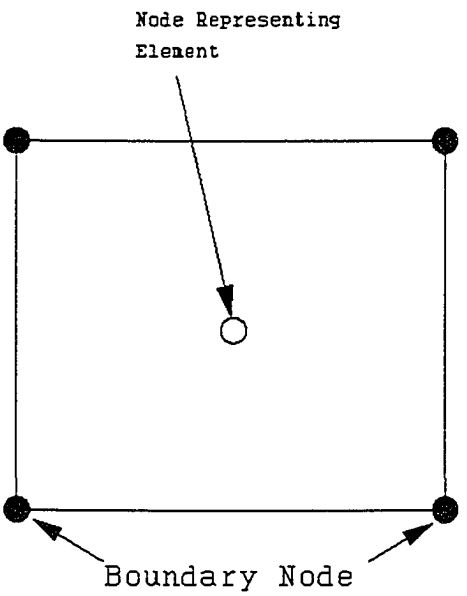

Figure 2.6 Three-Dimensional Constant Element.

The fundamental solution for three-dimensional space is

$$p^* = e^{-ik\bar{r}}/4\pi\bar{r}$$

and

$$q^* = -\frac{e^{-ik\bar{r}}}{4\pi}\left(1/\bar{r}^2 + ik/\bar{r}\right)\cos\theta. \qquad (2.24)$$

Substituting Equation (2.24) into Equation (2.23), the governing three-dimensional boundary element equation becomes

$$c_m\, p_m - \sum_{j=1}^{N}\left[\int_{\Gamma_j}\frac{e^{-ik\bar{r}}}{4\pi}\left(1/\bar{r}^2 + ik/\bar{r}\right)\cos\theta\; d\Gamma\right] p_j = \sum_{j=1}^{N}\left(\int_{\Gamma_j} e^{-ik\bar{r}}/4\pi\bar{r}\; d\Gamma\right) q_j, \qquad (2.25)$$

where the total boundary has been discretized into N elements. The values p_j and q_j have again been pulled outside the boundary integrals. Note that if linear elements were employed, the same approach as the two-dimensional case would follow with two dimensionless parameters, one in the x-direction and one in the y-direction.

2.4 System Equations and Solution Procedures

By applying the governing boundary element equation to each element, a set of equations is formed which can be represented in matrix form. The two-dimensional integrals in Equations (2.18) and (2.22) can be written as,

$$\left[\hat{H}_{mj}\right] = \int_{\Gamma_j} -\frac{ik}{4}H_1^{(1)}(k\bar{r})\cos\theta\; d\Gamma$$

and

$$[G_{mj}] = \int_{\Gamma_j} \frac{i}{4} H_o^{(1)}(k\bar{r})\, d\Gamma \qquad (2.26)$$

for constant elements, and

$$[\hat{H}_{mj}] = \int_{\Gamma_j} [\Phi_1 \ \Phi_2] \left[-\frac{ik}{4} H_1^{(1)}(k\bar{r}) \right] \cos\theta \ d\Gamma$$

and

$$[G_{mj}] = \int_{\Gamma_j} [\Phi_1 \ \Phi_2] \left[\frac{i}{4} H_o^{(1)}(k\bar{r}) \right] d\Gamma \qquad (2.27)$$

for linear elements. The subscript m represents the source element and j represents the observation boundary element. The three-dimensional integrals in Equation (2.25) can be expressed as

$$[\hat{H}_{mj}] = -\int_{\Gamma_j} \frac{e^{-ik\bar{r}}}{4\pi} \left(1/\bar{r}^2 + ik/\bar{r}\right) \cos\theta \ d\Gamma,$$

and

$$[G_{mj}] = \int_{\Gamma_j} e^{-ik\bar{r}} / 4\pi\bar{r} \ d\Gamma. \qquad (2.28)$$

From this point, the solution procedure is the same for two and three-dimensions using the appropriate $[\hat{H}_{mj}]$ and $[G_{mj}]$ matrices. Using matrix form, the governing boundary element equations can be written as

$$c_m \, p_m + [\hat{H}_{mj}]\{p_j\} = [G_{mk}]\{q_k\}. \qquad (2.29)$$

The subscript m sums from 1 to N, j sums from 1 to N and k sums from 1 to N for constant elements and from 1 to 2N for linear boundary elements.

The $c_m p_m$ term can be combined with the $[\hat{H}_{mj}]$ matrix to form a new matrix, $[H_{mj}]$, where $[H_{mj}]$ is given as

$$H_{mj} = \begin{cases} \hat{H}_{mj} + c_m & m=j \\ \hat{H}_{mj} & m \neq j \end{cases}. \tag{2.30}$$

Therefore, the system of equations in matrix form is,

$$[H]\ \{p\} = [G]\ \{q\}. \tag{2.31}$$

The matrices [H] and [G] are called the influence matrices because they relate how one element influences another. The integral expressions in the influence matrices are solved with a four-point Gauss integration scheme as shown in Appendix A. Both {p} and {q} vectors contain unknown values of p and q, respectively. For a particular element, p and/or q may be unknown. If an impedance boundary condition exists, then p and q are unknown and only the relationship between p and q is known. To solve Equation (2.31), the matrices must be transformed into a new matrix equation

$$[A]\ \{X\} = \{B\}, \tag{2.32}$$

where all of the unknown p and q values are collected in the vector {X}. The matrix [A] and the vector {B} contain complex values and hence all unknown p and q terms can be solved on the boundary. Also note that the matrix [A] is fully populated and unsymmetric. If any pressures or velocities of internal points are required, they can be found as a post processing operation only after the boundary pressures and

velocities have been calculated. The same system equation is used for determining pressure and velocity with the coordinates of the internal point and a different c_m value, substituted into Equation (2.29).

2.5 Boundary Element Singularities

Evaluating singularities is a big concern when using the boundary element method. Singularities occur when the observation point lies on the source element. Usually, the $\hat{H}_{mm}$ term does not produce any complications for smooth elements, since the normal is perpendicular to the element. When this occurs, $\hat{H}_{mm}$ equals zero due to the $\cos\theta$ term. However, the G_{mm} term almost always yields a singularity.

2.5.1 Two-Dimensional Problems

For the two-dimensional Helmholtz equation, a singularity occurs in the integral for constant elements, where the G_{mm} integral term is,

$$G_{mm}=\int_{\Gamma_m}\frac{i}{4}H_o^{(1)}(k\vec{r})\,d\Gamma=\frac{i}{4}\int_{\Gamma_m}\left(J_o(k\vec{r})+iY_o(k\vec{r})\right)d\Gamma. \qquad (2.33)$$

This study provides approximations to the singular integrals of the Bessel functions. As $\vec{r}$ approaches 0, the $Y_o(k\vec{r})$ term tends to $-\infty$. The integral in Equation (2.33) can be broken into two independent integrals,

$$G_{mm}=\frac{i}{4k}\int_0^{kl}J_o(\epsilon_o)\,d\epsilon_o+\frac{i}{4k}\int_0^{kl}Y_o(\epsilon_o)\,d\epsilon_o. \qquad (2.34)$$

A variable change was performed to help with the integration. The first integral is given by,

$$\int_0^{kl} J_o(\epsilon_o)\,d\epsilon_o = klJ_o(kl) + \frac{\pi kl}{2}\left[S_{To}(kl)J_1(kl) - S_{T1}(kl)J_o(kl)\right], \qquad (2.35)$$

where S_{T0} and S_{T1} are the Struve Functions and l is the length of the element. The second integral is expressed as,

$$\int_0^{kl} Y_o(\epsilon_o)\,d\epsilon_o = klY_o(kl) + \frac{\pi kl}{2}\left[S_{To}(kl)Y_1(kl) - S_{T1}(kl)Y_o(kl)\right], \qquad (2.36)$$

where the exact integration above is given in [66].

For linear elements, the G_{mm} term also produces a singularity. The G_{mm} integral term is,

$$G_{mm} = \int_{\Gamma_j} \Phi_1 \frac{i}{4} H_o^{(1)}(k\bar{r})\,d\Gamma = \frac{i}{8}\int_{\Gamma_j} (1-\epsilon_o)\left[J_o(k\bar{r}) + iY_o(k\bar{r})\right]d\Gamma. \qquad (2.37)$$

By changing the coordinate system from $\bar{r}$ to β_o, the initial integral is broken into four minor integrals,

$$G_{mm} = \frac{i}{8k}\int_0^{kl} \left[2J_o(\beta_o) + 2iY_o(\beta_o) - \frac{2\beta_o}{kl}J_o(\beta_o) - \frac{2\beta_o i}{kl}Y_o(\beta_o)\right]d\beta_o. \qquad (2.38)$$

The first two integrals in Equation (2.38) are solved using Equations (2.35) and (2.36), respectively. The third integral is solved with the identity,

$$\int_0^{kl} \beta_o J_o(\beta_o)\,d\beta_o = klJ_1(kl), \qquad (2.39)$$

and the fourth integral is solved by,

$$\int_0^{kl} \beta_o Y_o(\beta_o)\, d\beta_o = klY_1(kl) + \frac{2\Gamma_f(1)}{\pi}, \qquad (2.40)$$

where Γ_f is the Gamma function. A small error is produced in the G_{mm} terms, because the Struve functions are calculated by a series expansion approximation. The complete definitions and approximations of the Struve functions are given in Appendix A. Since the two-dimensional singularities are such a problem, many authors did not address two-dimensional acoustic problems. Working through the singularities is a difficult obstacle to overcome when using the boundary element method.

2.5.2 Three-Dimensional Problems

As with two-dimensional solutions, the $\hat{H}_{mm}$ term is zero due to the $\cos\theta$ term. However, the G_{mm} integral term gives a singularity because $\vec{r}$ is zero in the equation

$$G_{mm} = \frac{1}{4\pi} \int_x \int_y e^{-ik\vec{r}}/\vec{r}\, dxdy. \qquad (2.41)$$

The singularity can be removed by changing to polar coordinates and thus

$$G_{mm} = \frac{1}{2} \int_0^{R_o} e^{-ik\vec{r}}\, d\vec{r}. \qquad (2.42)$$

Chertock developed an approach that can easily solve the singularity problem in the [G] influence matrix [70]. Chertock's approach finds the radius R_o, of a circular element

that integrates over the same area as a rectangular element. Assuming that AR is the area of the m^{th} element, the singular integral becomes

$$G_{mm}=\frac{i}{2k}\left(e^{-ik\sqrt{AR/\pi}}-1\right). \qquad (2.43)$$

Thus, the singularity in the three-dimensional boundary element equation is easily removed.

Chapter 3

SOUND AND STRUCTURE INTERACTION

Over the past few years, the study of sound- structure interaction has received increased attention. The aircraft and automobile industries have rigorously studied sound-structure interaction effects. Currently the automobile industry is pursuing methods to model NVH (Noise, Vibration and Harshness) environments. Some components that have been modelled in the automotive industry include: carburetor manifolds, transmission housings, and tire/hub systems. The most popular and most effective coupling method employed for the study of their problems is the coupled boundary and finite element methods. In industry, most boundary element codes are written in-house, while most finite element codes are commercial programs. The most common finite element programs in use today are NASTRAN, ABAQUS, IDEAS, ANSYS, and ALGOR. SYSNOISE was the first program that coupled basic finite and boundary element analyses. In 1994, the COMET/BEA programming system was introduced into industry. This program couples the finite and boundary element methods in an attempt to model NVH

environments. Currently, composite laminates and random excitation can not be analyzed using the COMET/BEA system.

This chapter introduces the governing equations for the coupled boundary and finite element methods. Coupled BEM-FEM results are then compared with existing experimental data for a well-known cavity-backed plate problem in Chapter 4. Coupled BEM-FEM formulation for plates of composite materials is introduced and transmission loss characteristics are studied. Random response analysis of the structural and acoustic domains is also presented.

3.1 Acoustic Formulation (BEM)

In order to couple the boundary element method with the finite element method, the governing equations for the acoustic domain are slightly modified. The governing equations, representing the acoustic domain, for two and three-dimensions are the same. Only the influence matrices, in Equation (2.31), change as a result of the dimensionality of the problem. In this study, only three-dimensional systems are coupled. The acoustic domain is governed by the wave equation as shown in Equation (2.4). By assuming the time dependance as $e^{i\omega t}$, the wave equation reduces to the Helmholtz equation as seen in Equation (2.7). On applying the boundary element method over the domain, the governing equation in matrix form becomes

$$[H]\{p\} = [G]\{\frac{\partial p}{\partial n}\}. \qquad (3.1)$$

The elements of the influence matrices, [H] and [G], are given in Equation (2.28). The [H] and [G] matrices represent the transfer function of the acoustics and they are functions of the input frequency, ω, and the distance vector, $\vec{r}$. At the acoustic boundary, the normal derivative of pressure is related to the acoustic particle acceleration, velocity and displacement by

$$\frac{\partial p}{\partial n} = -\rho_a \frac{\partial^2 u_a}{\partial t^2} = -i\rho_a \omega \frac{\partial u_a}{\partial t} = \rho_a \omega^2 u_a, \qquad (3.2)$$

where u_a is the acoustic particle displacement at the boundary. This boundary condition can be easily derived using the continuity equation. On substituting Equation (3.2) into Equation (3.1), we get

$$[H]\{p\} = \rho_a \omega^2 [G]\{u_a\}. \qquad (3.3)$$

Equation (3.3) represents the boundary element method governing equation for the acoustic domain. Equation (3.3) is applied only on the acoustic boundary of the duct system and thus, Equation (3.3) can be modified to couple with the finite element method.

3.2 Structure Formulation (FEM)

The finite element method has become a very powerful tool in analyzing static and dynamic response of structures. The

finite element method is capable of handling complex structural analysis. The objective here is to model the plate or structure and obtain pertinent linear theory information needed to couple with the boundary element method.

3.2.1 Finite Element Specifications

Many rectangular and triangular type finite elements are currently being used in commercial and in-house codes. Any type of finite element can be applied to the following formulation. The element selected for this study is a four-node rectangular element and is shown in Figure 3.1 [67]. The characteristics of the element are given in Appendix B. The element displacement functions for the transverse and in-plane directions are

$$w_b = [H_w]\{\alpha\}, \tag{3.4}$$

and

$$u = [H_u]\{\beta\}$$

$$v = [H_v]\{\beta\}. \tag{3.5}$$

The shape functions, $[H_w]$, $[H_u]$ and $[H_v]$, and the generalized coordinates, α and β, for the rectangular element are also shown in Appendix B. The generalized coordinates are related to the element bending and membrane nodal displacements through

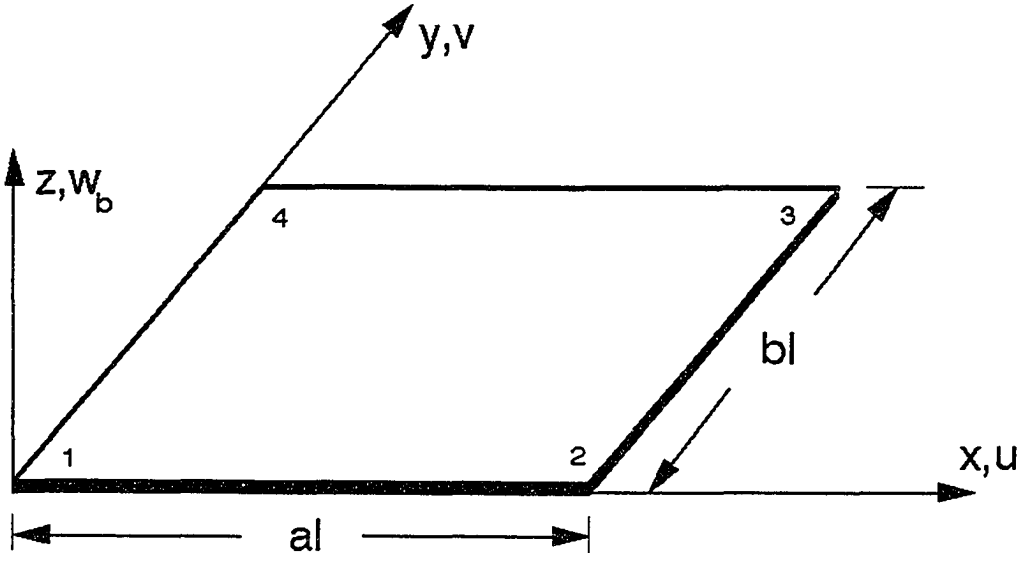

Figure 3.1 Finite Element Rectangular Plate Element.

$$\{\alpha\}=[T_b]\{W_b\}$$
$$\{\beta\}=[T_m]\{W_m\}, \tag{3.6}$$

where the transformation matrices, $[T_m]$ and $[T_b]$, are functions of the element lengths, al and bl. The transformation matrices are given in Appendix B along with the definition of the degrees of freedom in bending and membrane for the plate element.

3.2.2 Strain-Displacement and Stress-Strain Relations

The linear relationship between the strain and displacement is given as

$$\{\epsilon\}=\{\epsilon_m\}+z_o\{\kappa\}, \tag{3.7}$$

where $\{\epsilon_m\}$ is the membrane strain, $\{\kappa\}$ is the curvature, and z_o is the distance from the mid-surface. The curvature and the membrane strain are given by

$$\{\kappa\}=\begin{Bmatrix} -w_{,xx} \\ -w_{,yy} \\ -2w_{,xy} \end{Bmatrix}=\begin{bmatrix} -H_{w,xx} \\ -H_{w,yy} \\ -2H_{w,xy} \end{bmatrix}\{\alpha\}=[C_b]\{\alpha\}, \tag{3.8}$$

and

$$\{\epsilon_m\}=\begin{Bmatrix} u_{,x} \\ v_{,y} \\ u_{,y}+v_{,x} \end{Bmatrix}=\begin{bmatrix} H_{u,x} \\ H_{v,y} \\ H_{u,y}+H_{v,x} \end{bmatrix}\{\beta\}=[C_m]\{\beta\}, \tag{3.9}$$

where the subscripts b and m denote bending and membrane, respectively. The matrices, $[C_b]$ and $[C_m]$, are functions of x and y and are given in Appendix B.

The linear stress-strain relations for a composite layer are given by

$$\begin{Bmatrix} \sigma_1 \\ \sigma_2 \\ \tau_{12} \end{Bmatrix} = \begin{bmatrix} Q_{11} & Q_{12} & 0 \\ Q_{21} & Q_{22} & 0 \\ 0 & 0 & Q_{66} \end{bmatrix} \begin{Bmatrix} \epsilon_1 \\ \epsilon_2 \\ \gamma_{12} \end{Bmatrix}, \tag{3.10}$$

where the subscript 1 represents the direction of the fibers and subscript 2 represents the direction normal to the axis of the fibers. The Q_{ij}, (i,j=1,2,6), components are calculated with E_{11}, E_{22}, G_{12}, υ_{12} and υ_{21}. If the lamination angle, ϕ, is changed, the stress-strain relations for the kth layer becomes

$$\begin{Bmatrix} \sigma_x \\ \sigma_y \\ \tau_{xy} \end{Bmatrix}_k = \begin{bmatrix} \bar{Q}_{11} & \bar{Q}_{12} & \bar{Q}_{16} \\ \bar{Q}_{21} & \bar{Q}_{22} & \bar{Q}_{26} \\ \bar{Q}_{61} & \bar{Q}_{62} & \bar{Q}_{66} \end{bmatrix}_k \begin{Bmatrix} \epsilon_x \\ \epsilon_y \\ \gamma_{xy} \end{Bmatrix}. \tag{3.11}$$

where $[\bar{Q}]$ is the transformed stiffness matrix. Derivation of [Q] and $[\bar{Q}]$ is given in detail in Appendix B. The stress components of the kth layer are given by

$$\{\sigma\}_k = [\bar{Q}]_k (\{\epsilon_m\} + z_o\{\kappa\}), \tag{3.12}$$

which are substituted into the stress resultant expression,

$$(\{N\}, \{M_b\}) = \int_{-\frac{h}{2}}^{\frac{h}{2}} \{\sigma\}_k (1, z_o)\, dz_o. \tag{3.13}$$

This produces the constitutive relations for the forces and moments of a composite laminate as

$$\begin{Bmatrix} N \\ M_b \end{Bmatrix} = \begin{bmatrix} A & B \\ B & D \end{bmatrix} \begin{Bmatrix} \epsilon_m \\ \kappa \end{Bmatrix}. \tag{3.14}$$

where the [A], [B], and [D] laminate stiffness matrices are developed from

$$([A],[B],[D]) = \int_{-\frac{h}{2}}^{\frac{h}{2}} [\bar{Q}]_k (1, z_o, z_o^2)\, dz_o. \tag{3.15}$$

3.2.3 Derivation of Equations of Motion

The equations of motion of the plate structure are derived using the principle of virtual work. The principle of virtual work states that the net work done by a system in an equilibrium state under a virtual displacement tends to zero. The virtual work definition
is

$$\delta W = \delta W_{int} - \delta W_{ext} = 0. \tag{3.16}$$

The virtual work of the internal forces is

$$\delta W_{int} = \int_A (\{\delta \epsilon_m\}^T \{N\} + \{\delta \kappa\}^T \{M_b\})\, dA, \tag{3.17}$$

where the forces {N}, and the moments $\{M_b\}$, are given in Equation (3.14).

The total external virtual work is

$$\delta W_{ext} = \int_A -\rho h (\ddot{u}\delta u + \ddot{v}\delta v + \ddot{w}_b \delta w_b)\, dA + \int_A p(x,y,t)\, \delta w_b \, dA, \qquad (3.18)$$

where δu, δv, and δw_b are the infinitesimal virtual displacements. The pressure loading, p(x,y,t), in Equation (3.18) represents the combination of the external pressure and the acoustic pressure. The virtual strain and virtual curvature in Equation (3.17) are given as

$$\begin{aligned} \{\delta \epsilon_m\} &= \delta\{[C_m]\{\beta\}\} \\ &= [C_m]\{\delta\beta\}. \end{aligned} \qquad (3.19)$$

and

$$\begin{aligned} \{\delta \kappa\} &= \delta\{[C_b]\{\alpha\}\} \\ &= [C_b]\{\delta\alpha\}. \end{aligned} \qquad (3.20)$$

Substituting Equations (3.14), (3.19), and (3.20) into Equation (3.17), we get

$$\begin{aligned} \delta W_{int} = \int_A (&\{\delta\beta\}^T [C_m]^T ([A]\{\epsilon_m\} + [B]\{\kappa\}) \\ &+ \{\delta\alpha\}^T [C_b]^T ([B]\{\epsilon_m\} + [D]\{\kappa\}))\, dA. \end{aligned} \qquad (3.21)$$

Substituting Equations (3.8) and (3.9) into Equation (3.21), we get

$$\delta W_{int}=\int_A (\{\delta\beta\}^T[C_m]^T[A][C_m]\{\beta\} + \{\delta\beta\}^T[C_m]^T[B][C_b]\{\alpha\} + \{\delta\alpha\}^T[C_b]^T[B][C_m]\{\beta\} + \{\delta\alpha\}^T[C_b]^T[D][C_b]\{\alpha\})dA. \quad (3.22)$$

Equation (3.22) can be written in terms of the membrane and bending deflections, and the linear stiffness terms as

$$\delta W_{int}=\{\delta w_m\}^T[k_m]\{w_m\}+\{\delta w_b\}^T[k_b]\{w_b\} + \{\delta w_m\}^T[k_{mb}]\{w_b\}+\{\delta w_b\}^T[k_{bm}]\{w_m\}. \quad (3.23)$$

The linear membrane and bending stiffness matrices in Equation (3.23) are given as

$$[k_m]=[T_m]^T\int_A [C_m]^T[A][C_m]dA[T_m], \quad (3.24)$$

and

$$[k_b]=[T_b]^T\int_A [C_b]^T[D][C_b]dA[T_b]. \quad (3.25)$$

The linear coupled stiffness matrices are given by

$$[k_{mb}]=[k_{bm}]^T=[T_m]^T\int_A [C_m]^T[B][C_b]dA[T_b]. \quad (3.26)$$

The in-plane and transverse contributions to the external virtual work is given by Equation (3.18). Replacing u, v, and w_b with their approximations, and the external virtual work can be expressed as

$$\delta W_{ext} = -\int_A (\{\delta w_m\}^T [T_m]^T [H_u]^T \rho h [H_u] [T_m] \{\ddot{w}_m\} + \{\delta w_m\}^T [T_m]^T [H_v]^T \rho h [H_v] [T_m] \{\ddot{w}_m\} + \{\delta w_b\}^T [T_b]^T [H_w]^T \rho h [H_w] [T_b] \{\ddot{w}_b\}) \, dA + \{\delta w_b\}^T \{p_b(t)\}$$

$$= -\{\delta w_m\}^T ([m_{um}] + [m_{vm}]) \{\ddot{w}_m\} - \{\delta w_b\}^T [m_b] \{\ddot{w}_b\} + \{\delta w_b\}^T \{p_b(t)\}. \quad (3.27)$$

Substituting the expressions for the external and internal work, Equations (3.23) and (3.27), into the principle of virtual work equilibrium relation, Equation (3.16), we obtain the elemental equations of motion

$$[m]\{\ddot{w}\} + [k_{el}]\{w\} = \{p_b(t)\}. \quad (3.28)$$

The linear element mass and stiffness matrices from Equation (3.28) are represented as

$$[m] = \begin{bmatrix} m_b & 0 \\ 0 & m_m \end{bmatrix} \quad (3.29)$$

and

$$[k_{el}] = \begin{bmatrix} k_b & k_{bm} \\ k_{mb} & k_m \end{bmatrix}. \quad (3.30)$$

The load vector, $p_b(t)$, represents the bending load as

$$\{p_b(t)\} = [T_b]^T \int_A p(x,y,t) \{H_w\} dA. \quad (3.31)$$

3.2.4 Global Equations and Solution Procedure

Applying the elemental equation of motion for each element and summing each element's contribution, we obtain the global equation of motion as

$$[M]\{\ddot{W}\}+[K]\{W\}=\{F_T\}. \tag{3.32}$$

Assuming that the time dependance of the plate response is $e^{i\omega t}$, the free vibration problem can be reduced to

$$[K]\{\Phi\}_n=\omega_n^2[M]\{\Phi\}_n. \tag{3.33}$$

Equation (3.33) can now be solved for the natural frequencies ω_n and the normal mode shapes Φ_n for the structure. These frequencies and mode shapes are used to define the structural response function. The response function is then used to couple with the boundary element method.

The damping effects are now added to the structural system as

$$[M]\{\ddot{W}\}+[C]\{\dot{W}\}+[K]\{W\}=\{F_T\}. \tag{3.34}$$

The damping matrix [C] can be experimentally determined or assumed as proportional damping.

A modal transformation is now applied with

$$\{W\}=\begin{Bmatrix} W_b \\ W_m \end{Bmatrix}=\left[\{\Phi\}_1\cdots\{\Phi\}_n\cdots\right]\{d\}=[\Phi]\{d\}, \tag{3.35}$$

where {d} are the modal displacements and [Φ] is the modal matrix. This modal reduction allows the system to be reduced to a fixed number of modes. All analyses in this study was

done using ten modes for the modal reduction. Ten modes were selected to make sure all dominant modes were analyzed. The structural equation of motion, Equation (3.34), can now be expressed in modal coordinates as

$$\ddot{d}_n+2\zeta_n\omega_n\dot{d}_n+\omega_n^2 d_n=\frac{\{\Phi\}_n^T\{F_T\}}{M_n}, \tag{3.36}$$

where M_n and ζ_n are the modal mass and the damping ratio, respectively. From Equation (3.36), a response function is easily derived as

$$(H_s)_n=\frac{1}{M_n(\omega_n^2-\omega^2+2i\zeta_n\omega_n\omega)}. \tag{3.37}$$

Using the structural response function, the structural governing equation becomes

$$[H_s]\{d\}=[\Phi]^T\{F_T\}, \tag{3.38}$$

where the subscript s represents the structural response. The subscript used in Equation (3.37) is to distinguish the structural response from the influence matrix in Equation (2.31). The modal load vector can be separated into external forces and the forces applied by the acoustic pressure. Therefore, the governing equation becomes

$$[H_s]\{d\}=[\Phi]^T\{F_p\}+[\Phi]^T\{F_e\}, \tag{3.39}$$

where $\{F_p\}$ is the acoustic force and $\{F_e\}$ is the external or input force. The acoustic force vector $[\Phi]^T\{F_p\}$, is transformed from the boundary element system to the finite

element system as shown in Figure 3.2. A transformation matrix [LT], is created from the [Φ] matrix, and is used to transfer the acoustic loads from the center of the boundary element to the nodes of the finite element or vice versa. The [LT] matrix arises due to the difference in the definition of the element types. The boundary element is represented by a node in the center of the element, whereas the finite element is represented by its corner nodes. The [LT] matrix performs two tasks simultaneously; it performs the modal reduction and the element transformation. Rewriting Equation (3.39) with the load transformation matrix, we get

$$[H_s]\{d\}=[LT]^T\{F_p\}+[\Phi]^T\{F_e\}. \qquad (3.40)$$

Equation (3.40) is the final form of the governing equation for the linear finite element method for the structure.

3.3 Coupling System Equations and Solution Procedures For Harmonic Response

The structure and acoustic domains have been modelled using finite and boundary elements. Equation (3.3) is the governing boundary element equation for the acoustic domain and Equation (3.40) represents the finite element formulation of the structure. A coupled plate/cavity problem, is shown in Figure 3.3 to assist in the physical interpretation. The acoustic force F_p and the external force F_e are also shown in Figure 3.3. The acoustic domain and the structural domain are spatially separated. Coupling the two initially independent

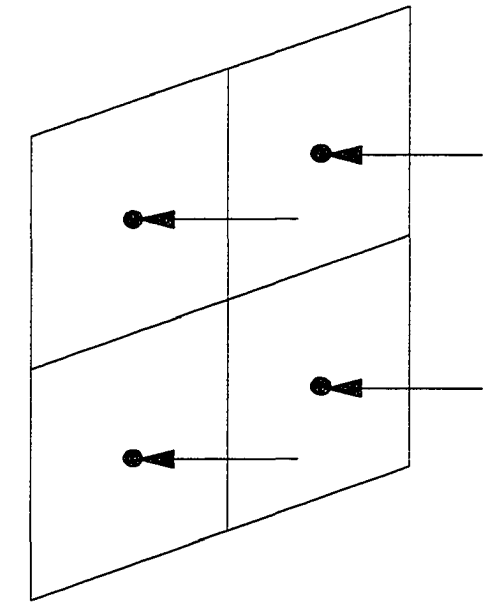

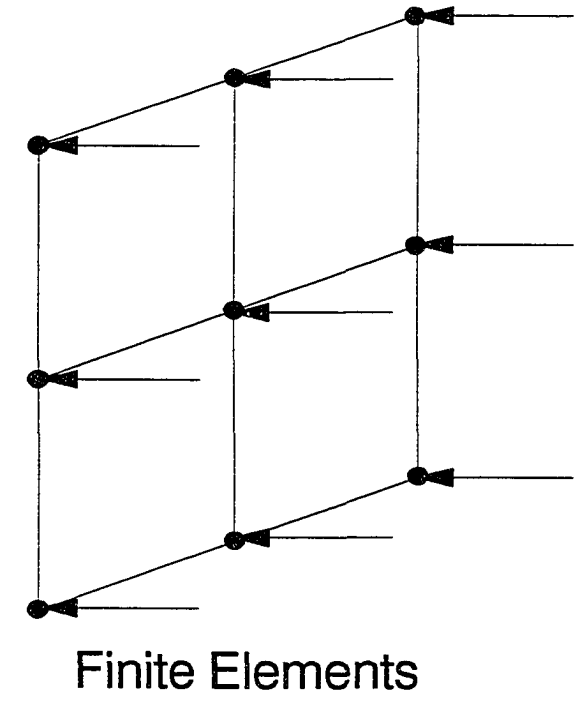

Figure 3.2 Definition of Transformation Matrix [LT] Between Finite and Boundary Elements.

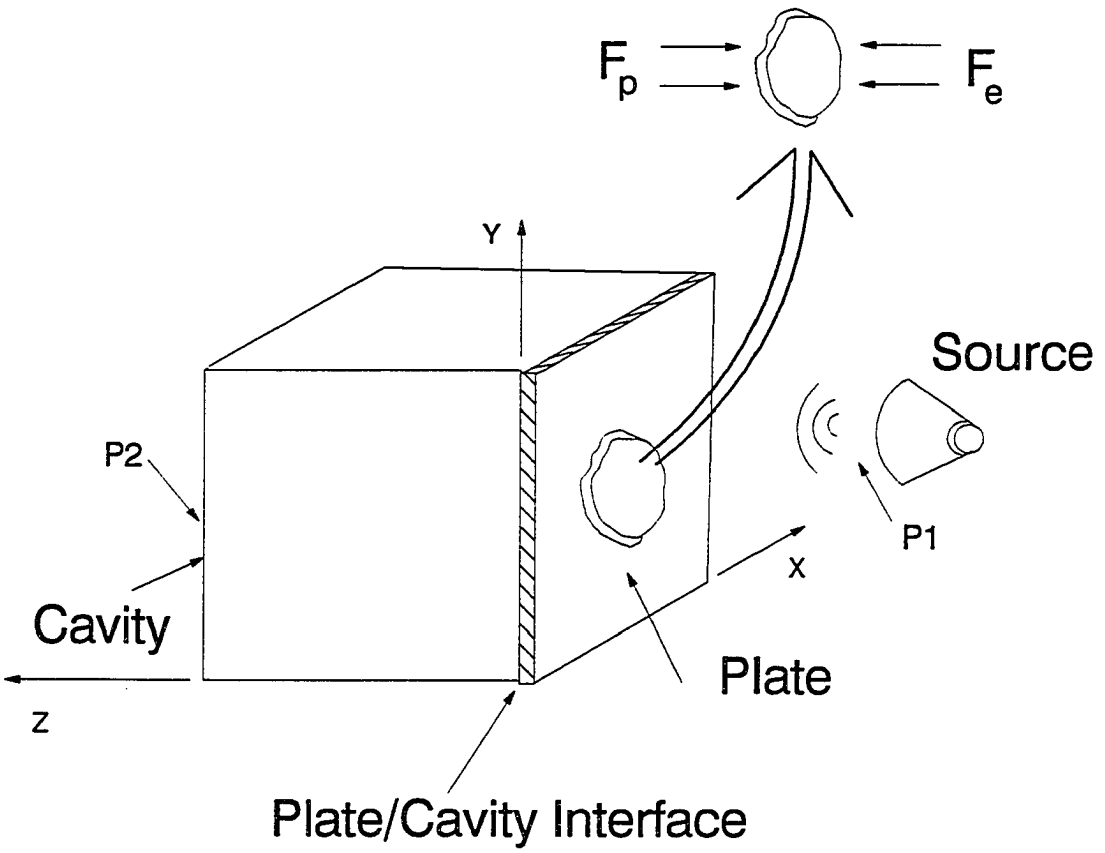

Figure 3.3 Coupled Plate/Cavity System.

systems takes place in terms of compatibility conditions across the interface of the plate and the acoustic domain. When the compatibility of displacements and forces applied at the interface are enforced, the two systems become coupled.

Applying the displacement compatibility over the interior plate surface requires that the acoustic displacement equals the out-of-plane plate displacement as

$$\{W_b\}=\{u_a\}=[LT]\{d\}, \tag{3.41}$$

which has been related to the modal displacement {d}. The definition relation of the out-of-plane displacement is seen as,

$$\{W\}=\begin{Bmatrix} W_b \\ W_m \end{Bmatrix}=\begin{bmatrix} \Phi_b \\ \Phi_m \end{bmatrix}\{d\}. \tag{3.42}$$

The force compatibility equation represents the force from the acoustic pressure as an additional force $\{F_p\}$, as seen in Equation (3.40). Assuming that the acoustic pressure is uniform over each plate element, the acoustic force vector, from Equation (3.40), may be represented as

$$[LT]^T\{F_p\}=[LT]^T[S_A]\{p_{act}\}, \tag{3.43}$$

where $\{p_{act}\}$ is the global acoustic pressure vector represented at the center of the boundary element. The diagonal matrix $[S_A]$, is composed of the elemental areas of each interface element.

The external force vector from Equation (3.40) may also be expressed in terms of pressure as

$$[\Phi]^T\{F_e\} = -[\Phi]^T\{P_b(t)\} = -p_{IN}[\Phi]^T\{P_{b1}(t)\} = -p_{IN}\{f_{mod}\}, \tag{3.44}$$

where $\{p_{IN}\}$ is the constant input pressure vector and $\{f_{mod}\}$ represents the modal force vector. The vector $\{P_b(t)\}$, is the global finite element force vector, which is composed of the contribution of the element forces $p_b(t)$, from Equation (3.27). The value p_{IN} has been pulled from $\{P_b(t)\}$ in Equation (3.44), since uniform pressure loads are assumed. In all transmission loss calculations, a unit input pressure vector is assumed. The acoustic and structure system can now be coupled, using Equations (3.3), (3.40), (3.41), (3.43) and (3.44). In matrix form, the coupled system is given as

$$\begin{bmatrix} [H] & -\rho_a\omega^2[G][LT] \\ -[LT]^T[S_A] & [H_s] \end{bmatrix} \begin{Bmatrix} p_{act} \\ d \end{Bmatrix} = \begin{Bmatrix} 0 \\ \{f_{mod}\} \end{Bmatrix}. \tag{3.45}$$

Equation (3.45) can now be solved for all acoustic pressures and modal displacements. The global pressure vector $\{p_{act}\}$, encompasses all pressures from the entire acoustic boundary. For instance, if the acoustic boundary is discretized into 150 boundary elements and the plate into 25 finite elements, the pressure vector $\{p_{act}\}$, contains all 150 acoustic pressures. Only the first 25 pressures are coupled with the plate system. Note that this system is only a function of frequency. After

solving for the acoustic boundary pressures and the modal displacements, a variety of other data becomes readily available. From Equation (3.35), the element plate velocities can easily be calculated. Using the boundary pressures $\{p_{act}\}$ as boundary conditions, any interior acoustic pressures or velocities can be calculated from Equation (3.3).

The importance of coupling the acoustic and structural domain will be shown in Chapter 4. In order to accurately model aerospace and automotive vehicle environments, coupled systems must be considered. This study is a step towards improving the modelling of such complicated environments.

3.4 Coupling System Equations and Solution Procedures For Random Response

The majority of real world systems involve random loading and random response. As stated in the introduction, this study is an attempt to accurately model structures in complex environments for aerospace and automobile industries. In order to satisfy this criteria, the previous harmonic analysis is now modified to include random loading and response. The goal of this section is to analyze the previously selected problem and model it with linear random analysis. The random response of the coupled plate/cavity system will be compared with the random response of the plate structure only. Therefore, a brief introduction of the random response of composite panels is now given.

3.4.1 Random Response of Plate Structure

The governing finite element equation for the linear plate structure is given in Equation (3.34). A standard eigenvalue/eigenvector solver is applied with the global mass and stiffness matrices and the natural frequencies and mode shapes can be calculated. The modal equation has been given in Equation (3.36). The spectral density of the plate response is given by

$$\left(S_d(\omega)\right)_n = |H_s(\omega)|_n^2 \, S_{IN}(\omega), \tag{3.46}$$

where

$$(H_s(\omega))_n = \frac{1}{M_n(\omega_n^2 - \omega^2 + 2i\zeta_n\omega_n\omega)}. \tag{3.47}$$

The $S_{IN}(\omega)$ value is the input spectral density of the external excitation P_b, from Equation (3.44). Equation (3.46) holds only for linear random analysis. From the definition of spectral density, the mean square response of the modal displacement can be written as

$$E(d_n^2) = S_p(\omega)\,(f_{\text{mod}})_n^2 \int_{-\infty}^{\infty} |H_s(\omega)|_n^2 \, d\omega, \tag{3.48}$$

or

$$E(d_n^2) = \frac{\pi S_p(\omega)\,(f_{\text{mod}})_n^2}{4\zeta_n M_n^2 \omega_n^3}. \tag{3.49}$$

The input spectral density is assumed as white noise and

$$S_p(\omega) = 8.4216 \times 10^{(SSL \times .1 - 18.0)}, \qquad (3.50)$$

where SSL is the input sound pressure level in dB. The mean square of the modal displacement can be related to the mean square of the displacement by

$$E[\{W\}\{W\}^T] = [\Phi] E[\{d\}\{d\}^T][\Phi]^T, \qquad (3.51)$$

where $[\Phi]$ is the modal matrix [67]. Since the terms $E[d_n d_j]$ $(n \neq j)$ are at least two orders of magnitude smaller than $E[d_n^2]$ $(n=j)$, all cross-correlation terms, $E[d_n d_j]$ $(n \neq j)$, are set to zero. Therefore, Equation (3.51) reduces to

$$E(W_n^2) = \sum_{j=1}^{\#of\ modes} \Phi_{nj}^2 \, E(d_j^2) . \qquad (3.52)$$

From Equation (3.52), the maximum root mean square (RMS) deflection can be calculated and the results can be compared with those from the coupled analysis results. A detailed derivation of the random response of plate structures can be found in [67] and [68].

3.4.2 Random Response of Coupled Structural-Acoustic System

The random response of the acoustic domain is formulated from the wave equation [68]. A classical continuum approach is used to relate the acoustic pressure and the modal displacement through a transfer function. The fundamental pressure response of the acoustic domain can be written as

$$P(x,y,z,t) = H_{pact}(x,y,z,\omega)u_a(t), \tag{3.53}$$

where H_{pact} is the acoustic transfer function. In other words, the acoustic pressure at any location in the duct can be related to the acoustic displacement through the acoustic transfer function. In order to find the acoustic transfer function, u_a is set to $1e^{i\omega t}$. Substituting Equation (3.53) into the three-dimensional wave equation, we get

$$\nabla^2 H_{pact} + k^2 H_{pact} = 0, \tag{3.54}$$

where k is the acoustic wavenumber and u_a represents a unit harmonic response. The boundary conditions for Equation (3.54) for the coupled system in Figure (3.3) are

$$\begin{aligned} \frac{\partial H_{pact}}{\partial n} &= 0 && \textit{on a rigid wall} \\ \frac{\partial H_{pact}}{\partial n} &= -\rho_a \omega^2 u_a && \textit{for a displacement at the interface.} \end{aligned} \tag{3.55}$$

To find the transfer function H_{pact}, the displacement vector is set to unity. Equation (3.54) can be applied to the acoustic domain utilizing the boundary element method, as

$$[H]\{H_{pact}\} = [G]\{\frac{\partial H_{pact}}{\partial n}\}. \tag{3.56}$$

An expression for the acoustic transfer function can be obtained by

$$\{H_{pact}\} = [H]^{-1}[G][LT]\{-\rho_a\omega^2\} = \{C_c\}, \qquad (3.57)$$

where the [G] matrix has been modified to account for only the vibrating wall of the duct and the element transformation has taken place through Equation (3.41).

By applying the boundary element method, a set of equations is created where $\{H_{pact}\}$ is now only a function of frequency and not space (x, y and z). The boundary conditions for the acoustic domain, Equation (3.55), have been applied to Equation (3.56), which yields a solution for the acoustic transfer function, $\{H_{pact}\}$. The vector $\{H_{pact}\}$ represents the acoustic transfer function for each boundary element due to a unit displacement at the structure. For linear random analysis, the spectral density of the pressure response can be related to the input spectral density by

$$\begin{aligned}\{S_{pact}(\omega)\} &= \{H_{pact}(\omega)\}\{H_{pact}(-\omega)\}^T\{S_d(\omega)\} \\ &= \{C_c(\omega)\}\{C_c(-\omega)\}^T\{S_d(\omega)\}.\end{aligned} \qquad (3.58)$$

Equation (3.58) is used to model the random response of the acoustic domain and it relates the spectral density of the acoustic pressure to the spectral density of the input acoustic displacement.

The structural system can be modelled through Equation (3.46), taking into account the acoustic spectral density and the input force or external force spectral density. Assuming that the input force spectral density is a constant white noise input and that the spectral density of the acoustic

pressure is also constant over each element, Equation (3.46) reduces to

$$\left(S_d(\omega)\right)_n = |H_s(\omega)|_n^2 S_p(\omega)\,(f_{\mathrm{mod}})_n^2 - |H_s(\omega)|_n^2 \sum_{j=1}^{NPEL} (LT_{jn}^2)\,(S_{pact}(\omega))_j, \tag{3.59}$$

where NPEL is the number of plate elements. In order to transfer Equation (3.59) to matrix form, we write

$$[LOAD] = \sum_{n=1}^{\#\ of\ modes} \sum_{j=1}^{NPEL} (LT_{jn}^2). \tag{3.60}$$

The coupled system can now be modelled using Equations (3.58), (3.59) and (3.60) as

$$\begin{bmatrix} I & -\{C_c(\omega)\}\{C_c(-\omega)\}^T \\ [LOAD]\,|H_s(\omega)|^2 & I \end{bmatrix} \begin{Bmatrix} S_{pact}(\omega) \\ S_d(\omega) \end{Bmatrix} = \begin{Bmatrix} 0 \\ S_p(\omega)\,\{f_{\mathrm{mod}}^2\}\,|H_s(\omega)|^2 \end{Bmatrix}, \tag{3.61}$$

where [I] is the identity matrix. Equation (3.61) couples the spectral densities of the plate\cavity system in the frequency domain. The unknowns in Equation (3.61) are the acoustic pressure spectral densities, $\{S_{pact}\}$, for each acoustic boundary element and the structure modal displacement spectral densities, $\{S_d\}$.

For simplicity, Equation (3.61) can be written as

$$[CPLG(\omega)]\ \{SD(\omega)\} = \{SD_{IN}(\omega)\}, \qquad (3.62)$$

where SD(ω) represents the unknown spectral densities from Equation (3.61). The matrix [CPLG(ω)] represents the total coupling matrix in Equation (3.61). Multiplying both sides of Equation (3.62) by the inverse of [CPLG] and integrating over the derived frequency range, ($-\omega_c<\omega<\omega_c$), we get

$$\begin{Bmatrix} E[p_{act}^2] \\ E[d^2] \end{Bmatrix} = \int_{-\omega_c}^{\omega_c} \{SD(\omega)\} d\omega = \int_{-\omega_c}^{\omega_c} [CPLG(\omega)]^{-1} \{SD_{IN}(\omega)\} d\omega. \qquad (3.63)$$

The integral in Equation (3.63) can be solved using a simple trapezoidal approximation. After applying the integration in Equation (3.63), the mean square response of the modal displacement and the acoustic pressure can be readily calculated.

Chapter 4

NUMERICAL RESULTS

In this chapter we present the results of the previous formulation and also provide some additional discussion. The results section has been subdivided into three sub-sections: acoustic results, coupled BEM-FEM results, and analysis of panels in the Thermal Acoustic Fatigue Apparatus (TAFA) at NASA Langley Research Center. The purpose of this chapter is to show that the boundary element method is a powerful numerical technique that can be used to solve a wide range of acoustic problems. The coupling of the boundary element and finite element methods, leads to a powerful tool that can be readily used to analyze structural-acoustic problems.

4.1 Acoustic Duct Results

The boundary element method has become a preferred method when modelling acoustic domains. BEM has advantages such as: reduction of discretized dimensionality of the domain, implementation of infinite domains, and shorter computation time. Here we will analyze two and three-dimensional interior acoustic domains.

4.1.1 Two-Dimensional Interior Domain Analysis

Due to the symmetry of structures, a two-dimensional analysis can be performed to save time and calculations. Very little work has been done in the study of 2-D acoustic fields using the boundary element method due to difficulties associated with singular Bessel functions. Therefore, some acoustic field problems with exact solutions are selected to see how well the boundary element method can approximate these solutions. Some very useful information is learned about the number of elements required to solve problems and the limits on the wavenumber for accurate results.

The first problem is a simple rectangular duct with an open outlet. The geometry is shown in Figure 4.1, and the boundary conditions are given as follows:

$$\begin{aligned} &\frac{\partial p}{\partial n}=0 \text{ at } y=0 \text{ and } 1m \\ &p=1 \text{ at } x=0m \\ &p=0 \text{ at } x=6m. \end{aligned} \tag{4.1}$$

The duct length is set at 6 meters and the wavenumber k, is 1. The exact solution is

$$p(x)=\frac{\sin k(L-x)}{\sin kL}, \tag{4.2}$$

where the pressure p(x) only depends on the x coordinate since a plane wave solution is assumed. The pressure along the boundary is calculated versus the x-distance. The comparison between constant and linear boundary elements with the exact solution is shown in Figure 4.2. Eighty boundary elements are

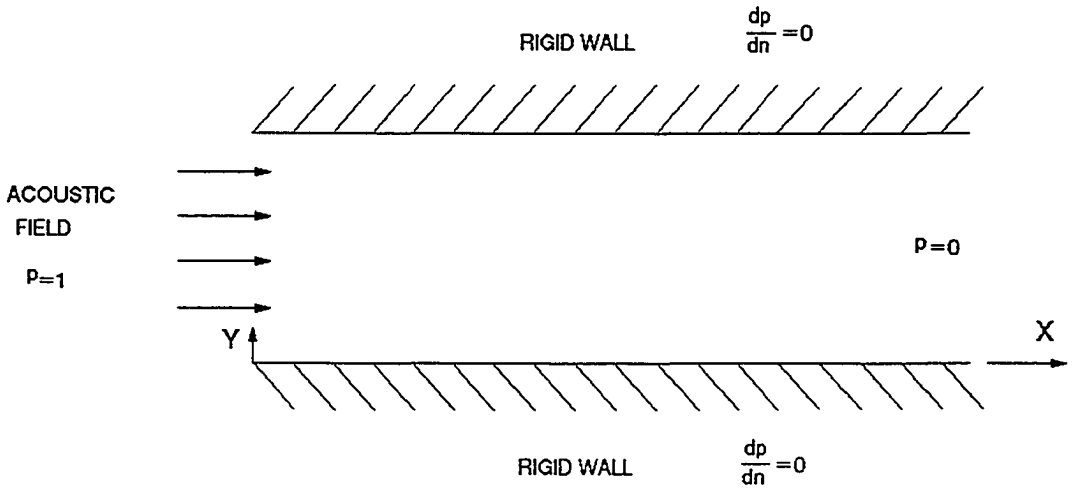

Figure 4.1 Open Outlet Rectangular Duct.

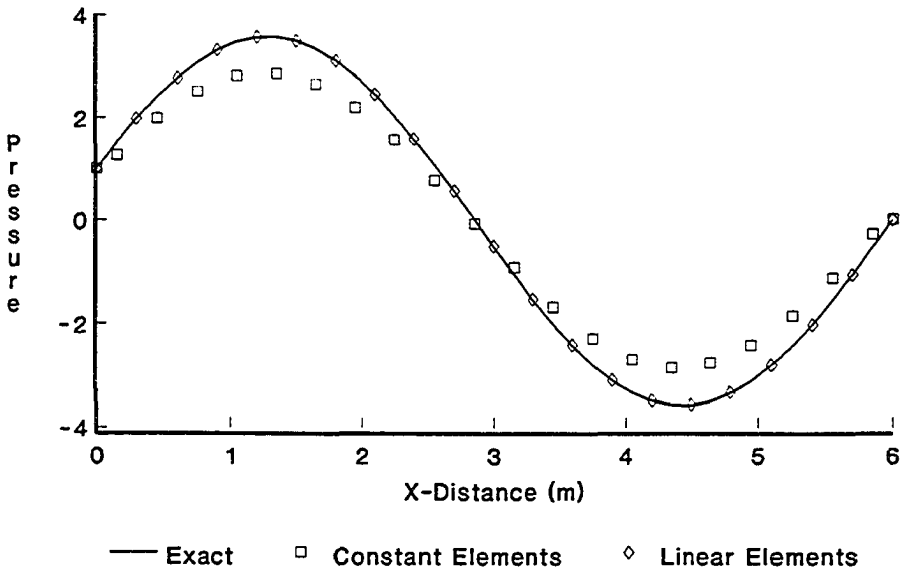

Figure 4.2 Open Outlet Rectangular Duct Results.

used for both the linear and constant element cases. The element distribution is as follows: 32 boundary elements on y=0.0, 32 boundary elements on y=1.0 m., 8 boundary elements on x=0.0 and 8 boundary elements on x=6.0 m. All elements are of equal length on each individual surface. As expected, the linear elements give a better approximation to the exact solution than the constant elements.

Also for the open outlet case, the pressure is plotted at (x,y)=(1.5,0) versus the wavenumber. The wavenumber is varied from 0 to 4 as shown in Figure 4.3. The natural frequencies of the cavity appear at the pressure discontinuities. Figure 4.3 shows the pressure variation for linear elements only. The exact cavity frequencies can also be easily calculated. The acoustic natural frequencies for constant and linear elements are compared with the exact frequencies in Table 4.1. Both the constant elements and the linear elements give very good approximations to the acoustic natural frequencies. Knowing that the boundary element method can approximate the pressure accurately at the acoustic frequencies becomes very important when coupling BEM and FEM.

The convergence of the pressure values versus the number of elements is also very important. The same type of problem is considered except that the length of the duct in the y direction is set at 6 meters which is the same as the x direction length. The wave number is set at .001 to ensure the plane wave assumption and the pressure was observed at

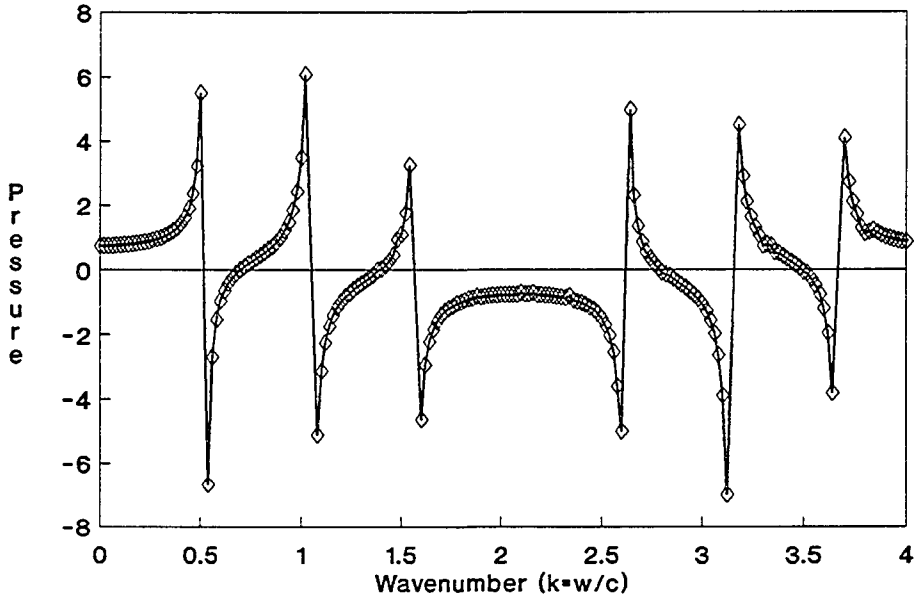

Figure 4.3 Pressure Variation at x=1.5 meters and y=0.

Table 4.1 Comparison of Wavenumber for Acoustic Natural Frequencies.

EXACT SOLUTION	CONSTANT ELEMENTS	LINEAR ELEMENTS
0.524	0.54	0.52
1.047	1.06	1.05
1.571	1.59	1.57
2.618	2.63	2.62
3.142	3.18	3.14
3.665	3.71	3.67

(x,y)=(3,5) for linear elements. The convergence data is shown in Table 4.2. As the number of elements increases, the error sharply decreases as expected.

The second example problem used to validate the boundary element method is a rectangular duct with a closed outlet as shown in Figure 4.4. The closed outlet is assumed to be a rigid wall at the exit. The boundary conditions for the duct in Figure 4.4 are,

$$\begin{aligned} \frac{\partial p}{\partial n}&=0 \ at \ y=0,1m \\ \frac{\partial p}{\partial n}&=0 \ at \ x=6m \\ p&=1 \ at \ x=0m. \end{aligned} \tag{4.3}$$

As before, the wavenumber is set at 1 and the length of the duct in the x-direction is 6 meters. The exact solution is easily found as,

$$p(x)=\frac{\cos k(L-x)}{\cos kL}. \tag{4.4}$$

The pressure, p(x), is only a function of the x-direction due to the assumption of plane wave propagation. As before, 80 elements are used for the constant and linear element cases. The boundary element comparison with the exact solution is shown in Figure 4.5. Both constant and linear element cases give very good approximations.

In most realistic duct problems, the velocity or the pressure is not known at the duct outlet. Only the relationship between the normal pressure and the normal

Table 4.2 Pressure Convergence with Number of Elements.

Number of Linear Elements	Pressure
4	0.47561
8	0.49979
12	0.49987
80	0.50000
Exact	0.50000

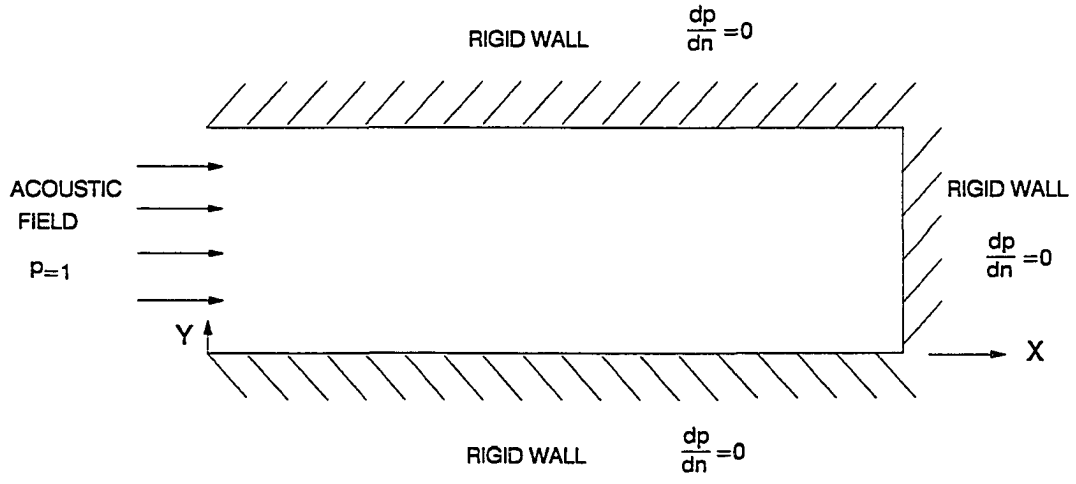

Figure 4.4 Closed Outlet Rectangular Duct.

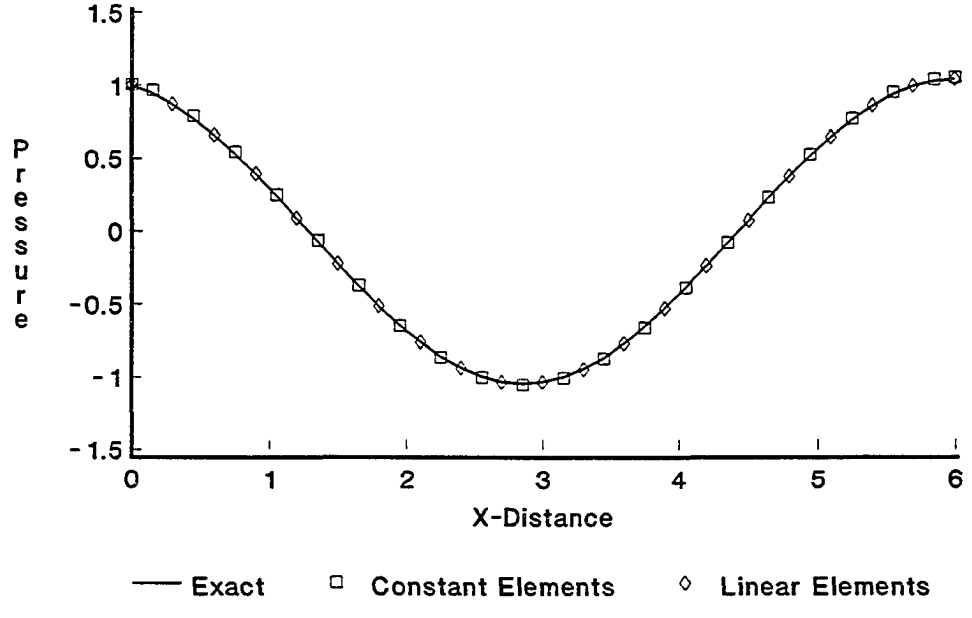

Figure 4.5 Closed Outlet Rectangular Duct Results.

velocity is known. This is known as an impedance boundary condition, where $z=p/v_a$ is some arbitrary complex constant. A realistic condition at the exit requires that no reflected acoustic waves are encountered at the outlet. Since a plane wave assumption is made, the no-reflection exit condition requires that the impedance be set to $\rho_a c$, where ρ_a is the medium density and c is the medium sound speed. Knowing the relationship between the pressure and the velocity at the exit, a boundary condition in terms of p and q can be derived.

The next example problem includes an impedance boundary condition at the outlet. The example problem in Figure 4.6 includes the following boundary conditions:

$$\begin{aligned} &\frac{\partial p}{\partial n}=0 \text{ at } y=0,1m \\ &z=\frac{p}{v_a}=\rho_a c \text{ at } x=6m \\ &p=1 \text{ at } x=0m. \end{aligned} \tag{4.5}$$

The duct is discretized into 80 elements for both constant and linear element cases and the wavenumber is set at 0.05. In Figure 4.7, the pressure results for the linear and constant element cases are plotted along with the exact solution versus the x distance of the duct. Both element cases give extremely accurate results. The constant element case gives continuously higher values than the linear case, however the maximum error for the constant element case is only 0.3 percent. The results of this case are very good because the

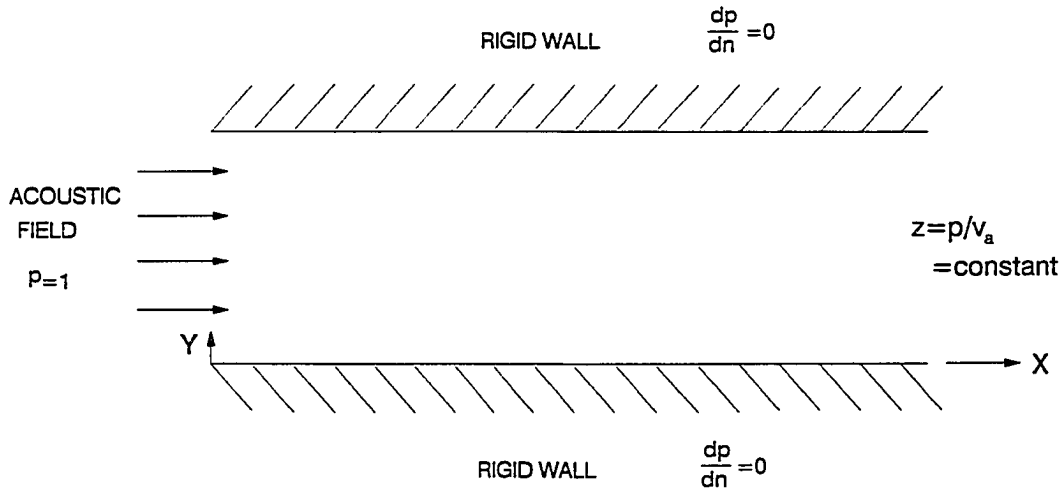

Figure 4.6 Rectangular Duct with Impedance Boundary Condition.

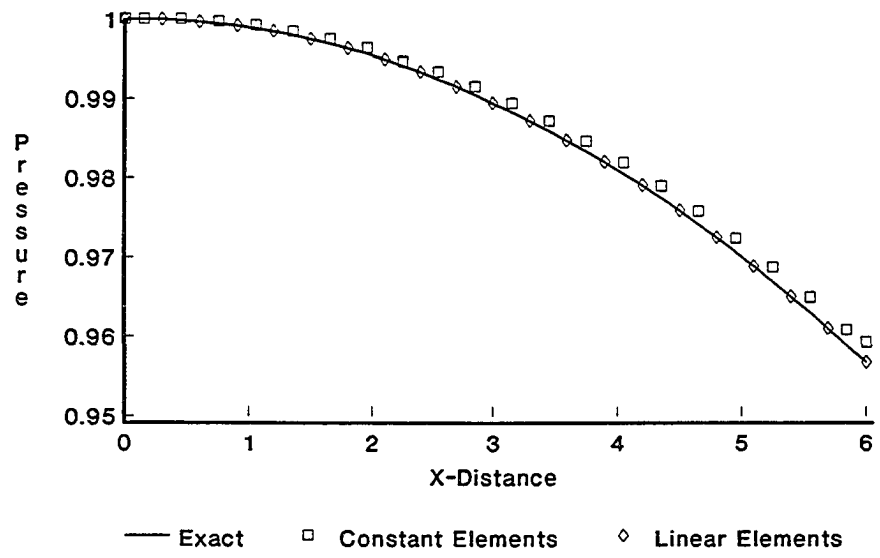

Figure 4.7 Results for a Rectangular Duct with an Impedance Outlet Condition.

acoustic wavelength is large compared with the duct element dimensions.

The boundary element method has shown that it can handle any type of boundary condition of pressure and velocity on the surface of the duct system. The next objective is to see how BEM handles sound propagation in rectangular ducts with complex geometries. A muffler-type problem with an exact solution is modelled and compared with the approximations of the boundary element method.

The variable geometry of the muffler-shaped duct is shown in Figure 4.8. The side walls are considered rigid and there is a unit pressure distribution at the inlet of the duct. In order to assume no reflection at the outlet, an impedance boundary condition is used, where $z=p/v_a=\rho_a c$. The transmission loss coefficient is calculated between the input pressure and the outlet pressure. The cross-sectional areas S_1 and S_2, are set at 1.0 m and 2.0 m respectively. Thus the ratio of the two areas, S_2/S_1, is set at 2.0 and the rectangular duct is discretized into 80 elements. The inlet section and the outlet section use 20 boundary elements each and the mid-section of the duct uses 40 boundary elements for the discretization. The length of section 2 as shown in Figure 4.8 is set at L_2=1.0 m.

The exact solution for the transmission coefficient can easily be derived in terms of complex amplitudes of incident,

reflected, and transmitted pressures [64]. At low frequencies corresponding to $kL_2 \ll 1$, leads to a transmission coefficient of

$$\alpha_t = \frac{1}{1+\left[\frac{S_2 k L_2}{2S_1}\right]^2}. \qquad (4.6)$$

Equation (4.6) shows that the transmission coefficient is near unity for low frequencies and tends to zero as the frequency is increased. The equations derived for pressure transmission are valid only when the wavelength is large compared with the smallest dimension of the duct section.

As the wavenumber is increased, the transmission coefficient is evaluated for both constant and linear elements as shown in Table 4.3. The transmission coefficient decreases as the frequency increases as expected. Both constant and linear elements give very good approximations with average errors of 1.36% and 1.08%, respectively. The error values are calculated up to k=.4 because the exact solution may not be valid due to the $kL_2 \ll 1$ assumption for larger k values.

From the pressure comparisons in the above example problems, it can be seen that the boundary element method is a very good approximating method for two-dimensional domains. The next objective is to show the versatility of the boundary element method through an example. A multi-section duct was created as shown in Figure 4.9. The side walls are considered to be rigid and a unit pressure field is applied at the entrance of the duct. An impedance boundary condition is

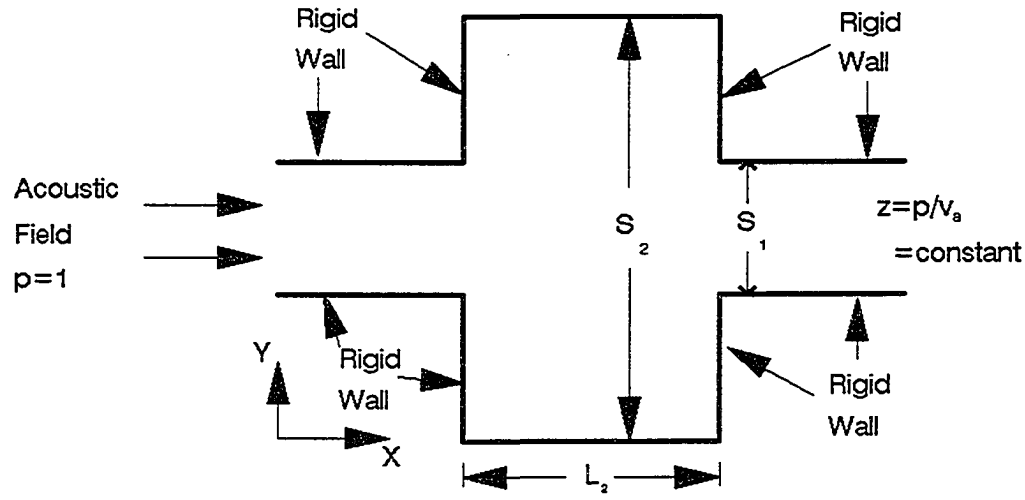

Figure 4.8 Muffler-Shaped Duct System.

Table 4.3 Pressure Values for Muffler-Shaped Duct.

k	Exact Sol.	Linear Elem.	Constant Elem.
0.01	0.9999	0.9999	0.9999
0.1	0.9901	0.9959	0.9965
0.2	0.9615	0.9806	0.9829
0.3	0.9174	0.9437	0.9475
0.4	0.8621	0.8622	0.8679
0.5	0.8000	0.6941	0.6985

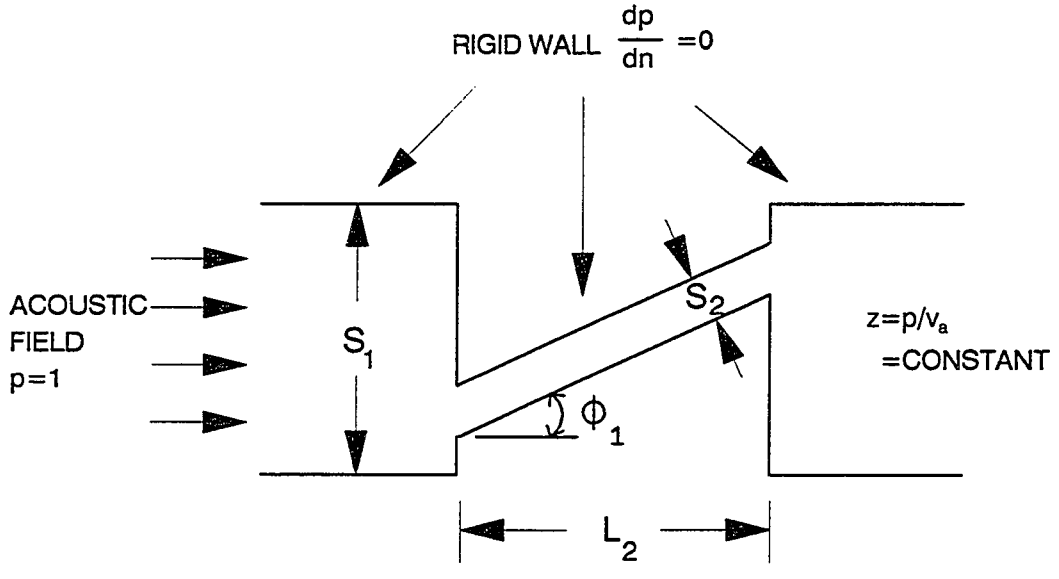

Figure 4.9 Three-Section Rectangular Duct.

employed at the outlet to assume no acoustic reflection and the wavenumber is set at 0.1. The three-duct system is discretized into 70 boundary elements and the transmitted pressure is observed at the center of the outlet duct.

The transmitted pressure is calculated for both constant and linear elements as the angle ϕ_1 is varied from 0 to 45 degrees. The results are plotted in Figure 4.10 for angle values, ϕ_1, in increments of 5 degrees. Both constant and linear element cases give very close results due to the low frequency assumption applied at the beginning. In Table 4.4, a frequency-pressure response is tabulated for different values of the wavenumber. The angle of the mid-section duct is set at 20 degrees and the transmitted pressure is obtained at the center of the outlet section. The transmission loss is calculated with the relationship between the input pressure and the output transmitted pressure, $TL=20\log(p_{in}/p_{out})$. A negative transmission loss value means the output pressure is greater than the input pressure. The distance of the mid-section duct in Figure 4.9 is set at 1.0 m. and the ratio of cross-sectional areas S_2/S_1, equals 0.25. As the wavenumber tends towards unity, higher order modes begin to propagate and the transmitted pressure begins to rapidly change. Due to the odd geometrical configuration of the duct system, higher order modes begin to propagate at lower frequencies than typical rectangular duct systems.

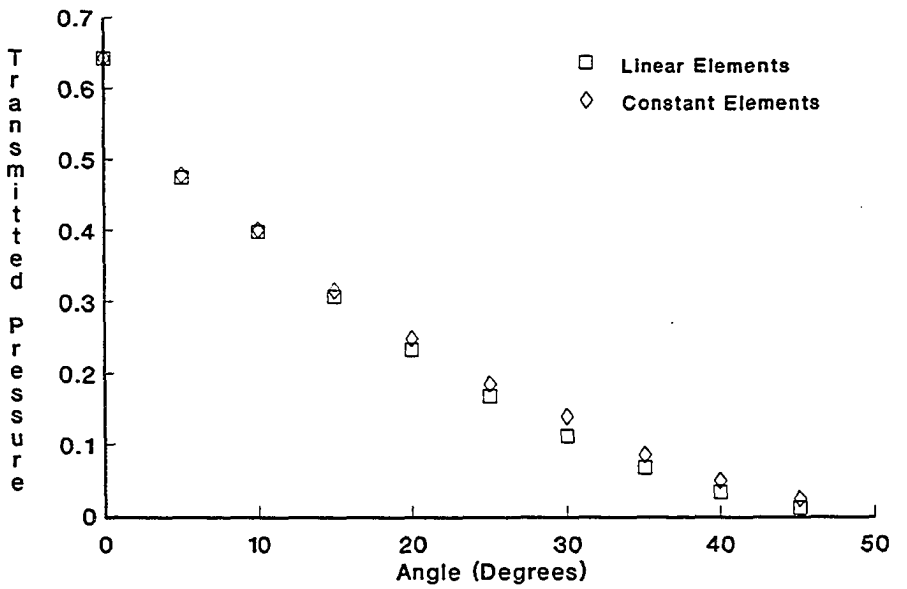

Figure 4.10 Three-Section Rectangular Duct Results.

Table 4.4 Pressure Values at the Center of the Outlet Section of a Three-Section Duct with ϕ_1=20°.

k	Constant Elements	Linear Elements
0.001	0.24735	0.22416
0.01	0.24736	0.22419
0.1	0.25617	0.23268
0.2	0.28206	0.25893
0.3	0.29800	0.29063
1.0	-0.18069	-0.18105

As seen from the comparisons above, the boundary element method gives very accurate and reliable solutions for the two-dimensional duct analysis. Bessel function singularities have been approximated.

4.1.2 Three-Dimensional Interior Domain Analysis

Acoustic analysis on most realistic structural components are three-dimensional in nature. Since the components of the wavenumber analysis are affected by the dimensionality, three-dimensional analysis must be performed. For example, the majority of commercial mufflers, particularly the ones embodying flow-reversing chambers, are three-dimensional. Thus, one and two-dimensional frequency-domain acoustic theories as well as time-domain finite wave theories are not applicable [65]. One has to resort to the numerical solution techniques in order to solve such complex systems.

As mentioned before, three-dimensional acoustic analysis is easier to apply than the two-dimensional analysis simply because the approximate function deals with exponential functions instead of Bessel functions. This section first shows that the boundary element method is accurate by comparing it to some problems with exact solutions. Next some example problems with complex geometry features are analyzed using BEM to show the versatility of the method.

The example problems are derived from a typical rectangular duct as shown in Figure 4.11. The duct shows how the boundary is discretized with two-dimensional elements.

Each example problem assumes that each side of the duct is 20 cm and the entire duct is discretized using boundary elements. The two end surfaces (inlet and outlet) are each modelled by a 5x5 mesh or 25 elements, and the duct side walls are also modelled by a 5x5 mesh or 25 elements each. Thus, the total number of elements is 150 constant boundary elements, as shown in Figure 4.11. The frequency is varied in each case and the pressure is measured at the center of the duct outlet. A unit pressure field is assumed at the duct entrance (z=0.0 cm) and all of the exterior walls are assumed rigid. For the first example problem, a null pressure field is applied at the duct outlet and the transmission loss is plotted versus the input frequency in Figure 4.12.

In each case, the input acoustic waves are considered to be plane waves and thus the one-dimensional exact solutions are valid. From Figure 4.12, the boundary element method gives very accurate results compared to the exact solution. However, at the acoustic natural frequency of the duct system, the boundary element method results vary from the exact solution slightly. The cut-off frequency is selected at 1200 Hz due to the accuracy of the boundary element method. This frequency dependent accuracy will be discussed at the end of this section. For three-dimensional domains, only constant

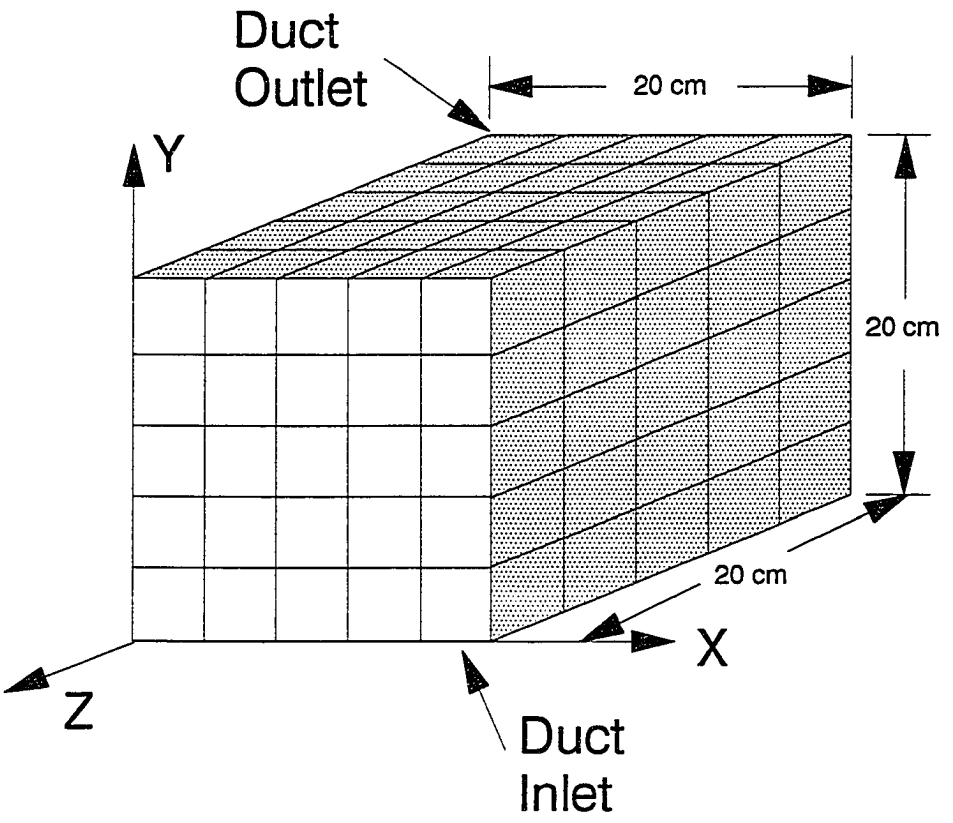

Figure 4.11 Three-Dimensional Rectangular Duct.

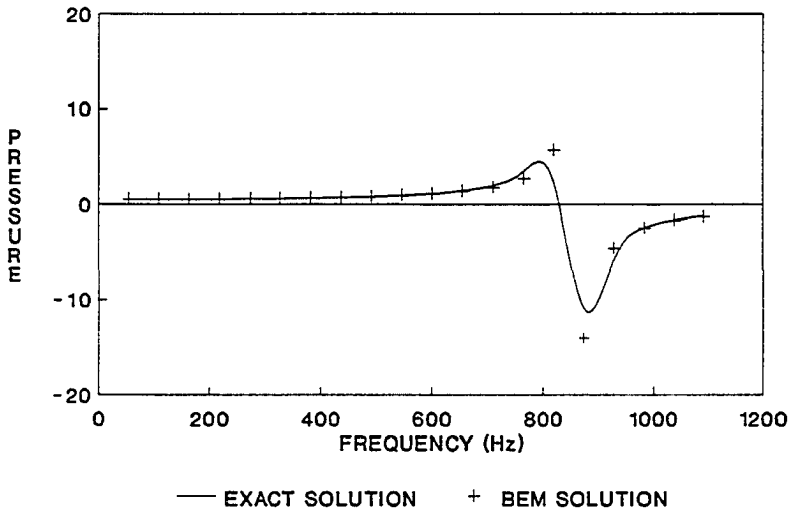

Figure 4.12 Results for Three-Dimensional Duct with Null Pressure at Outlet.

elements are used since the two-dimensional analysis showed that the discrepancy between linear and constant elements was nominal.

The second example problem uses the same duct dimensions and the same acoustic assumptions. The outlet boundary condition assumes a rigid wall at z=20 cm. By assuming a rigid wall boundary condition, the normal velocity and q are set equal to zero. The results for a rigid wall boundary condition are shown in Figure 4.13. Once again, at the acoustic natural frequency, the boundary element method gives erroneous results. BEM gives very accurate approximations, except at the acoustic natural frequencies, because the influence matrices become singular.

The last example problem applies an impedance boundary condition at the outlet of the duct. A no-reflection condition is used, which assumes the relationship between p and v equals $\rho_a c$ for the plane wave assumption. The density for air is 1.21 kg/m^3 and the speed of sound in air is given as 343 m/s^2. Obviously, the no-reflection condition assumes the total plane acoustic wave is transmitted at the outlet. The results for the impedance boundary condition case are shown in Figure 4.14.

Notice that as the frequency increases, the boundary element results tend to diverge from the exact solution. This is a result of two things. Once again, an increase in the number of elements for higher frequencies must be applied to

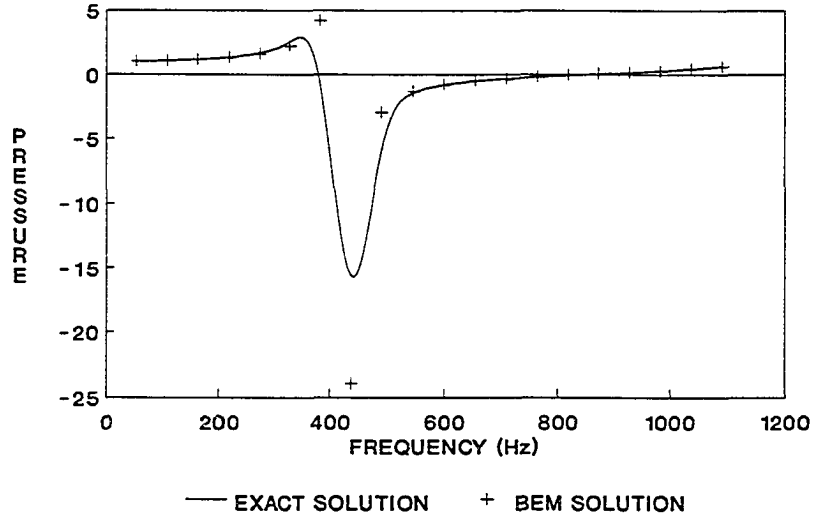

Figure 4.13 Results for Three-Dimensional Duct with Rigid Wall Outlet.

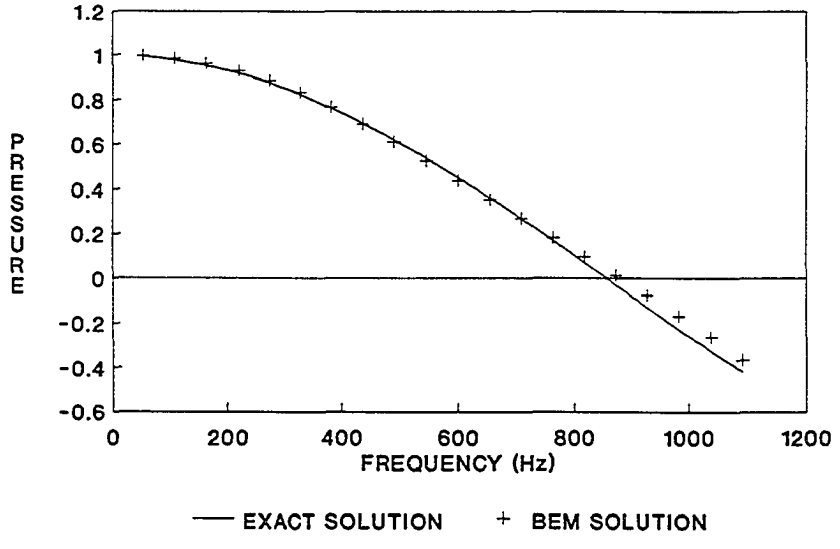

Figure 4.14 Results for Three-Dimensional Duct with Impedance Boundary Condition.

assure accurate results. This will be discussed later. Second, at higher frequencies, the higher order modes come into play in the BEM approximations and thus the comparison with the exact solution tends to diverge. Therefore, these two phenomena contribute to the divergence of the boundary element results.

From the previous results, the boundary element method has shown that it gives accurate results for three-dimensional domains. The next objective is to model a three-dimensional duct with complex geometry. Munjal has solved an offset inlet-outlet duct as shown in Figure 4.15 [64]. The inlet of the duct system enters at the bottom right of the main section and the outlet exits at the top left. Munjal approximates the transmission loss of the system with 40 finite elements. Three case studies are considered with the boundary element method: 50, 82, and 328 elements, as shown in Figure 4.16. The 50 element case discretizes the inlet and outlet sections with 5 boundary elements each and the mid-section with 40 boundary elements. The 82 element case discretizes the inlet and outlet sections with 9 elements each and the mid-section with 64 boundary elements. The 328 element case discretizes the inlet and outlet sections with 36 boundary elements each and the mid-section with 256 boundary elements. The 50 element case gives a good general approximation. The 82 and 328 element cases give extremely close approximations to the finite element results. Notice that the 50 element BEM case,

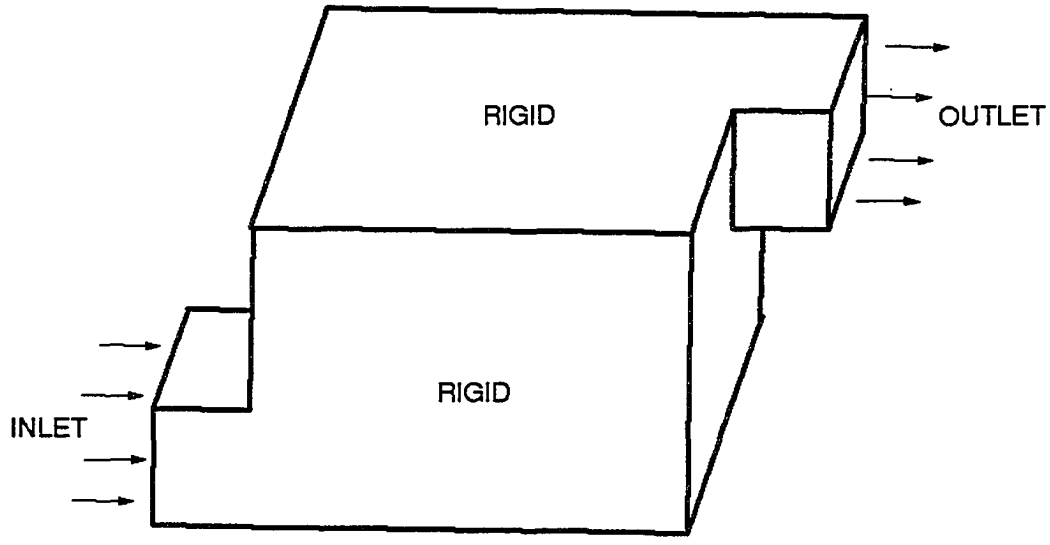

Figure 4.15 Three-Dimensional Offset Inlet-Outlet Duct.

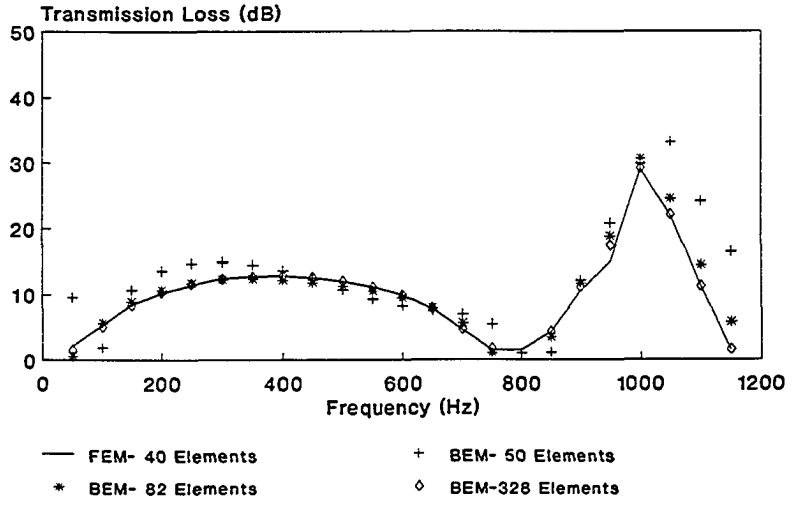

Figure 4.16 Transmission Loss of Offset Inlet-Outlet Duct.

gives erroneous results at very low frequencies. This phenomena has been noted before by Hussain and Peat [22]. They proposed a small change in their formulation for low-frequency calculations. Careful consideration has to be taken into account when modelling complex duct systems.

With confidence in modelling three-dimensional domains, a very complex system can now be solved. In Figure 4.17, the complex duct system has four inlets and four outlets. All inlets and outlets have the same dimensions and are located at the corners of the main duct system. Two boundary element cases are considered: transmission loss for 74 and 130 elements as shown in Figure 4.18. The 74 element case discretizes each inlet and outlet section with 5 boundary elements each and the mid-section with 24 elements. The remaining 10 boundary elements are used to discretize the inlet and outlet surfaces. The 130 element case discretizes each inlet and outlet section with 9 boundary elements each and the mid-section with 48 elements. The remaining 10 boundary elements are again used to model the inlet and outlet surfaces. A unit pressure field is activated at each inlet and an impedance boundary condition, $z=\rho_a c$, is assumed at each outlet boundary. At various frequencies, the 74 element case gives varying transmission loss results from the 130 element case. However, both cases give very similar approximation trends.

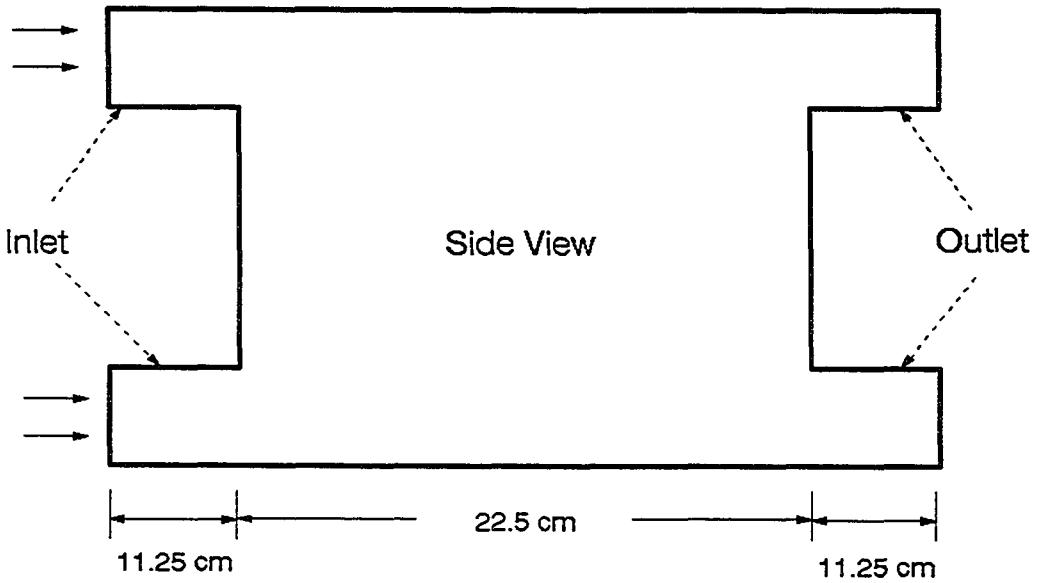

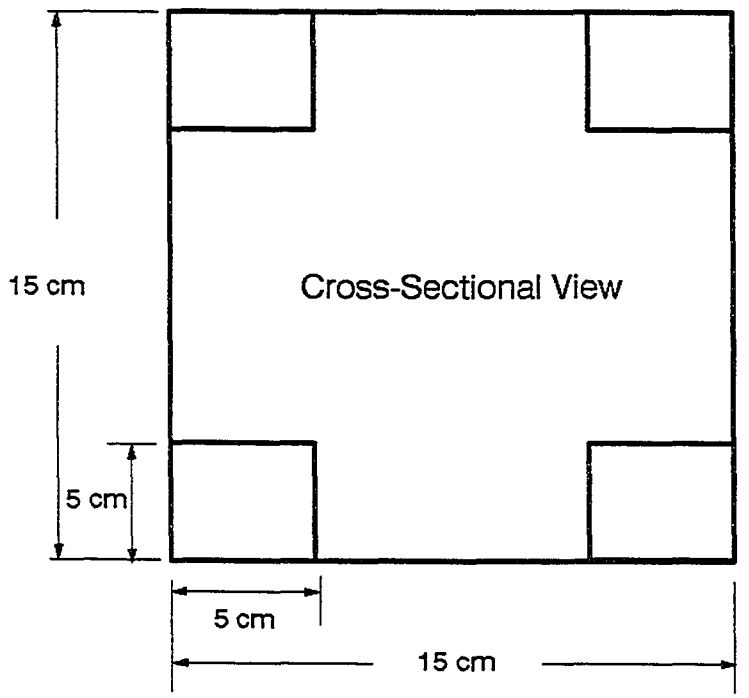

Figure 4.17 Four-Inlet and Outlet Irregular Duct System.

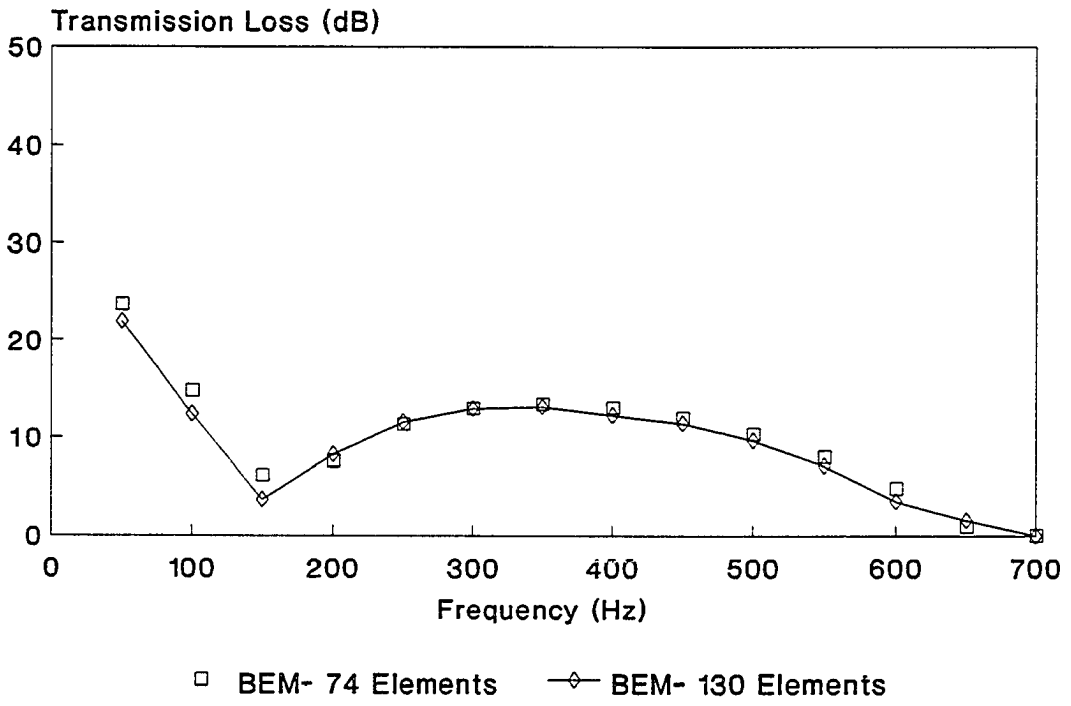

Figure 4.18 Four-Inlet and Outlet Duct Results.

From the previous results, the boundary element method has shown that it gives very accurate solutions for regular and irregular-shaped three-dimensional ducts. Some interesting aspects have been noted. Some erroneous results can occur with low-element, low-frequency modelling. It has been found that four to five elements per acoustic wavelength are needed to accurately model acoustic domains. Note that this generalization applies only to constant elements. It is also shown at certain acoustic natural frequencies, that the boundary element method can give erroneous results. Many authors have addressed and solved this problem with the "CHIEF" and "CONDOR" methods [8,48]. These methods solve the singular matrix system and provide very accurate solutions at natural frequencies.

At this point, the boundary element method has shown that it gives accurate solutions for two and three-dimensional domains. Some very complex geometric systems have been modelled. The most attractive advantage of the boundary element method is that only the boundary is discretized. This cuts down considerably on user modelling time.

4.2 Coupled Harmonic Response of Structural-Acoustic Problems

Coupling the structure and acoustic domains is essential when trying to accurately model harsh environments. Previously, isotropic panels have been coupled with acoustic domains as mentioned in Chapter 1. The first objective of

this section is to validate the coupled BEM-FEM approach by comparing with known analytical and experimental results for isotropic panels. Two selected problems with different plate boundary conditions are used for the validation.

Composite panels are then coupled with the acoustic domain and transmission loss characteristics are studied. No exact solutions or experimental data are available for sound-structure interaction problems using composite panels. Random analysis results are included in the last section.

4.2.1 Isotropic Structures

As mentioned in Chapter 1, analytical, experimental and exact solutions are available for isotropic panels backed by an acoustic cavity as shown in Figure 3.3. Guy and Bhattacharya provided modal summation approximations along with valuable experimental data for two coupled problems [57]. Bokil developed exact solutions using Laplace transforms for the same two coupled problems [58]. The data from references [57] and [58] are very valuable because they give coupled frequencies to compare with the BEM-FEM procedure. The first cavity backed structure (see Figure 3.3), is a simply supported brass panel with the following plate and duct characteristics:

Panel/Cavity Problem - Simply Supported Brass Plate

Cavity

X axis length = 20 cm.
Y axis length = 20 cm.
Z axis length = 20 cm.
All walls are considered rigid
Air medium: ρ_a=1.21 kg/m^3, c=343 m/s

Plate

X axis length = 20 cm.
Y axis length = 20 cm.
Thickness = 0.9144 mm.
Young's Modulus = 10.4E10 Pa.
Poisson's Ratio = 0.37
Density = 8500 kg/m^3.

Two element-mesh cases were run for this coupled system, one case consisted of 25 (5x5 mesh), finite elements and 150 (5x5 mesh for each of the 6 duct walls), boundary elements, and the second case used 64 (8x8 mesh), finite elements and 384 (8x8 mesh for each of the 6 duct walls), boundary elements. The pressure was calculated at the back wall of the cavity (p_{out}) and the transmission loss was calculated using the source pressure as the input pressure (p_{in}). The coupled BEM-FEM results are compared in Figure 4.19 with approximate analytical, experimental and exact solutions from references [57] and [58]. The results in Figure 4.19 indicate that the coupled boundary element/finite element procedure reproduces results that are of comparable accuracy with existing analytical, experimental and exact solutions.

The second case considered analyzes the same plate/cavity system as shown in Figure 3.3. However, this time the panel

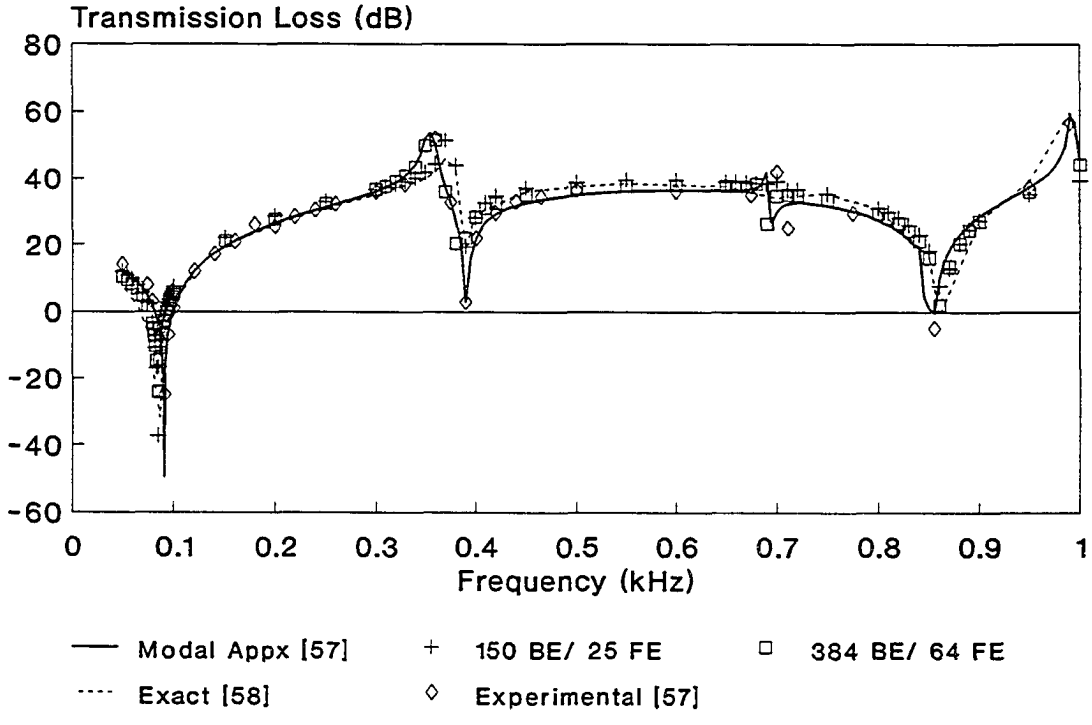

Figure 4.19 BEM-FEM Comparison for Simply Supported Sound-Structure Interaction Problem.

is made of aluminum and clamped instead of simply supported. The cavity and plate dimensions and properties are given below:

Panel/Cavity Problem - Clamped Aluminum Plate

Cavity

X axis length = 30.48 cm.
Y axis length = 15.24 cm.
Z axis length = 15.24 cm.
All walls are considered rigid
Air medium: ρ_a=1.21 kg/m^3, c=343 m/s

Plate

X axis length = 30.48 cm.
Y axis length = 15.24 cm.
Thickness = 0.16256 cm.
Young's Modulus = 7.0E10 Pa.
Poisson's Ratio = 0.33
Density = 2400 kg/m^3.

The transmission loss is once again plotted in Figure 4.20 with the analytical, experimental and exact results from references [57] and [58]. The same two element-mesh cases were used for the boundary and finite elements. Again, both element-mesh cases give very good results.

When studying the coupled system, the coupled natural frequencies are of vast importance. In Table 4.5, a comparison of the first few natural frequencies between the coupled BEM-FEM procedure and references [57] and [58] are given. The uncoupled natural frequencies are given, where the numbers in bold represent the uncoupled plate frequencies and the numbers in italics represent the acoustic uncoupled

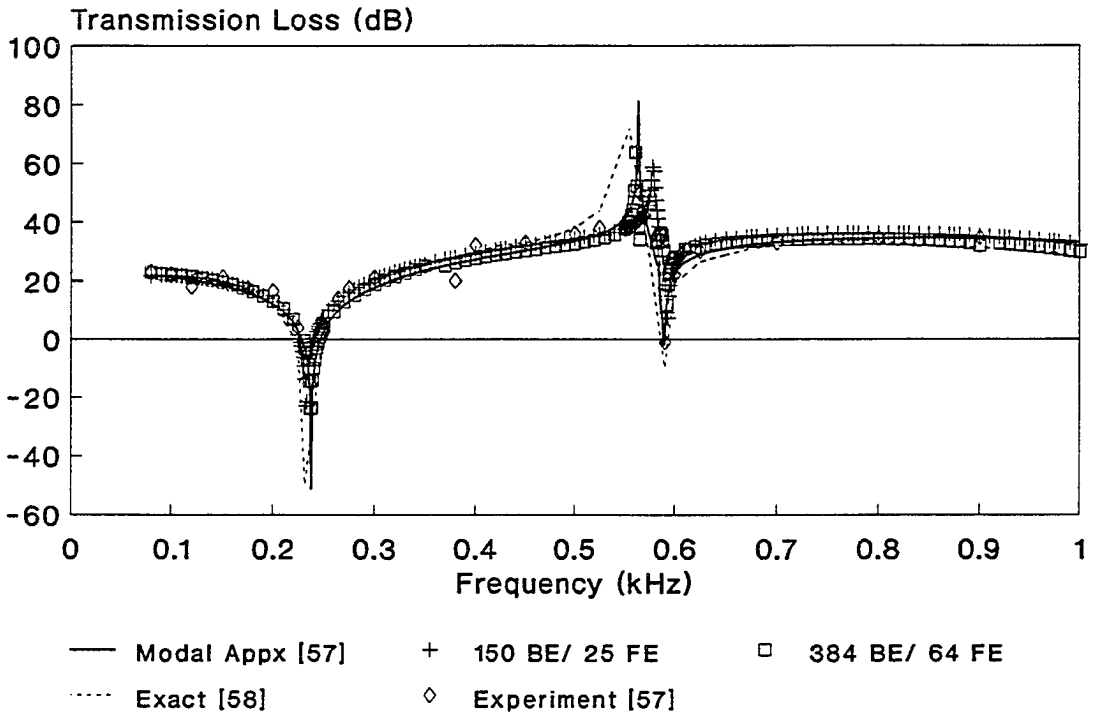

Figure 4.20 BEM-FEM Comparison for Clamped Sound-Structure Interaction Problem.

Table 4.5 Comparison of Natural Frequencies (Hz) for Coupled Boundary Element and Finite Element Method.

Modal [57]	Exact [58]	Exper. [57]	BEM-150 FEM-25	BEM-384 FEM-64	Uncoupled Plate/*Acoustic*
Simply Supported Brass Plate					
91.5	87.0	91.0	85.0	86.0	**78.1**
390.0	390.4	397.0	384.0	385.0	**390.3**
695.0	702.5	730.0	697.0	705.0	**702.5**
860.0	860.0	864.0	860.0	861.0	*860.0*
Clamped Aluminum Plate					
238.1	234.4	235.0	234.0	238.0	**227.0**
564.0	588.5	565.0	578.0	562.0	**590.1**

frequencies. The uncoupled natural frequencies are given in order to show how the coupling affects the total system response. Note that the first natural frequency of the coupled system with the simply supported plate is greater than the first uncoupled plate natural frequency. This is because the acoustic chamber "spring-loads" the plate and thus increases the coupled natural frequency. Also note that the coupled system is affected by the first acoustic natural frequency at 860 Hz. The same phenomena occurs with the first coupled natural frequency of the clamped aluminum panel. However, note that only the first natural frequency is affected by the coupled system.

From the two systems above, the coupled BEM-FEM procedure gives very reliable results. Both element cases seem to favorably approximate all of the analytical, experimental and exact solutions.

Another interesting aspect of the structural-acoustic system is the effect of the cavity depth on the plate mode shape. Figure 4.21 shows the first mode shape of the square brass plate driven at the coupled natural frequency of 86 Hz. Increasing and decreasing the length of the acoustic chamber greatly affects the mode shape of the panel. If the acoustic chamber is reduced from 20 cm. to .2 mm., the plate appears to vibrate like the third mode shape as shown in Figure 4.22.

The outlet boundary condition can provide another interesting study. In all of the above problems, the outlet

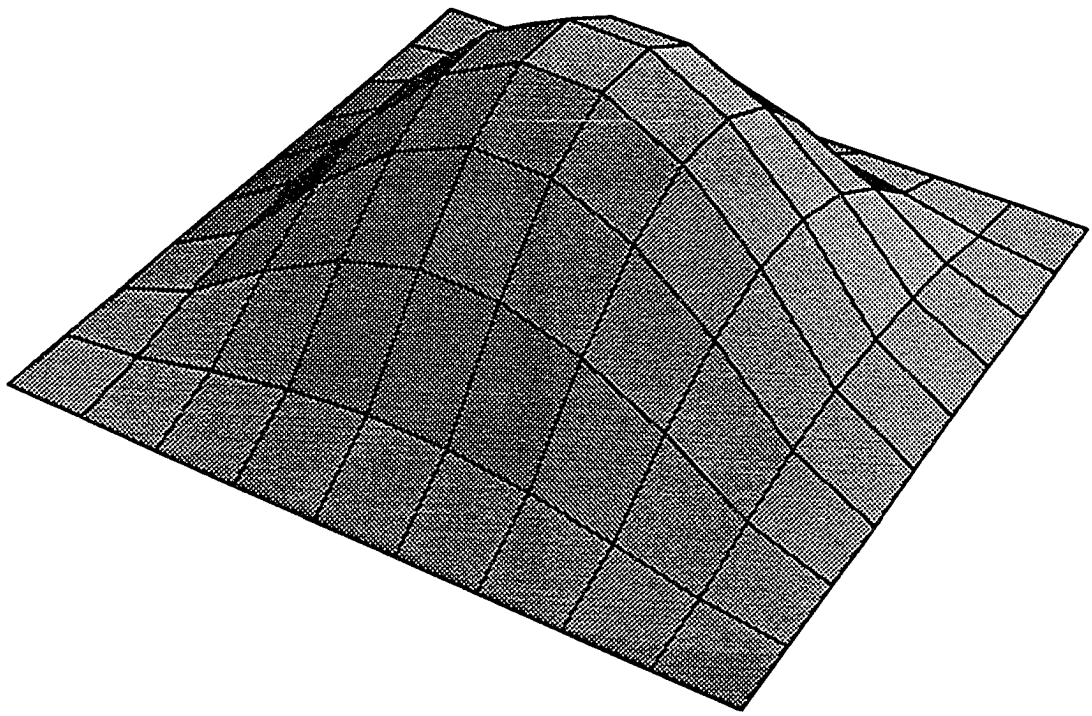

Figure 4.21 First Mode Shape of Brass Plate Vibrating at 86 Hz with Duct Length of 20 cm.

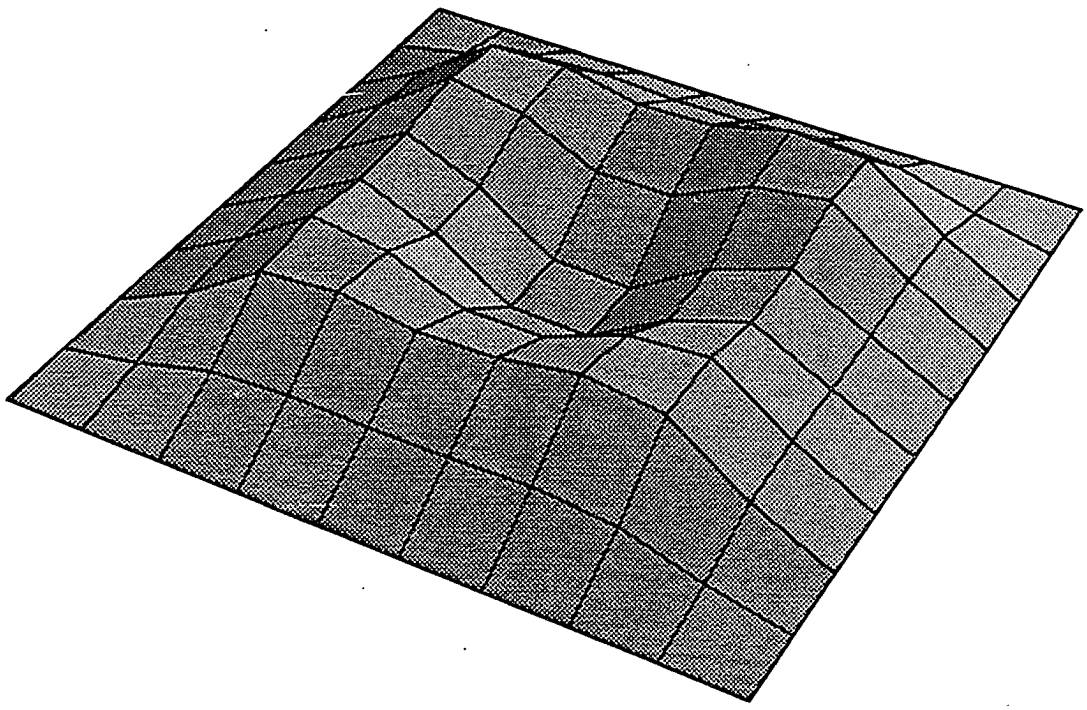

Figure 4.22 Third Mode Shape of Brass Plate Vibrating at 86 Hz with Duct Length of .20 mm.

boundary condition is assumed to be a rigid wall. Here, we will assume that the outlet boundary condition has a constant impedance value. Thus the relationship between pressure and velocity is varied from $\rho_a c$ to 1, ($.0415 < z < 1.0$). As z increases towards 1, the rigid wall approximation is applied. When z equals $\rho_a c$, there is no impedance mismatch at the outlet, and the acoustic wave travels out of the duct system. From Figure 4.23, the coupled natural frequency is equal to the uncoupled natural frequency of the panel (78 Hz) in the low impedance range. As the impedance value increases, the coupled natural frequency increases up to the maximum coupled natural frequency of 85 Hz (the same as the rigid wall condition).

4.2.2 Composite Structures

As the next step towards exploring the area of sound-structure interaction, this study offers numerical results on an acoustic cavity-backed composite panel by harnessing the strengths of the coupled BEM-FEM technique. The composite panel used in this study has the following properties:

Graphite/Epoxy

E_{11} = 15.57E10 Pa
E_{22} = 0.807E10 Pa
ν_{12} = 0.22
G_{12} = 0.455E10 Pa
ρ = 1550 kg/m^3.

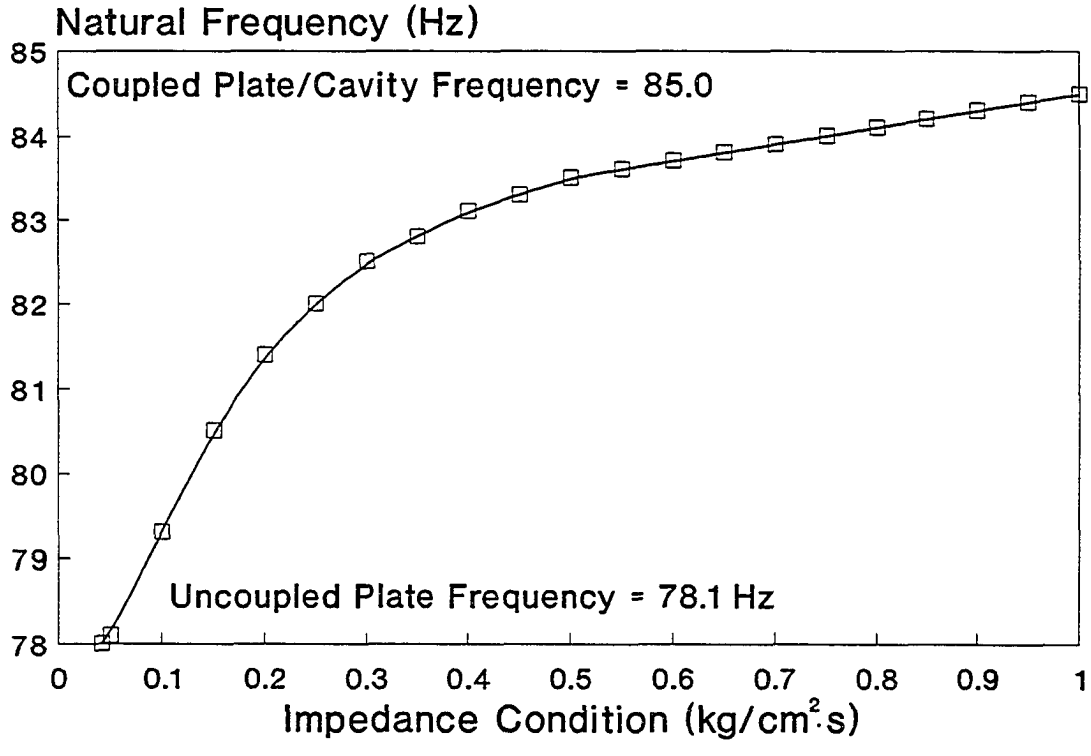

Figure 4.23 Coupled Natural Frequency Results With Variable Impedance at the Outlet.

The first transmission loss analysis is performed on the coupled system shown in Figure 3.3 and the same dimensions (20x20x0.09144 cm) are used from the Brass Panel problem in the previous section. The composite panel is simply supported and four panels with a different number of symmetrical cross-ply layers are considered. The number of layers is varied from 1, 3, 5 and 7. The one-layer laminate is a 0° degree layer, the three-layer laminate has a (0°/90°/0°) layup, the five-layer laminate has a (0°/90°/0°/90°/0°) layup and the seven-layer laminate has a (0°/90°/0°/90°/0°/90°/0°) layup. Figure 4.24 shows the transmission loss comparison for the 1 and 7-layer composite panels and the brass panel. The transmission loss data for the 3 and 5-layer composite panels lay between the curves of the 1 and 7-layer laminates and thus are not shown. The first coupled natural frequency of the composite panels is much greater than the coupled natural frequency of the brass panel. Note that the second coupled natural frequency for the one-layer composite is less and for the seven-layer composite is greater than the second coupled natural frequency of the brass panel. On an average, the brass panel give a greater transmission loss than the composite panel. However, remember that the brass panel is about 5½ times heavier than the composite panels.

The composite panels are also utilized in the second problem of the previous section and transmission loss data are compared with the aluminum clamped panel in Figure 4.25. The

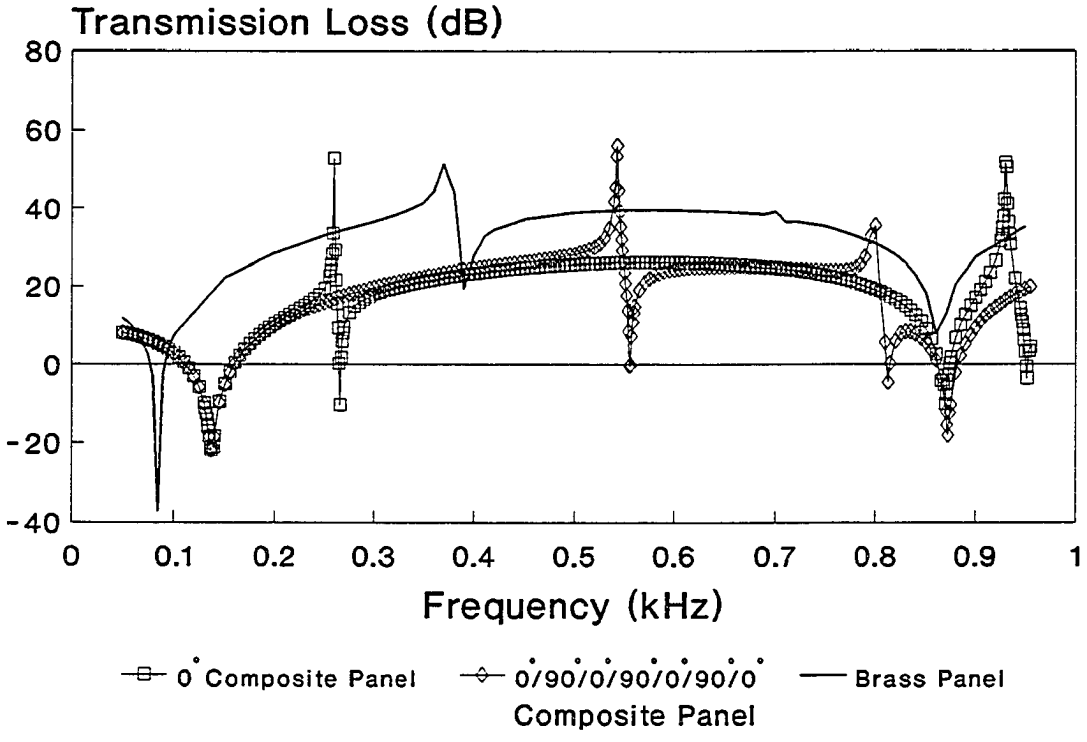

Figure 4.24 Composite Panel Analysis of Simply Supported Structure-Acoustic Interaction Problem.

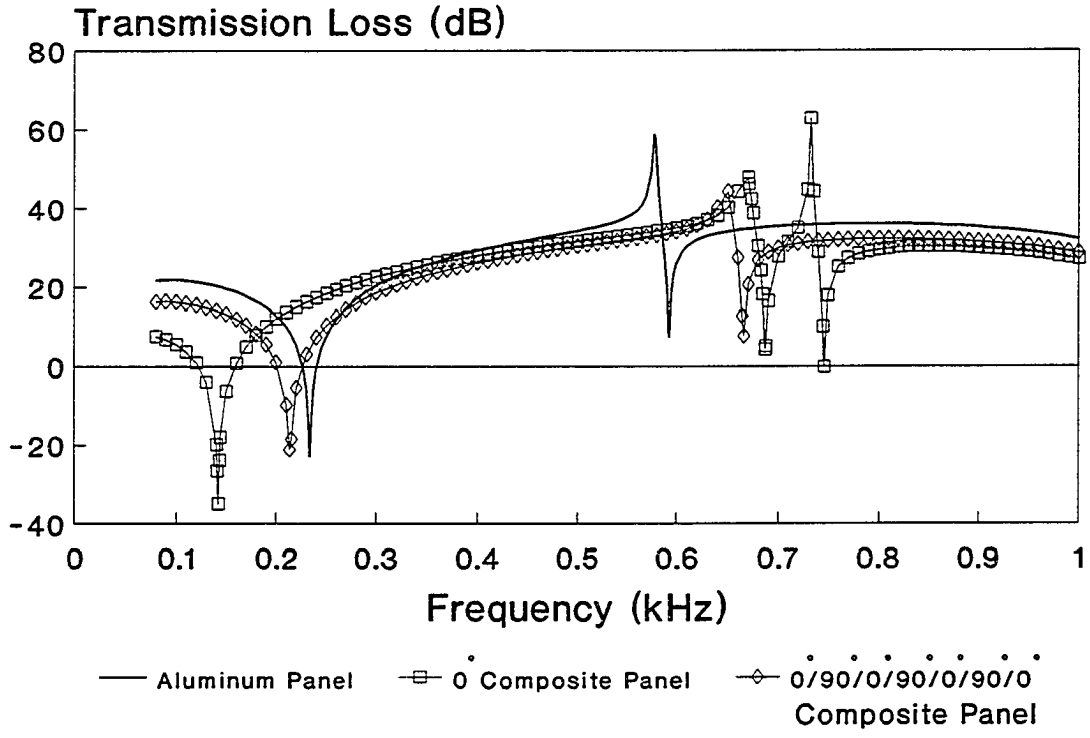

Figure 4.25 Composite Panel Analysis of Clamped Structure-Acoustic Interaction Problem.

transmission loss of one-layer and seven-layer composite panels are again shown along with the aluminum panel curve. As before, the three-layer and the five-layer composite panel transmission loss curves are bounded by the 1 and 7-layer curves and thus are not shown. Note, for this clamped case, the first coupled natural frequency of the composite laminates is less than the coupled natural frequency of the aluminum panel. The second coupled natural frequency of the composite laminates is greater than that of the aluminum panel. This effect occurs because the first coupled frequency is considered "mass-loaded" and the second frequency is considered "stiffness-loaded". From Figure 4.25, the composite panels give approximately the same transmission loss characteristics in an average sense. Remember again that the aluminum panel is about 1½ times heavier than the composite panels. Therefore, utilizing composite panels can greatly increase the strength-to-weight ratios.

The next composite study varies the lamination angle (ϕ,-ϕ,ϕ) of a three-layer symmetric angle-ply laminate. Again, two cases were run to compare transmission loss data. The first case uses the same data as the simply supported case above. Figure 4.26 shows the composite panel data versus the brass panel at 80 Hz. For the square panel, note that all transmission loss data for the composite panel are higher than the data for the brass panel. The uncoupled natural frequency is close to the coupled frequency for the brass panel. Thus

the output pressure is higher than the input pressure and the transmission loss values are negative. Remember, the transmission loss characteristics are totally dependent on the input frequency.

The second case uses the same data as the clamped case above. Figure 4.27 shows the comparison of the transmission loss results between the composite panel and the aluminum panel. Both panels have a dimensional ratio of 2:1 and the results show that in the case of the composite panel, the transmission loss is highly dependent on the lamination angle of the different layers.

The results above for the composite panels are simple examples showing the coupling of the plate/cavity system. At this point, the design process becomes critical in selecting the correct composite laminate. Composites offer many design variables, such as lamination angle, layer thickness and volume-fraction of graphite fibers. The designer must know the operating frequency range of the vibrating structure before deciding which laminate to use. Using this coupled BEM-FEM technique, along with the design variables, an optimal composite laminate can be chosen, which will offer excellent transmission loss characteristics with a low weight advantage.

4.3 Coupled Random Response of Structural-Acoustic Problems

As shown in the harmonic response problems, modelling the coupling of a system becomes very important. For cavity-

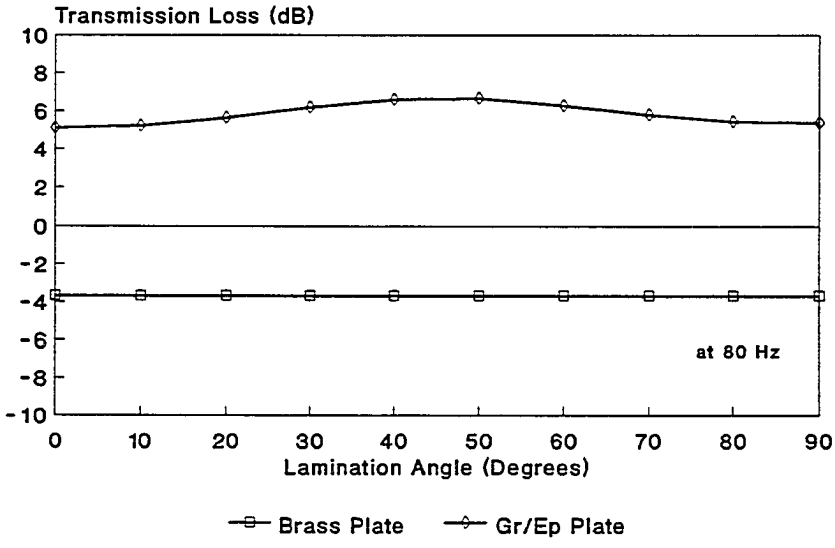

Figure 4.26 Transmission Loss of Simply Supported, Three-Layer Composite Panel ($\phi/-\phi/\phi$).

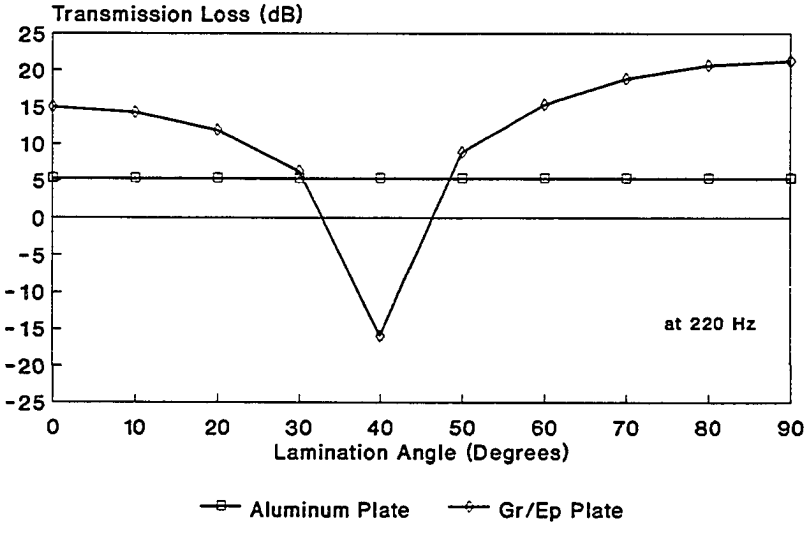

Figure 4.27 Transmission Loss of Clamped, Three-Layer Composite Panel ($\phi/-\phi/\phi$).

backed plate problems, as shown in Figure 3.3, the first coupled natural frequency of the system is increased. The same problems from Section 4.2 are now analyzed with random white noise excitation. Isotropic and composite panels with the same structure and acoustic characteristics are modelled. The coupled random response is compared with the uncoupled structure response to show the effect of coupling. The coupled system involves analysis of the duct and the structure together whereas the uncoupled system neglects the effect of the cavity.

First, the system with a simply supported panel is modelled. The square brass panel is 20 cm. by 20 cm. and 0.09144 cm. thick. Figure 4.28 shows the random response of the brass panel for the coupled and the uncoupled systems. The input sound pressure level is varied from 90 to 150 dB. The maximum Root Mean Square (RMS) value of deflection (W_{max}) at 150 dB is approximately half of the thickness. As expected, the coupled system produces lower RMS (W_{max}) values, since the first coupled natural frequency is increased. Similar to Equation (3.49), the response is dependent on the inverse of ω_n^3 and thus the RMS response is increased since the first coupled natural frequency is increased. Figure 4.29 models the same simply supported plate and cavity setup, but this time the panel is made of graphite/epoxy. The duct cavity characteristics and brass panel properties are given on page 84 and the seven-layer Graphite/Epoxy panel

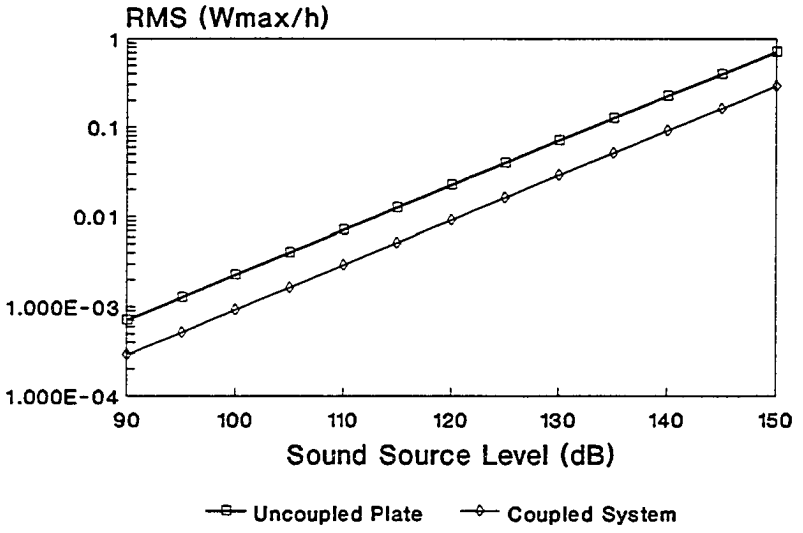

Figure 4.28 Random Response of Simply Supported Brass Panel and Acoustic Duct System.

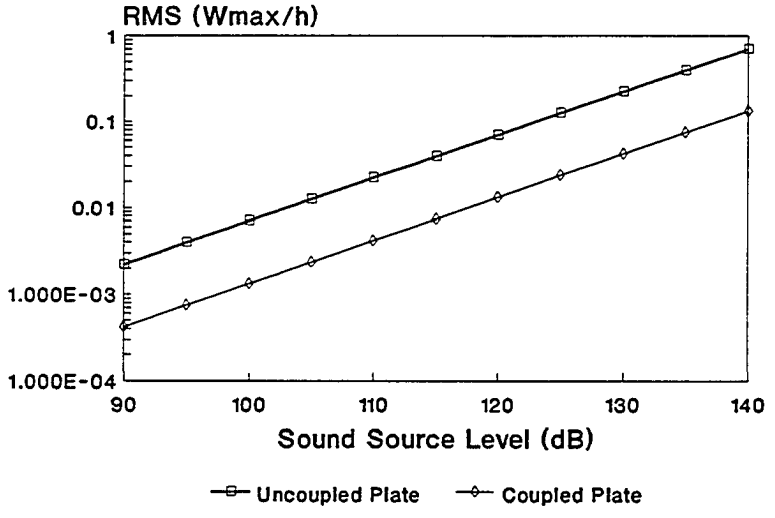

Figure 4.29 Random Response of Simply Supported Composite Panel and Acoustic Duct System.

(0°/90°/0°/90°/0°/90°/0°) properties are given on page 92. As in the earlier case, 25 finite elements and 150 boundary elements are used. Once again, the coupled system produces lower RMS (W_{max}) values. Note that the composite panel response is affected to a greater extent by the coupling than the brass panel. The composite panel is affected more, because the coupled natural frequency is increased from the uncoupled natural frequency by a greater amount. The uncoupled panel results agree with classical and other finite element solutions.

The next coupled system consists of a clamped rectangular panel and the acoustic duct. The panel is 30.48 x 15.24 cm. and 0.16256 cm. thick. The duct cavity characteristics and aluminum panel properties are given on page 86 and the same Graphite/Epoxy panel is used from above. Figure 4.30 shows the random response of the coupled and uncoupled clamped aluminum panel. Figure 4.31 shows the random response of a clamped composite panel. Once again, 25 finite elements and 150 boundary elements are used. As expected, the RMS (W_{max}) responses of the coupled systems are less than the responses of the uncoupled system.

Figures 4.28 to 4.31 help us to infer that the coupling between sound and structure, greatly affects the random response of the system.

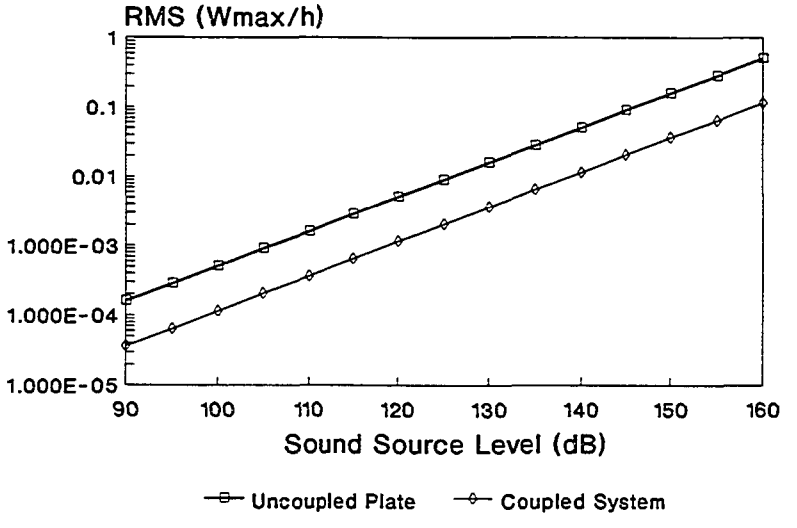

Figure 4.30 Random Response of Clamped Aluminum Panel and Acoustic Duct System.

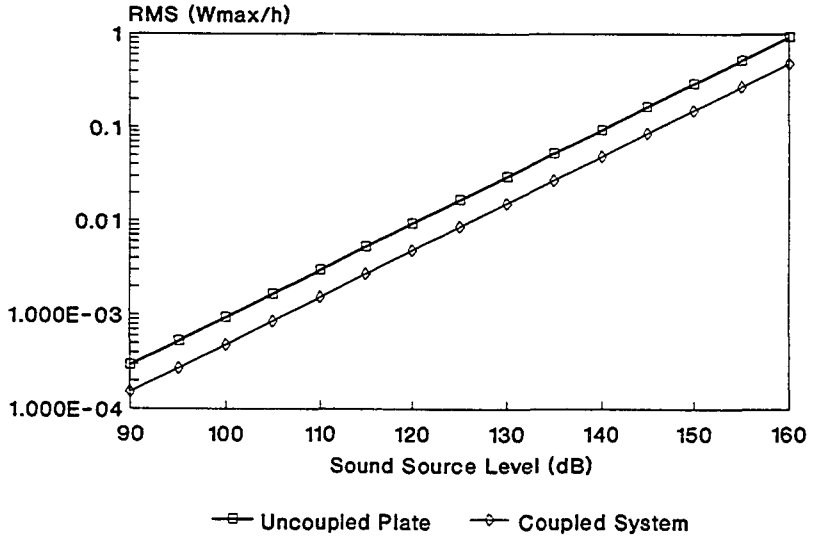

Figure 4.31 Random Response of Clamped Composite Panel and Acoustic Duct System.

4.4 Modelling The Thermal Acoustic Fatigue Apparatus (TAFA) at NASA Langley Research Center

Until now, we have seen that the coupled boundary/finite element procedure gives accurate and reasonable results. Future high speed aircraft such as the National Aerospace Plane (NASP), High Speed Civil Transport (HSCT) and the next generation of fighters will be subjected to intense thermal and acoustic environments [69]. In an attempt to test these environments, the Thermal Acoustic Fatigue Apparatus (TAFA) at NASA Langley Research Center was built. TAFA, shown in Figure 4.32, is a grazing incidence, high-intensity noise apparatus with capability of generating sound pressure levels of 168 dB and temperatures of 2000 °F. In this study, the temperature effects are not considered, but we account for acoustic pressures to be harmonic or random with a frequency input range of 0-500 Hz.

4.4.1 Harmonic Response of Panels in TAFA Facility

Three plates, brass, aluminum and graphite/epoxy, of 15x15x0.036 in. are considered. The plate and the acoustic test section are discretized into 9 finite elements and 384 boundary elements, respectively. The input and output pressure levels are specified as boundary conditions. The output boundary condition is set at 60 dB and the input pressure level varies from 90 to 140 dB. The input frequency of the external source is set at 20 Hz, because this is close

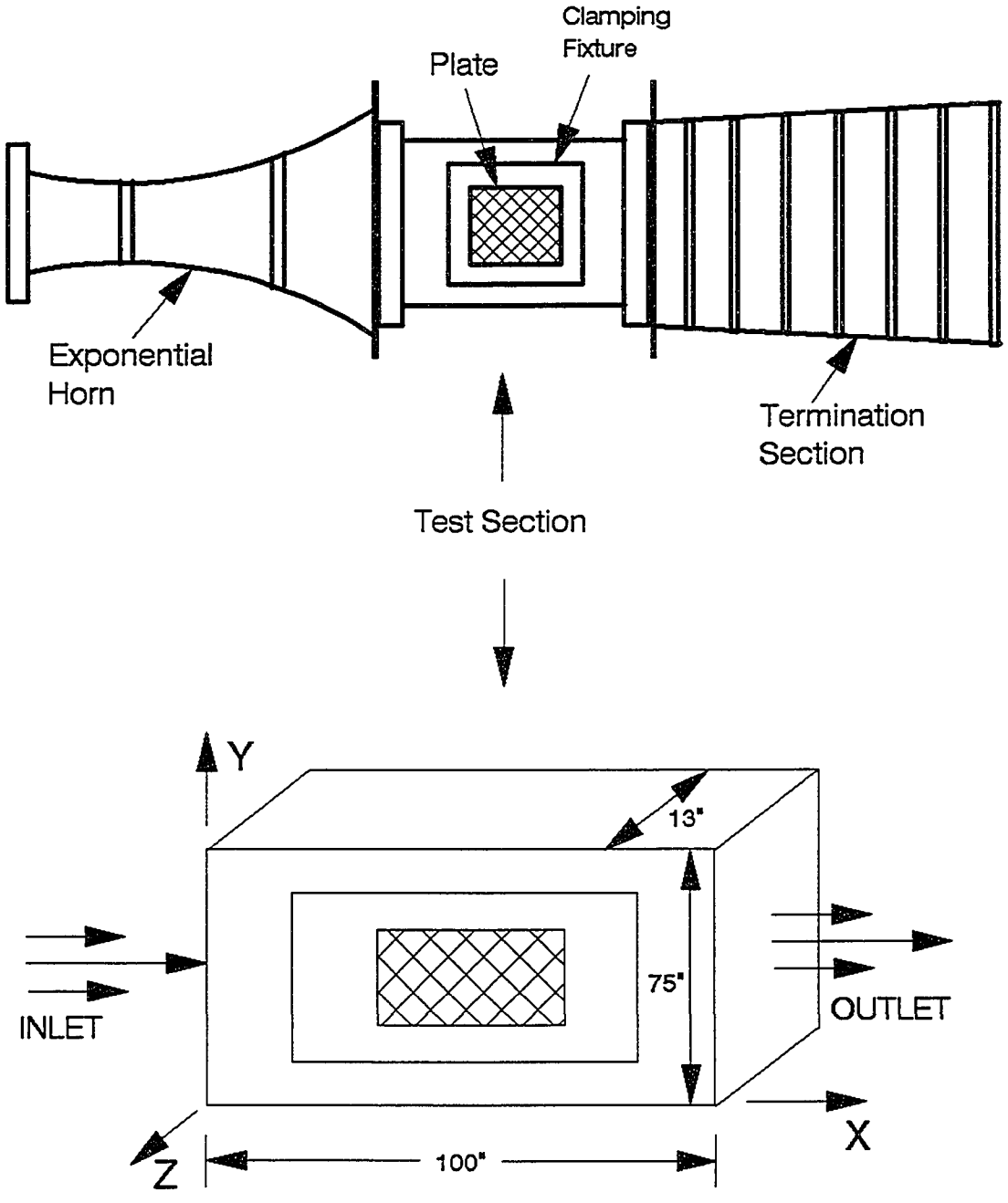

Figure 4.32 Thermal Acoustic Fatigue Apparatus (TAFA).

to the first natural frequency of the brass panel. This excites a first mode shape of each plate. The center displacements of the simply supported plates of the coupled system versus the input sound pressure level are shown in Figure 4.33. The composite panel is made of graphite/epoxy with a $[45°/-45°/45°/-45°]_s$ layup. The composite panel has the following properties: E_{11}=22.5E6 psi, E_{22}=1.17E6 psi, ν_{12}=.22, G_{12}=0.66E6 psi, ρ=0.056 lb/in^3 and ζ_1=0.01.

Figure 4.34 shows the displacement results for the clamped aluminum, brass and composite panels. From the Figures 4.33 and 4.34, we notice that the deflections of the composite panel are lower or equivalent to the deflections of the aluminum and brass panels. The considerable advantage of the composite panel is in the strength-to-weight ratio. The weights of the composite, aluminum and brass panels are .45 lb, .81 lb and 2.49 lb, respectively.

Two other features of the TAFA facility were also analyzed. First, the center panel deflection was calculated as a function of frequency for the simply supported composite panel listed above. Secondly, the pressure was analyzed 1/2" from the center of the panel on the interior of the duct. The center panel deflection and the acoustic pressures, as well as the uncoupled acoustic response, are seen in Figure 4.35. The acoustic response is defined as a sound pressure level,

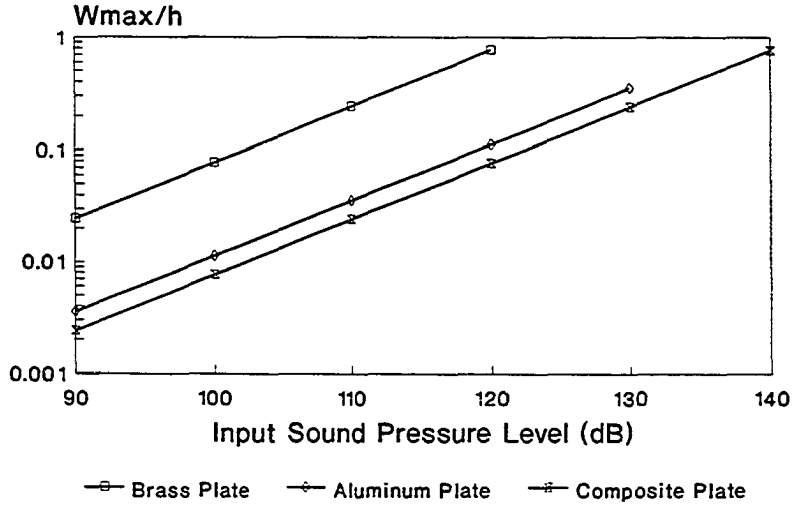

Figure 4.33 Harmonic Response of Simply Supported Panels.

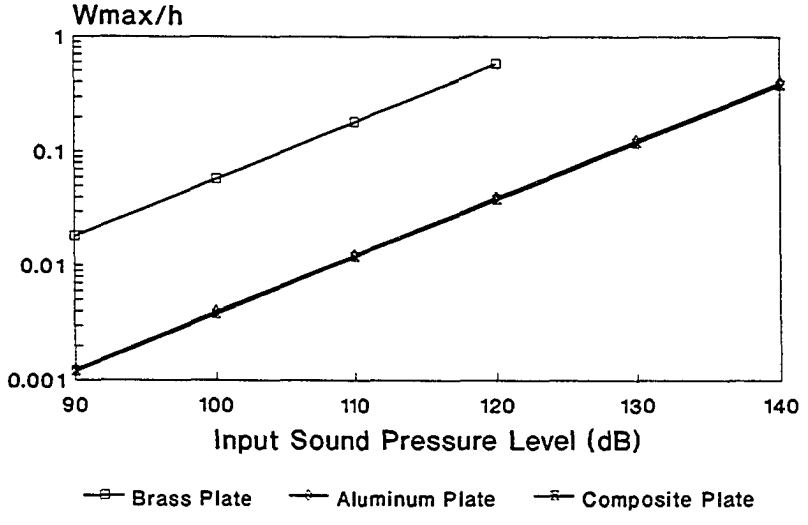

Figure 4.34 Harmonic Response of Clamped Panels.

$$Sound\ Pressure\ Level = 20 Log \left[\frac{P_{center}}{P_{ref}} \right], \qquad (4.7)$$

where $P_{ref}=2x10^{-5}$ Pa. From Figure 4.35, we can see that the first coupled natural frequency of the panel is around 42 Hz. As the panel resonates at its natural frequencies, large displacements are occurring in the panel and the acoustic domain. These large acoustic displacements produce higher acoustic pressures and hence lead to the higher acoustic response peaks.

In order to find the uncoupled acoustic natural frequencies, the same analysis was run in the TAFA facility with a rigid wall in place of the panel. The first three acoustic natural frequencies are 109 Hz, 179 Hz, and 240 Hz. The second uncoupled plate natural frequency was 98.7 Hz. Figure 4.36 shows the structure and acoustic response plotted at x=12.5 in. and y=7.5 in. Figure 4.36 shows that the structure is driving the system at the second natural frequency of the panel (98.7 Hz). Also from Figure 4.35, we can see that the acoustic response curve mirrors the structure response curve. This figure shows the strength of the coupled BEM-FEM formulation. The acoustic and structure response can simultaneously be monitored in the coupled system.

The mode shape of the panel and the distribution of acoustic pressure are shown for the first coupled natural frequency (42 Hz) in Figure 4.37. Figure 4.38 shows the mode

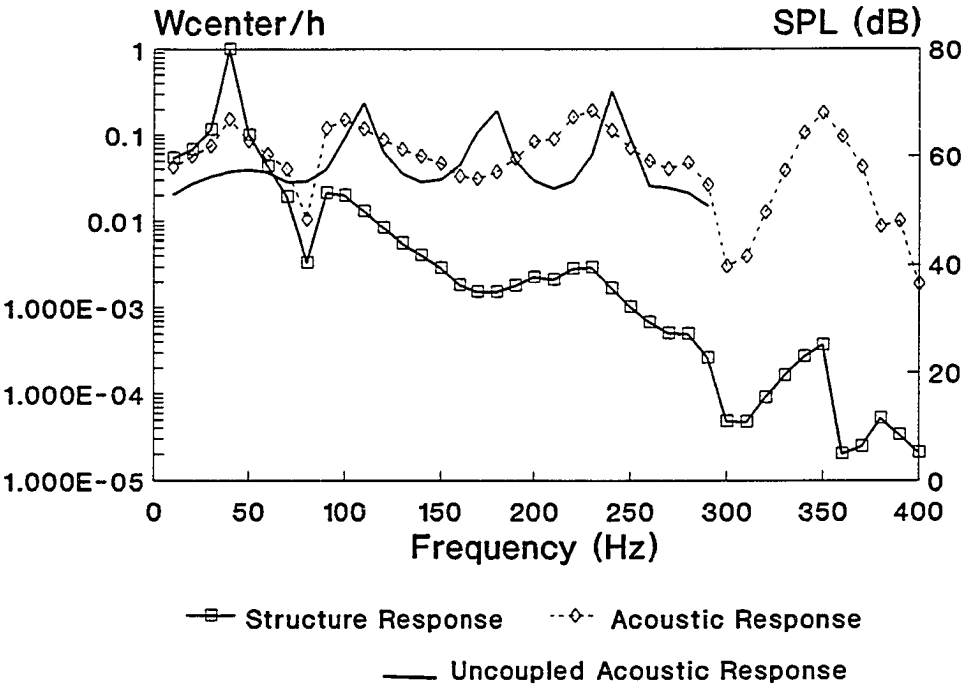

Figure 4.35 Structure and Acoustic Response for Simply Supported Composite Panel in TAFA.

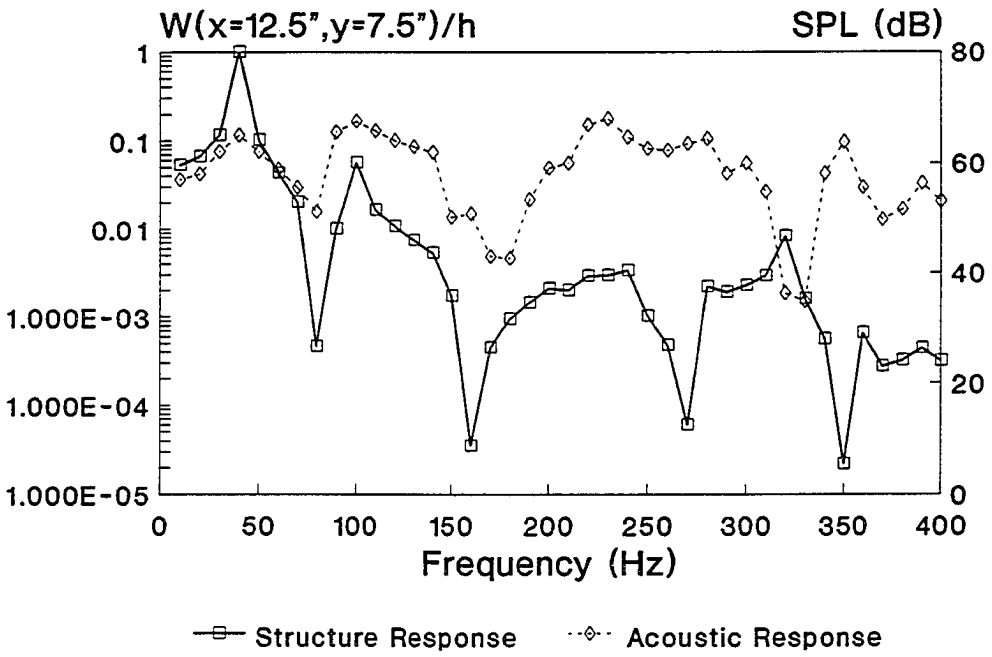

Figure 4.36 Structure and Acoustic Response for Simply Supported Composite Panel in TAFA at x=12.5" and y=7.5".

shape and the pressure distribution at 100 Hz, which is close to the second coupled natural frequency. Figure 4.38 shows that the panel is vibrating similar to a 2:1 mode shape.

4.4.2 Random Response of Panels in TAFA Facility

A random response of the coupled system is now analyzed, since the TAFA facility can produce a random acoustic input. A cut-off frequency of 400 Hz is assumed, which easily covers the first few modes of the composite panel. The same composite panel from Section 4.4.1 is used again. Figure 4.39 shows the random response for the simply supported and the clamped composite panels, where the output noise level is set at 60 dB and the input noise level is varied from 130 to 160 dB. The overall sound spectral level in Figure 4.39 is the difference between the input noise and the output noise. The random response of the clamped composite panel is compared with the response of the simply supported composite panel in Figure 4.39. The coupled RMS displacement of the clamped panel is less than the displacement of the simply supported panel.

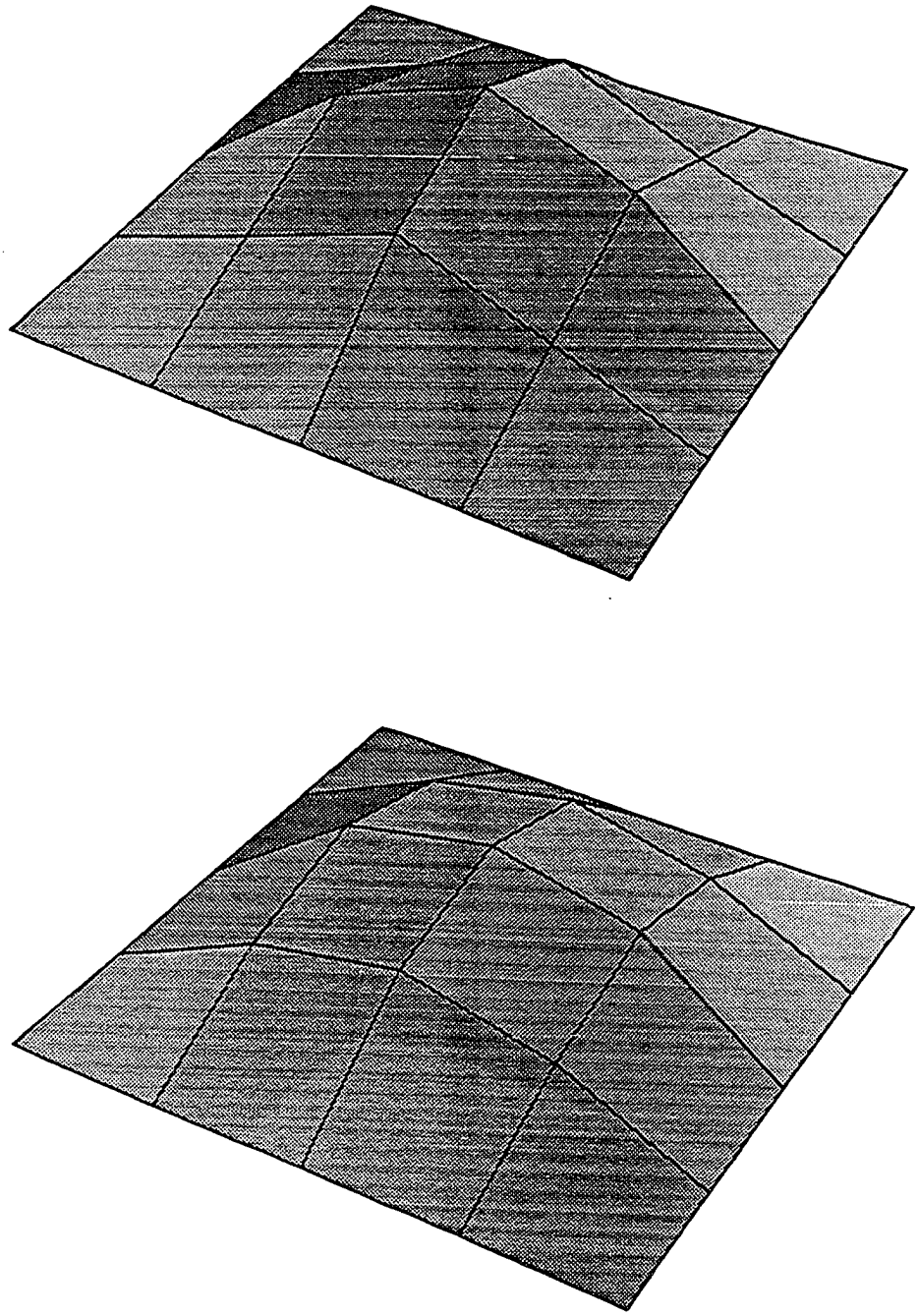

Figure 4.37 Panel Mode Shape (Top) and Acoustic Pressure Distribution (Bottom) at 42 Hz.

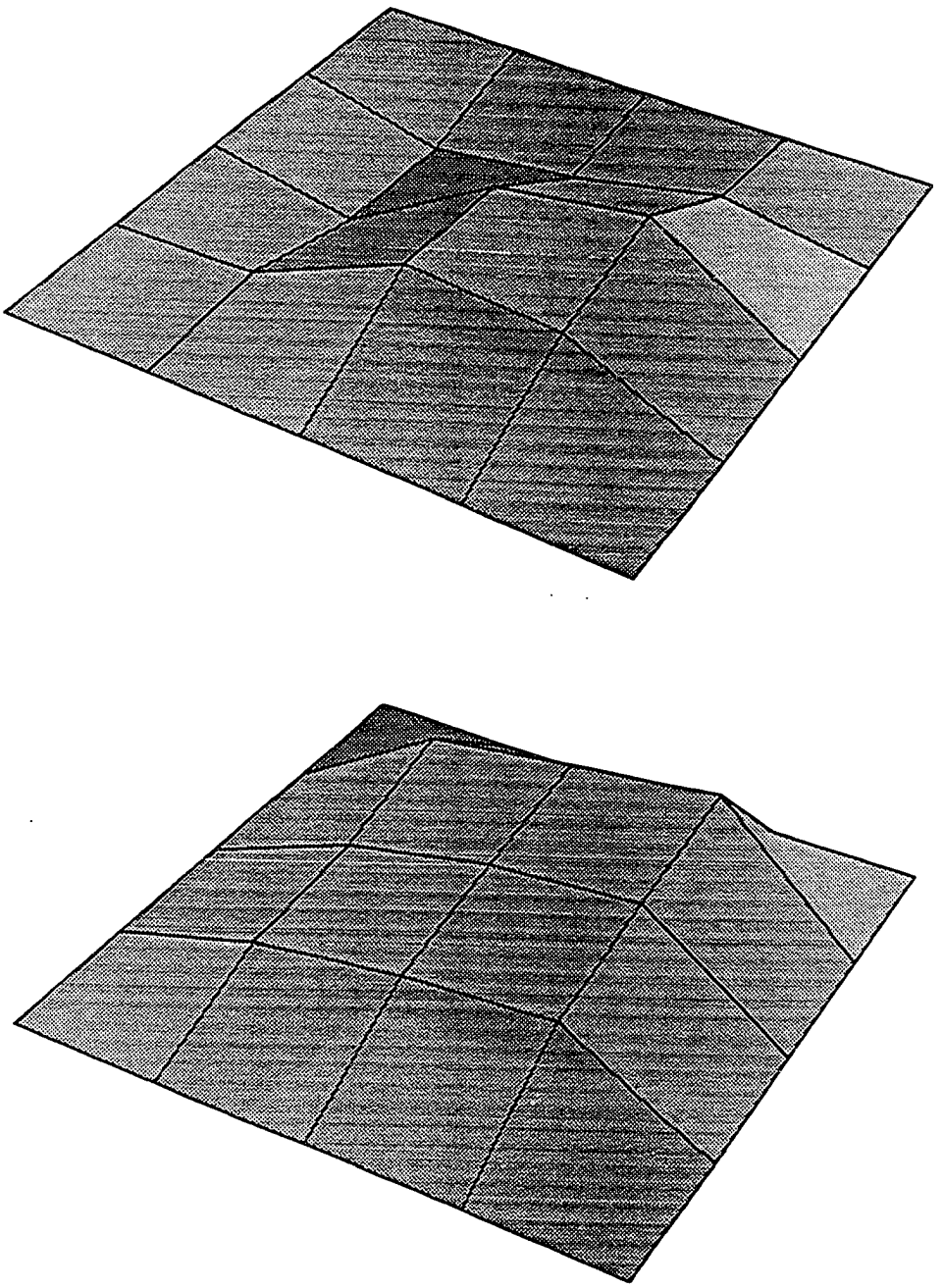

Figure 4.38 Panel Mode Shape (Top) and Acoustic Pressure Distribution (Bottom) at 100 Hz.

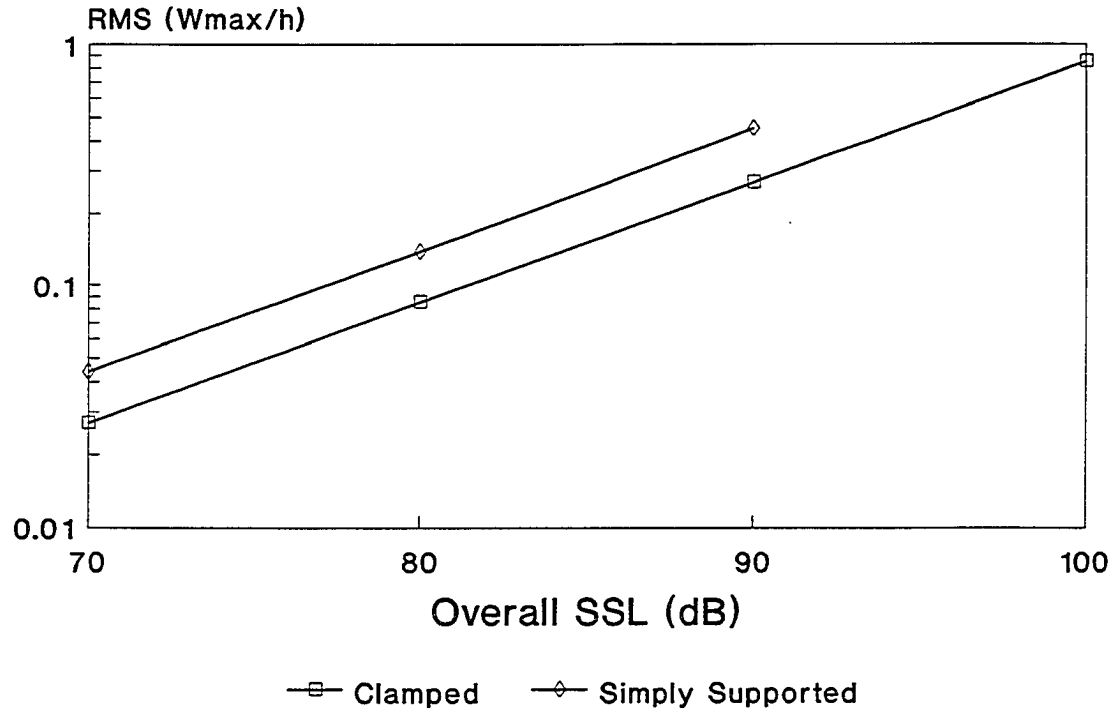

Figure 4.39 Random Response of Clamped and Simply Supported Panels in the TAFA Facility.

Chapter 5

Summary and Conclusions

5.1 Concluding Remarks

In this study, we have presented the principles of a very useful tool for analyzing real world, sound-structure environments. In order to accurately model these complex coupled problems, coupling of the structure and acoustic environments must be done carefully. The coupled system effects were shown to be very important for certain types of problems. For example, the cavity-backed plate problem showed a significant first frequency shift due to the coupling. In our attempt to model real environments, random response analysis of the coupled system was also performed. The coupled harmonic response gave very accurate results when compared with existing analytical, exact and experimental data for simplistic problems. The Thermal Acoustic Fatigue Apparatus at NASA Langley Research Center was modelled and analyzed. The coupled BEM-FEM method shows the relationship between the interior acoustic pressure and the structure response for a 0-400 Hz frequency range.

The boundary element method was also applied to interior acoustic domain problems. Two and three-dimensional analyses

were performed on simple and complex geometric-shaped ducts. Constant and linear boundary elements gave very satisfactory results for the 2-D case and constant elements for the 3-D case.

Currently, industry is striving to couple the boundary element and finite element methods in order to more effectively model aerospace and automobile systems. This study is an attempt to enhance our understanding in that direction. Applying random analysis and adapting to composite materials allows designers to model real world problems. The random response formulation of the coupled finite element and boundary element method can provide a tremendous approximation method for complex coupled structural-acoustic systems.

5.2 Future Work

Many areas of research still need to be considered in order to more accurately model real world systems. In order to continue this study, four areas of research can be completed in the near future. First, the three-dimensional constant boundary element needs to be extended to a linear or even a quadratic type element. This will allow users to model more complex geometry systems as well as improve the accuracy of the results. Secondly, temperature effects can also be considered for the acoustic and the structural domains. Temperature effects will greatly affect the structure, which will in-turn greatly affect the acoustic response. The next

area of research could be in the harmonic nonlinear area. The structure can be modelled with nonlinear analysis where the time components of the nonlinear terms neglect the period doubling effects. The last area of interest is in the random nonlinear analysis. The nonlinear analysis of the structure can be incorporated into the current finite element analysis of the structure.

REFERENCES

1. Edson, J.R., "Review of Testing and Information on Sonic Fatigue," Doc. No. D-17130, Boeing Co., 1957.

2. Powell, C.A. and Parrott, T.L., "A Summary of Acoustic Loads and Response Studies," Tenth National Aero-Space Plane Technology Symposium, Paper No. 106, April, 1991.

3. Bernhard, R.J. and Kipp, C.R., "Prediction of Acoustical Response of Three-Dimensional Cavities Using an Indirect Boundary Element Method," NASA Conference Publication 2404, 1985.

4. Beskos, D.E., "Boundary Element Methods in Dynamic Analysis,"*Appl Mech Rev*, Vol. 40, No. 1, January 1987, pp. 1-23.

5. Bernhard, R.J., Gardner, B.K., Mollo, C.G., and Kipp, C.R., "Prediction of Sound Fields in Cavities Using Boundary Element Methods," Proceedings of AIAA 10th Aeroacoustic Conference, Seattle, WA, 1986, pp. 4-12.

6. Jiang, J.K. and Prasad, M.G., "On the Applications of the Boundary-Element Method to Acoustical Field Studies of Vibrating Structures," *J. of Vibration, Acoustics, Stress, and Reliability in Design*, Vol. 108, October 1986, pp. 454-461.

7. Prasad, M.G., Yeh, C.J. and Jiang, J.K., "Evaluation of Sound Radiation Efficiency Using Boundary Element Method, "International Congress on Recent Developments in Air-and Structure-Borne Sound and Vibration, 1990, pp. 475-482.

8. Pijaca, J. and Prasad, M.G., "A Review of the Developments in Application of Boundary Element Method to Sound Radiation Analysis," International Congress on Recent Developments in Air-and Structure-Borne Sound and Vibration, 1990, pp. 467-474.

9. Koopmann, G.H., Song, L. and Fahnline, J.B., "A Method for Computing Acoustic Fields Based on the Principle of Wave Superposition," *J. Acoust. Soc. Am.*, Vol 86, No. 6, December 1989, pp. 2433-2438.

10. Wu, T.W., Seybert, A.F. and Wan, G.C., "On the Numerical Implementation of a Cauchy Principal Value Integral to Insure a Unique Solution for Acoustic Radiation and Scattering," *J. Acoust. Soc. Am.*, Vol. 90, No. 1, July 1991, pp. 554-560.

11. Amini, S., Ke, C. and Harris, P.J., "Iterative Solution of Boundary Element Equations for the Exterior Helmholtz Problem, "*J. of Vibration and Acoustics*, Vol. 112, April 1990, pp. 257-262.

12. Seybert, A.F, Soenarko, B., Rizzo, R.J. and Shippy, D.J., "An Advanced Computational Method for Radiation and Scattering of Acoustic Waves in Three Dimensions," *J. Acoust. Soc. Am.*, Vol. 77, No. 2, February 1985, pp. 362-368.

13. Hall, W.S. and Robertson, W.H., "Boundary Element Methods for Acoustic Wave Scattering," *Boundary Elements X: Geomechanics, Wave Propagation, and Vibrations*, Vol. 4, Springer-Verlag, Berlin, 1988, pp. 301-315.

14. Dokumaci, E., "An Integral Equation Formulation for Boundary Element Analysis of Acoustic Radiation Problems in Viscous Fluids," *J. of Sound and Vibration*, Vol. 147, No. 2, 1991, pp. 335-348.

15. Park, J., and Eversman, W., "Two-Dimensional Sound Propagation Over a Ridge," Proceedings of AIAA 13th Aeroacoustic Conference, Tallahassee, FL, 1990, pp. 1-8.

16. Coyette, J.P. and Fyfe, K.R., "An Improved Formulation for Acoustic Eigenmode Extraction from Boundary Element Models, "*J. of Vibration and Acoustics*, Vol. 112, July 1990, pp. 392-398.

17. Kane, J.H., Mao, S. and Everstine, G.C., "A Boundary Element Formulation for Acoustic Shape Sensitivity Analysis," *J. Acoust. Soc. Am.*, Vol. 90, No. 1, July 1991, pp. 561-573.

18. Pates, C.S. and Shirahatti, U.S., "Application of the Boundary Element Method to Predict the Acoustic Field in a Two-Dimensional Duct," Proceedings of the 13th Biennial ASME Conference for Mechanical Vibration and Noise, Paper No. 54, Miami, FL, 1991.

19. Pates, C.S., "Analysis of Two-Dimensional Ducts with Sudden Area Changes Using the Boundary Element Method," Proceedings of the 33rd Structures, Structural Dynamics, and Materials Conference, AIAA-92-2296-CP, Vol. 1, Dallas, TX, 1992, pp.360-367.

20. Utsuno, H., Wu, T.W. and Seybert, A.F., "Prediction of Sound Fields in Cavities with Sound Absorbing Materials," *AIAA Journal*, Vol. 28, No. 11, November 1990, pp. 1870-1876.

21. Cunefare, K.A. and Koopman, G.H., "A Boundary Element Approach to Optimization of Active Noise Control Sources on Three-Dimensional Structures," *J. of Vibration and Acoustics*, Vol. 113, July 1991, pp. 387-394.

22. Hussain, K.A. and Peat, K.S., "Boundary Element Analysis of Low Frequency Cavity Acoustical Problems," Internal Report #A158, Sponsored by the Dept. of Trade & Industry, London, England, April 1992, pp. 1-24.

23. Seybert, A.F. and Wu, T.W., "Recent Developments and Applications of the BEM in Acoustics and Noise Control, "*Boundary Elements X: Geomechanics, Wave Propagation, and Vibrations*, Vol. 4, Springer-Verlag, Berlin, 1988, pp. 289-299.

24. Soenarko, B. and Seybert, A.F., "Recent Developments of The Boundary Element Method (BEM) to Noise Control Problems, "Proceedings of Inter-Noise 91, Vol. 2, Sydney, Australia, December 1991, pp. 1169-1172.

25. Munjal, M.L., "State of the Art of Acoustics of Active and Passive Mufflers," Vibration Inst, *The Shock and Vibration Digest*, Vol. 22, No. 2, 1990, pp. 3-12.

26. Pates, C.S. and Shirahatti, U.S., "Boundary Element Analysis of the Acoustic Field in Three-Dimensional Regular and Irregular Ducts," Proceedings of the 1993 National Conference of Noise Control Engineering, Paper No. 91, Williamsburg, VA, May, 1993, pp. 111-116.

27. Suzuki, S., Maruyama, S. and Ido, H., "Boundary Element Analysis of Cavity Noise Problems with Complicated Boundary Conditions," *J. of Sound and Vibration*, Vol 130, No. 1, 1989, pp. 79-91.

28. Kipp, C.R., "Prediction of Sound Fields in Acoustical Cavities Using BEM," Master's Thesis, Purdue University, 1985.

29. Brebbia, C.A. and Dominguez, J., *Boundary Elements An Introductory Course*, McGraw-Hill, New York, 1989.

30. Seybert, A.F., Wu, T.W. and Wu, X.F., "Radiation and Scattering of Acoustic Waves from Elastic Solids and Shells Using the Boundary Element Method," *J. Acoust. Soc. Am.*, Vol. 84, No. 5, November 1988, pp.1906-1912.

31. Kipp, C.R. and Bernhard, R.J., "Prediction of Acoustical Behavior in Cavities Using an Indirect Boundary Element Method," *J. of Vibration, Acoustics, Stress, and Reliability in Design*, Vol. 109, January 1987, pp. 22-28.

32. Loeffler, C.F. and Mansur, W.J., "Analysis of Time Integration Schemes for Boundary Element Applications to Transient Wave Propagation Problems," *Boundary Element Techniques Applications in Stress Analysis and Heat Transfer,* McGraw-Hill, New York, 1987.

33. Shaw, R.P., "Integral Equation Methods in Acoustics," *Boundary Elements X: Geomechanics, Wave Propagation, and Vibrations*, Vol. 4, Springer-Verlag, Berlin, 1988, pp. 241-243.

34. Belytschko, T., Chang, H.S. and Lu, Y.Y., "A Variationally Coupled Finite Element-Boundary Element Method," *J. of Computers and Structures*, Vol. 33, No. 1, 1989, pp. 17-20.

35. Hsiao, G.C., "The Coupling of Boundary Element and Finite Element Methods," *ZAMM Z. angew. Math. Mech.*, Vol. 70, 1990, pp. 493-503.

36. Girija Vallabhan, C.V., "Coupling of BEM/FEM Technology: An Overview," *Boundary Element Techniques Applications in Stress Analysis and Heat Transfer,* McGraw-Hill, New York, 1987.

37. Poterasu, V.F. and Mihalache, N., "Analysis by BEM and FEM of a Plane Model With a Complex Geometry," *Variational Methods in Engineering*, McGraw-Hill, New York, 1985, pp. 21-28.

38. Jiang, J.K. and Prasad, M.G., "Studies on Acoustical Fields of Beam-Type Vibrating Structures," Proceedings of Noise-Con 85, Columbus, OH, 1985, pp. 165-170.

39. De Paula, F.A., Telles, J.C.F., and Mansur, W.J., "Combination of Boundary Elements and Finite Elements to Solve Two-Dimensional Elasticity Problems,"*Boundary Element Techniques Applications in Stress Analysis and Heat Transfer,* McGraw-Hill, New York, 1987.

40. Cox, J., "Coupling of The Finite and Boundary Element Methods in Elastostatics," NCEL Technical Note, November 1988.

41. Sawada, T. and Sakaguchi, H., "Indentation by Circular Punch with BEM/FEM Combination Analysis," *Theory and Applications of BEM*, McGraw-Hill, New York, 1990, pp. 329-336.

42. Jianqiao, Y., "Non-Linear Bending Analysis of Plates and Shells by Using a Mixed Spline Boundary Element and Finite Element Method," *Int. J. for Numerical Methods in Engineering*, Vol. 31, 1991, pp. 1283-1294.

43. Seybert, A.F., Cheng, C.Y.R. and Wu, T.W., "The Solution of Coupled Interior/Exterior Acoustic Problems Using the Boundary Element Method," *J. Acoust. Soc. Am.*, Vol. 88, No. 3, September 1990, pp. 1612-1618.

44. Niku, S.M., Adey, R.A., Klein, M., Teichert, W. and Kries, M., "Analysis of Fluid Structure Interaction of Spacecraft's Fluid Tanks Using Combined Boundary Element and Finite Element Methods," Proceedings of the International Conf. on Spacecraft Structures and Mechanical Testing, Noordwijk, The Netherlands, April 1991, pp. 525-533.

45. Everstine, G.C. and Cheng, R.S., "Coupled BE/FE/BE Approach for Scattering From Fluid-Filled Structures," 18th NASTRAN User's Colloquium, 1990, pp. 150-164.

46. Amini, S. and Harris, P.J., "Boundary Element and Finite Element Methods for the Coupled Fluid-Structure Interaction Problems," *Boundary Elements X*, McGraw-Hill, New York, 1988, pp. 509-520.

47. Everstine, G.C., Henderson, F.M. and Schuetz, L.S., "Coupled NASTRAN/Boundary Element Formulation for Acoustic Scattering," 15th NASTRAN User's Colloquium, 1987, pp. 250-265.

48. Schenck, H.A. and Benthien, G.W., "The Application of a Coupled Finite-Element Boundary-Element Technique to Large-Scale Structural Acoustic Problems," *Advances in Boundary Elements: Volume 2 - Field and Fluid Solutions*, McGraw-Hill, New York, 1990, pp. 309-318.

49. Kagawa, Y. and Murai, T., "Simulation of Nonlinear Acoustic Wave Scattering by Boundary Element-Finite Element Combination Approach," *Theory and Applications of the Boundary Element Method*," McGraw-Hill, New York, 1990, pp. 313-320.

50. Everstine, G.C. and Henderson, F.M., "Coupled Finite Element/Boundary Element Approach for Fluid-Structure Interaction," *J. Acoust. Soc. Am.*, Vol. 87, No. 5, May 1990, pp. 1938-1947.

51. Fronk, T.H. and Mahan, J.R., "Boundary Element Model of the Acoustic Field Radiated by a Baffled Rectangular Plate," International Congress on Recent Developments in Air-and Structure-Borne Sound and Vibration, 1990, pp. 439-444.

52. Yuying, H., "A Mixed FE-BE Method for Coupled Vibration of Floating Plates With Complicated Shape," *Theory and Applications of the Boundary Element Method*," McGraw-Hill, New York, 1990, pp. 321-328.

53. Suzuki, S., Imai, M. and Ishiyama, S., "Boundary Element Analysis of Structural-Acoustic Problems," *Boundary Elements VI*, McGraw-Hill, New York, 1984, pp. 27-35.

54. Tanaka, M. and Masuda, Y., "Boundary Integral Equation Approach to Structural-Acoustic Coupling Problems," *Boundary Elements IX Volume 3 - Fluid Flow and Potential Applications*, McGraw-Hill, New York, 1987, pp. 19-33.

55. Mariem, J.B. and Hamdi, M.A., "A New Boundary Finite Element Method for Fluid-Structure Interaction Problems," *Int. J. for Numerical Methods in Engineering*, Vol. 24, 1987, pp. 1251-1267.

56. Tanaka, M. and Masuda, Y., "Boundary Element Method Applied to Certain Structural-Acoustic Coupling Problems," *Computer Methods in Applied Mechanics and Engineering*, Vol. 71, 1988, pp. 225-234.

57. Guy, R.W. and Bhattacharya, M.C., "The Transmission of Sound Through a Cavity-Backed Finite Plate," *J. of Sound and Vibration*, Vol. 27, No. 2, 1973, pp. 207-223.

58. Bokil, V.B., "Modal Analysis of Gyroscopically Coupled Sound-Structure Interaction Problems," Master's Thesis, Old Dominion University, 1992.

59. Fyfe, K.R., Coyette, J.P.G. and van Vooren, P.A., "Acoustic and Elasto-Acoustic Analysis Using Finite Element and Boundary Element Methods," *Sound and Vibration*, Vol. 25, No. 12, December 1991, pp. 16-22.

60. Suzuki, S., "Boundary Element Analysis of Structural-Acoustic Problems With Complicated Boundary Conditions," *Advances in Boundary Elements: Volume 2 - Field and Fluid Solutions*, McGraw-Hill, New York, 1990, pp. 341-353.

61. Sung, S.H. and Nefske, D.J., "A Coupled Structural-Acoustic Finite Element Model for Vehicle Interior Noise Analysis," *J. of Vibration, Stress, and Reliability in Design*, Vol. 106, April 1984, pp. 314-318.

62. Seybert, A.F. and Oswald, F.B., "Experimental Validation of Boundary Element Methods for Noise Prediction," NASA-TM-105729, 1992.

63. Seto, W.W., *Acoustics*, McGraw-Hill, New York, 1971, Chapter 4.

64. Munjal, M.L., *Acoustics of Ducts and Mufflers*, Wiley and Sons, New York, 1987, Chapter 2.

65. Kinsler, L.E., Frey, A.R., Coppens, A.B. and Sanders, J.V., *Fundamentals of Acoustics*, Wiley and Sons, New York, 1982, pp. 98-108.

66. Abramowitz, M. and Stegun, I.A., *Handbook of Mathematical Functions*, Dover Publications, New York, 1972, pp. 496-499.

67. Chiang, C.K., *A Finite Element Large Deflection Multiple-Mode Random Response Analysis of Complex Panels with Initial Stresses Subjected to Acoustic Loading*, PhD. Dissertation, Old Dominion Univ., 1988.

68. Yang, C.Y., *Random Vibration of Structures*, John Wiley and Sons, New York, 1986.

69. Clevenson, S.A. and Daniels, E.F., "Capabilities of the Thermal Acoustic Fatigue Apparatus," NASA Technical Memorandum 104106, February 1992.

70. Chertock, G., "Integral Equation Methods in Sound Radiation and Scattering from Arbitrary Surfaces," Rep. 3538, David Taylor Naval Ship Research and Development Center, Bethesda, MD, 1971.

APPENDIX A

The integrals in Equations (2.18), (2.22) and (2.25) must be evaluated in order to obtain each element of the influence matrices, G_{mj} and $\hat{H}_{mj}$. The easiest and most efficient way of solving these integrals is approximating them with the Gauss quadrature scheme. The first step using Gauss quadrature is to approximate the integral by transferring the limits from -1 to 1 and then apply the Gauss rule to the new integral. In other words,

$$I=\int_{b}^{a} f(x)\,dx = \int_{-1}^{1} F(x_k)\,dx_k = \tilde{I} \cong \sum_{w=1}^{nn} W_w F(x_w)\,, \qquad \text{(A.1)}$$

where W_w are the weighting functions, x_w are the gauss points, and nn is the total number of gauss points. A four-point gauss scheme is used and the weight and point values are shown below,

Table A.1 Gauss Points and Gauss Weights

Point	Gauss Point x_w	Weight W_w
1,2	±.86113631	.34785485
3,4	±.33998104	.65214515

Note that the transfer from the exact integral to the Gauss integral requires a transformation in the coordinates

and hence a scaling factor in terms of the element size is produced. A four-point Gauss scheme was found to be sufficient in calculating the integrals of Equations (2.18), (2.22) and (2.25).

The Struve functions given in Equations (2.35) and (2.36) are not defined as Fortran functions or in the IMSL libraries. Therefore, approximations to the Struve functions must be incorporated. The approximation to the Struve function of the first kind is

$$S_{T0}(z) = \frac{4}{\pi}\sum_{k=0}^{\infty} \frac{J_{2k+1}(z)}{2k+1}, \qquad (A.2)$$

or

$$S_{T0}(z) = \frac{4}{\pi}\left\{\frac{J_1(z)}{1} + \frac{J_3(z)}{3} + \frac{J_5(z)}{5} + \frac{J_7(z)}{7} + \cdots\right\}, \qquad (A.3)$$

where J_i is the first Bessel function of the ith kind. The approximation to the Struve function of the second kind is

$$S_{T1}(z) = \frac{2}{\pi} - \frac{2}{\pi}J_o(z) + \frac{4}{\pi}\sum_{k=1}^{\infty} \frac{J_{2k}(z)}{4k^2-1} \qquad (A.4)$$

or

$$S_{T1}(z) = \frac{2}{\pi} - \frac{2}{\pi}J_o(z) + \frac{4}{\pi}\left\{\frac{J_2(z)}{3} + \frac{J_4(z)}{15} + \frac{J_6(z)}{35} + \cdots\right\}. \qquad (A.5)$$

These approximations to the Struve functions give very accurate solutions [66].

APPENDIX B

The element selected for this study is a four-node rectangular element as shown in Figure 3.1 [67]. The element is a C^1 conforming element with twenty-four degrees of freedom (six at each node w, w_x, w_y, w_{xy}, u, and v). The shape functions for the transverse and in-plane displacements are

$$H_w=\{1 \;\; x \;\; y \;\; x^2 \;\; xy \;\; y^2 \;\; x^3 \;\; x^2y \;\; xy^2 \;\; y^3 \;\; x^3y \;\; x^2y^2 \;\; xy^3 \;\; x^3y^2 \;\; x^2y^3 \;\; x^3y^3\}, \tag{B.1}$$

and

$$H_u=\{1 \;\; x \;\; y \;\; xy \;\; 0 \;\; 0 \;\; 0 \;\; 0\},$$

$$H_v=\{0 \;\; 0 \;\; 0 \;\; 0 \;\; 1 \;\; x \;\; y \;\; xy\}. \tag{B.2}$$

The generalized coordinates from Equations (3.4), (3.5) and (3.6) are defined as

$$\alpha = \{\alpha_1 \;\; \alpha_2 \;\; \alpha_3 \;\; \alpha_4 \;\; \alpha_5 \;\; \alpha_6 \;\; \alpha_7 \;\; \alpha_8 \;\; \alpha_9 \;\; \alpha_{10} \;\; \alpha_{11} \;\; \alpha_{12} \;\; \alpha_{13} \;\; \alpha_{14} \;\; \alpha_{15} \;\; \alpha_{16}\},$$

and

$$\beta=\{\beta_1 \;\; \beta_2 \;\; \beta_3 \;\; \beta_4 \;\; \beta_5 \;\; \beta_6 \;\; \beta_7 \;\; \beta_8\}. \tag{B.3}$$

The degrees of freedom in bending and membrane are

$$\{W_b\}^T=[W_1\ W_2\ W_3\ W_4\ W_{x1}\cdots W_{x4}\ W_{y1}\cdots W_{y4}\ W_{xy1}\cdots\ W_{xy4}], \qquad \text{(B.4)}$$

and

$$\{W_m\}=[u_1\ u_2\ u_3\ u_4\ v_1\ v_2\ v_3\ v_4]. \qquad \text{(B.5)}$$

The inverse of the transformation matrix, $[T_b]$ from Equation (3.6) is given as

$$[T_b]^{-1} = \begin{bmatrix}
1 & 0 & 0 & 0 & 0 & 0 & 0 & 0 \\
1 & al & 0 & al^2 & 0 & 0 & al^3 & 0 \\
1 & al & bl & al^2 & al\ bl & bl^2 & al^3 & al^2\ bl \\
1 & 0 & bl & 0 & 0 & bl^2 & 0 & 0 \\
0 & 1 & 0 & 0 & 0 & 0 & 0 & 0 \\
0 & 1 & 0 & 2al & 0 & 0 & 3al^2 & 0 \\
0 & 1 & 0 & 2al & bl & 0 & 3al^2 & 2al\ bl \\
0 & 1 & 0 & 0 & bl & 0 & 0 & 0 \\
0 & 0 & 1 & 0 & 0 & 0 & 0 & 0 \\
0 & 0 & 1 & 0 & al & 0 & 0 & al^2 \\
0 & 0 & 1 & 0 & al & 2bl & 0 & al^2 \\
0 & 0 & 1 & 0 & 0 & 2bl & 0 & 0 \\
0 & 0 & 0 & 0 & 1 & 0 & 0 & 0 \\
0 & 0 & 0 & 0 & 1 & 0 & 0 & 2al \\
0 & 0 & 0 & 0 & 1 & 0 & 0 & 2al \\
0 & 0 & 0 & 0 & 1 & 0 & 0 & 0
\end{bmatrix}$$

$$
\begin{bmatrix}
0 & 0 & 0 & 0 & 0 & 0 & 0 & 0 \\
0 & 0 & 0 & 0 & 0 & 0 & 0 & 0 \\
al\ bl^2 & bl^3 & al^3bl & al^2bl^2 & al\ bl^3 & al^3bl^2 & al^2bl^3 & al^3bl^3 \\
0 & bl^3 & 0 & 0 & 0 & 0 & 0 & 0 \\
0 & 0 & 0 & 0 & 0 & 0 & 0 & 0 \\
0 & 0 & 0 & 0 & 0 & 0 & 0 & 0 \\
bl^2 & 0 & 3al^2bl & 2al\ bl^2 & bl^3 & 3al^2bl^2 & 2al\ bl^3 & 3al^2bl^3 \\
bl^2 & 0 & 0 & 0 & bl^3 & 0 & 0 & 0 \\
0 & 0 & 0 & 0 & 0 & 0 & 0 & 0 \\
0 & 0 & al^3 & 0 & 0 & 0 & 0 & 0 \\
2al\ bl & 3bl^2 & al^3 & 2al^2bl & 3al\ bl^2 & 2al^3bl & 2al^2bl^2 & 3al^3bl^2 \\
0 & 3bl^2 & 0 & 0 & 0 & 0 & 0 & 0 \\
0 & 0 & 0 & 0 & 0 & 0 & 0 & 0 \\
0 & 0 & 3al^2 & 0 & 0 & 0 & 0 & 0 \\
2bl & 0 & 3al^2 & 4al\ bl & 3bl^2 & 6al^2bl & 6al\ bl^2 & 9al^2bl^2 \\
2bl & 0 & 0 & 0 & 3bl^2 & 0 & 0 & 0
\end{bmatrix}.
$$

(B.6)

The transformation matrix $[T_m]$ is given by

$$
[T_m] = \begin{bmatrix}
1 & 0 & 0 & 0 & 0 & 0 & 0 & 0 \\
\frac{-1}{al} & \frac{1}{al} & 0 & 0 & 0 & 0 & 0 & 0 \\
\frac{1}{al\ bl} & \frac{-1}{al\ bl} & \frac{1}{al\ bl} & \frac{-1}{al\ bl} & 0 & 0 & 0 & 0 \\
0 & 0 & 0 & 0 & 1 & 0 & 0 & 0 \\
0 & 0 & 0 & 0 & \frac{-1}{al} & \frac{1}{al} & 0 & 0 \\
0 & 0 & 0 & 0 & \frac{-1}{bl} & 0 & 0 & \frac{1}{bl} \\
0 & 0 & 0 & 0 & \frac{1}{al\ bl} & \frac{-1}{al\ bl} & \frac{1}{al\ bl} & \frac{-1}{al\ bl}
\end{bmatrix},
$$

(B.7)

where al and bl are the length and width of the element.

From Equation (3.8), the matrix $[C_b]$ is given as

$$[C_b] = \begin{bmatrix} -H_{w,xx} \\ -H_{w,yy} \\ -2H_{w,xy} \end{bmatrix} = - \begin{bmatrix} 0 & 0 & 0 & 2 & 0 & 0 & 6x & 2y \\ 0 & 0 & 0 & 0 & 0 & 2 & 0 & 0 \\ 0 & 0 & 0 & 0 & 2 & 0 & 0 & 4x \end{bmatrix}$$

$$\begin{bmatrix} 0 & 0 & 6xy & 2y^2 & 0 & 6xy^2 & 2y^3 & 6xy^3 \\ 2x & 6y & 0 & 2x^2 & 6xy & 2x^3 & 6x^2y & 6x^3y \\ 4y & 0 & 6x^2 & 8xy & 6y^2 & 12x^2y & 12xy^2 & 18x^2y^2 \end{bmatrix}. \qquad \text{(B.8)}$$

The matrix $[C_m]$ from Equation (3.9) is given as

$$[C_m] = \begin{bmatrix} H_{u,x} \\ H_{v,y} \\ H_{u,y}+H_{v,x} \end{bmatrix} = \begin{bmatrix} 0 & 1 & 0 & y & 0 & 0 & 0 & 0 \\ 0 & 0 & 0 & 0 & 0 & 0 & 1 & x \\ 0 & 0 & 1 & x & 0 & 1 & 0 & y \end{bmatrix}. \qquad \text{(B.9)}$$

The stress-strain relationship in Equation (3.10) involves the reduced stiffness matrix, [Q]. The Q_{16}, and Q_{26} terms are set to zero, due to orthogonality. Each element of the [Q] matrix is a function of the composite material characteristics including: Young's modulus (E_{11} and E_{22}), Poisson's ratio (ν_{12} and ν_{21}), and the shear modulus (G_{12}). The [Q] matrix components are defined as:

$$Q_{11}=\frac{E_{11}}{1-\nu_{12}\nu_{21}}$$

$$Q_{22}=\frac{E_{22}}{1-\nu_{12}\nu_{21}}$$

$$Q_{12}=\frac{\nu_{12}\ E_{22}}{1-\nu_{12}\nu_{21}}$$

$$Q_{66} = G_{12}. \qquad \text{(B.10)}$$

If a layer is rotated by an angle ϕ, then the reduced stiffness matrix must be transformed to the $[\bar{Q}]$ reduced stiffness matrix. The transformation matrix, [T], is given by

$$[T] = \begin{bmatrix} \cos^2\phi & \sin^2\phi & 2\sin\phi\cos\phi \\ \sin^2\phi & \cos^2\phi & -2\sin\phi\cos\phi \\ -\sin\phi\cos\phi & \sin\phi\cos\phi & \cos^2\phi-\sin^2\phi \end{bmatrix}. \qquad \text{(B.11)}$$

The transformed reduced stiffness matrix, $[\bar{Q}]$, is calculated as

$$[\bar{Q}] = [T]^{-1}\ [Q]\ [T]^{-T}. \qquad \text{(B.12)}$$

The terms of the transformed stiffness matrix are given as

$$\bar{Q}_{11} = Q_{11}\cos^4\phi+2(Q_{12}+2Q_{66})\sin^2\phi\cos^2\phi+Q_{22}\sin^4\phi$$

$$\bar{Q}_{12} = (Q_{11}+Q_{22}-4Q_{66})\sin^2\phi\cos^2\phi+Q_{12}(\sin^4\phi+\cos^4\phi)$$

$$\bar{Q}_{22} = Q_{11}\sin^4\phi + 2(Q_{12}+2Q_{66})\sin^2\phi\cos^2\phi + Q_{22}\cos^4\phi$$

$$\bar{Q}_{16} = (Q_{11}-Q_{12}-2Q_{66})\sin\phi\cos^3\phi + (Q_{12}-Q_{22}+2Q_{66})\sin^3\phi\cos\phi$$

$$\bar{Q}_{26} = (Q_{11}-Q_{12}-2Q_{66})\sin^3\phi\cos\phi + (Q_{12}-Q_{22}+2Q_{66})\sin\phi\cos^3\phi$$

$$\bar{Q}_{66} = (Q_{11}+Q_{22}-2Q_{12}-2Q_{66})\sin^2\phi\cos^2\phi + Q_{66}(\sin^4\phi+\cos^4\phi).$$

(B.13)